

Aus dem Fachbereich medizinische Biochemie und Molekularbiologie

Primary cilium biogenesis and signaling

der Medizinischen Fakultät

der Universität des Saarlandes, Homburg (Saar)

Jun.-Prof. Dr. David Mick

**Identification and Characterization of the putative phosphatase  
PALD1 as a previously unknown component of the Sonic  
Hedgehog Signaling Pathway**

Dissertation

zur Erlangung des Grades eines Doktors der Naturwissenschaften

Dr. rer. nat.

der medizinischen Fakultät

der Universität des Saarlandes

2021

vorgelegt von

**Elena Alexandra May**

Geboren am 24.11.1991 in München

Tag der Promotion: 03.03.2022

Dekan: Prof. Dr. M. D. Menger

Prüfer: Jun.-Prof. Dr. David Mick  
Prof. Dr. Frank Schmitz

*“And what greater might do we possess as human beings than our capacity  
to question and to learn?”*

Ann Druyan

*“If you wish to succeed, you must brave the risk of failure.”*

Garry Kasparov

I dedicate this work with the deepest appreciation to my parents and grandparents.

## Table of Content

<b>List of figures</b>	5
<b>List of tables</b>	6
<b>List of Abbreviations</b>	7
<b>1. Summary</b>	10
<b>2. Zusammenfassung</b>	12
<b>3. Introduction</b>	14
3.1. A Brief History of Cilia.	14
3.2. Physiological Relevance of Cilia described by the Example of Selected Ciliopathies.	16
3.3. Architecture and Function of Primary Cilia.	18
3.4. Cilia-APEX - A Tool For Studying The Ciliary Proteome.	23
3.5. Ciliary Signaling – the Sonic Hedgehog Signaling Pathway.	25
3.6. Objectives of this work.	29
<b>4. Material</b>	30
4.1. Antibodies	30
4.2. Bacteria	31
4.3. Buffer & Solutions	31
4.4. Cells & Consumables	35
4.5. Kits	37
4.6. Culture Media & media supplement	38
4.7. Laboratory equipment	39
4.8. Cloning	40
4.9. Reagents	41
4.10. Software & clouds	43
<b>5. Methods</b>	44
5.1. Sequence analysis	44
5.2. Phylogenetic Analysis via Gene Clime	44
5.3. Bacterial transformation	44
5.4. Bacterial overnight cultures	44
5.5. Cell lines	45
5.5.1. Inner Medullary Collecting Duct 3 (IMCD3) cells	45
5.5.2. 3T3 immortalized fibroblasts	45
5.5.3. C2C12 Myoblasts	45
5.6. Cell culture	45
5.7. APEX Labeling	46
5.8. Sonic conditioned-medium	46
5.9. Sonic Hedgehog Signaling Assays	47
5.10. Immunofluorescence (IF) Microscopy	47
5.11. Cilia Quantification	47

5.12. Bradford Assay	48
5.13. Quantitative Fluorescence Western Blot (WB) Analysis	48
5.14. Ponceau Stain	49
5.15. CRISPR-Cas9 based Genome Editing	49
5.16. Mammalian Cell Transfection	50
5.17. Fluorescence Activated Cell Sorting (FACS)	52
5.18. Muscle differentiation assay	52
5.19. Scratch Assay	53
5.20. Reverse transcription Quantitative real-time Polymerase Chain Reaction (qRT-PCR)	53
5.21. Statistics	53
<b>6. Results</b>	54
6.1. Improved Cilia-APEX2 cell line enables proteomic screen to investigate the remodeling of the primary cilium proteome in response to SHH signaling.	54
6.2. Enhanced proteomic screen identifies a new potential SHH Signaling component.	59
6.3. The role of PALD1 in ciliary signaling in IMCD3 cells.	60
6.4. PALD1 is a cell type specific factor conserved among species.	65
6.5. IMCD3 <i>Pald1</i> <sup>-/-</sup> cells show mild pre-activation phenotype.	72
6.6. Molecular mechanisms of PALD1 accumulation.	79
6.7. PALD1 accumulation is dependent on cAMP.	81
6.8. PALD1 in SHH related and non-related signaling of Myoblasts and Fibroblasts.	85
6.9. Prospect – pre-liminary qPCR analysis confirms pre-activation of <i>Pald1</i> <sup>-/-</sup> in IMCD3s and surprisingly also in 3T3 but not in C2C12 cells.	90
<b>7. Discussion</b>	92
7.1. Improved Cilia-APEX2 study enlightens our understanding of the ciliary proteome.	92
7.2. Identification of PALD1 as a new component of SHH signaling.	93
7.3. The relation between PALD1 and PKA.	100
7.4. Proposed mechanism and Perspectives.	101
<b>8. References</b>	103
<b>9. Acknowledgements</b>	125
<b>10. Publications</b>	126
<b>11. Curriculum vitae</b>	127

## List of figures

Fig. 1: The structure of a primary cilium.	18
Fig. 2: Different types of cilia, their structural differences and an exemplary cell types.	21
Fig. 3: Overview of the APEX labeling reaction.	24
Fig. 4: The Sonic Hedgehog Signaling Pathway in Mammalian Cells.	27
Fig. 5: The Cilia-APEX construct vs. the improved Cilia-APEX2 construct.	54
Fig. 6: Cilia-APEX2 exhibits weaker transgene expression.	55
Fig. 7: Cilia-APEX2 labels ciliary proteins with a higher efficiency than Cilia-APEX at lower transgene expression.	56
Fig. 8: Detection of GPR161 in WT, Cilia-APEX and Cilia-APEX2 expressing cells	58
Fig. 9: Domain structure of PALD1.	60
Fig. 10: PALD1 and SMO after treatment with different concentrations of Shh-N or SAG.	61
Fig. 11: CYC-treated IMCD3 cells show ciliary SMO but not PALD1 accumulation.	64
Fig. 12: Steady state protein expression levels of PALD1 vary in dependence of the cell line.	66
Fig. 13: Accumulation of PALD1 was observed in primary cilia of C2C12 cells but in no other cell line.	67
Fig. 14: Co-evolutionary analysis of PALD1.	69
Fig. 15: PALD1 accumulation is impaired in the IMCD3 <i>Ift27<sup>-/-</sup></i> cell line.	71
Fig. 16: Generation of a IMCD3 <i>Pald1<sup>-/-</sup></i> cell line and analysis in comparison to WT cells.	73
Fig. 17: GLI3 <sup>FL</sup> /GLI3 <sup>R</sup> in IMCD3 <i>Pald1<sup>-/-</sup></i> cells indicates pre-activation of SHH signaling after loss of PALD.	75
Fig. 18: Ciliary GPR161 signals in IMCD3 <i>Pald1<sup>-/-</sup></i> are decreased in unstimulated cells compared to the WT cells.	76
Fig. 19: SMO accumulation is increased in IMCD3 <i>Pald1<sup>-/-</sup></i> cells compared to WT cells after induction with Shh-N.	77
Fig. 20: PALD1 accumulation in the primary cilium is TULP3 dependent.	80
Fig. 21: PALD1 accumulation in stimulated Cilia-PKI cells does not differ from unstimulated Control-PKI cells.	82
Fig. 22: PALD1 accumulation is induced by changes in cAMP levels.	84
Fig. 23: Generation of a <i>Pald1</i> knock out in C2C12 and 3T3 cells.	85
Fig. 24: Scratch assay of 3T3 and 3T3 <i>Pald1<sup>-/-</sup></i> cells shows no significant differences.	86
Fig. 25: Muscle differentiation assay of C2C12 WT cells in comparison to C2C12 <i>Pald1<sup>-/-</sup></i> cells.	88
Fig. 26: C2C12 <i>Pald1<sup>-/-</sup></i> cells showed no SHH or cilia defects in comparison to C2C12 WT cells.	89
Fig. 27: qPCR analysis of <i>Pald1<sup>-/-</sup></i> and respective WT cells reveals differences in signaling status.	91

## List of tables

Tab. 1: Primary antibodies	30
Tab. 2: Secondary antibodies & dyes	31
Tab. 3: Bacterial strains	31
Tab. 4: Cell lines	35
Tab. 5: List of consumables	36
Tab. 6: Kits used within this work	37
Tab. 7: Culture media & supplements	38
Tab. 8: List of equipment	39
Tab. 9: Oligonucleotides	40
Tab. 10: Plasmids	40
Tab. 11: List of reagents	41
Tab. 12: List of used software and cloud systems	43

## List of Abbreviations

%	-	percentage
° C	-	degree Celsius
µm	-	micrometer
3T3	-	3T3-Swiss albino Fibroblasts
ac-tub	-	acetylated-tubulin
ADP	-	Adenosin Diphosphat
ADPKD	-	autosomal dominant polycystic kidney disease
AKAP	-	A Kinase Anchoring Protein
APEX	-	Ascorbate Peroxidase
APEX2	-	improved Ascorbate Peroxidase 2
APS	-	Ammoniumpersulfate
ANOVA	-	single factor analysis of variance
ARL13B	-	ADP-ribosylation factor-like protein 13B
BBS	-	Bardet Biedl Syndrome
BBSome	-	Bardet Biedl Syndrome associated protein complex
BSA	-	Bovine Serum Albumin
C2C12	-	C2C12 mouse myoblasts
cAMP	-	cyclic Adenosin Monophosphat
CaCl <sub>2</sub>	-	Calcium chloride
Cas9	-	CRISPR associated endonuclease 9
cDNA	-	complementary DNA
Cilia-APEX	-	Cilia localized Ascorbate Peroxidase
Cilia-APEX2	-	Cilia localized Ascorbate Peroxidase 2
CO <sub>2</sub>	-	Carbon dioxide
CRISPR	-	Clustered Regularly Interspaced Short Palindromic Repeats
Cy	-	Cyanine dye
CYC	-	Cyclopamine
<i>D. melanogaster</i>	-	<i>Drosophila Melanogaster</i>
Dest. H <sub>2</sub> O	-	distilled water
DMEM	-	Dulbeccos's Modified Eagle Medium
DMSO	-	Dimethylsulfoxid
DNA	-	deoxyribonucleic acid
DTT	-	Dithiothreitol
<i>E. coli</i>	-	<i>Escherichia coli</i>
<i>e.g.</i>	-	<i>exempli gratia</i>
EDTA	-	Ethylendiaminetetraacetic acid
ESRD	-	End Stage Renal Disease
FACS	-	Fluorescence Activated Cell Sorting



FBS	-	Fetal Bovine Serum
Fig.	-	Figure
GFP	-	Green Fluorescent Protein
GLI1	-	Gliom Associated Transcriptionfactor 1
GLI2	-	Gliom Associated Transcriptionfactor 1
GLI3	-	Gliom Associated Transcriptionfactor 3
GPCR	-	G-Protein Coupled Receptor
GPR161	-	G-Protein Coupled Receptor 161
h	-	hour
H <sub>2</sub> O <sub>2</sub>	-	hydrogen peroxide
H <sub>2</sub> O	-	water
HCl	-	Hydrogen chloride
HEK	-	Human Embryonic Kidney
<i>i.e.</i>	-	<i>id est</i>
IF	-	Immunofluorescence
IFT	-	Intraflagellar Transport
IFT	-	Intraflagellar Transport Protein
IMCD3	-	Inner Medullary Collecting Duct Clone 3
KCl	-	Potassium chloride
kDa	-	kilo Dalton
M	-	molar
MIN6β	-	mouse pancreatic islet cell line 6β
min	-	minutes
mM	-	mili molar
MKS	-	Meckel Gruber Syndrome
ml	-	mililitres
MS	-	Mass-Spectrometry
n.a.	-	not applicable
n.s.	-	not significant
NaCl	-	Sodium chloride
NG	-	NeonGreen
NPHP3	-	Nephrocystin 3
PALD1	-	Paladin 1
PBS	-	Phosphate Buffered Saline
PCR	-	Polymerase Chain Reaction
PFA	-	paraformaldehyde
pH	-	<i>potentia hydrogenii</i>
PI(4,5)P2	-	Phosphatidylinositol-4,5-bisphosphat 2
PIP	-	Phosphatidylinositolphosphate
PKA	-	cyclic adenosine monophosphate dependent protein kinase A

PKA-R1 $\alpha$	-	Protein Kinase A Regulatory Subunit I $\alpha$
PKA-C	-	Protein Kinase A Catalytic Subunit
PMSF	-	Phenylmethylsulfonyl fluoride
PTCH1	-	Patched I
RFU	-	Relative Fluorescence Units
RNA	-	ribonucleic acid
RPE	-	Retinal Pigment Epithelium
RT	-	room temperature
s	-	seconds
SAG	-	Smoothened Antagonist
SD	-	Standard Deviation
SHH	-	Sonic Hedgehog
Shh-N	-	Sonic Hedgehog N-terminus
SMO	-	Smoothened
Tab.	-	Table
TBS	-	Tris-buffered saline
TBS-T	-	Tris-buffered saline with Tween
two-way ANOVA	-	two factor analysis of variance
TZ	-	Transition Zone
UdS	-	Universität des Saarlandes
v/v	-	volume per volume
WB	-	Western Blot
WT	-	wild type
w/v	-	weight per volume
qRT-PCR	-	quantitative Reverse Transcriptase PCR
YFP	-	Yellow Fluorescent Protein

## 1. Summary

### ***Identification and Characterization of the putative phosphatase PALD1 as a previously unknown component of the Sonic Hedgehog Signaling Pathway.***

During the past decades primary cilia were brought into the focus of research. Despite the greatly increased interest in primary cilia, many questions remain unanswered. The small reaction space of primary cilia is associated with low amounts of protein which poses enormous challenges for research. Furthermore, primary cilia cannot be isolated like completely membrane-enclosed organelles because they do possess a highly specialized membrane but which is continuous with the plasma membrane. Based on the first methodological approach to study the ciliary proteome easily and reliably using proximity labeling and mass-spectrometric analysis, a new technique to study the ciliary proteome was established within this work using Cilia-APEX2. The Cilia-APEX2 construct consists of an improved cilia-localized ascorbate peroxidase, APEX2, which allows higher labeling efficiency at lower transgene expression than the previously used Cilia-APEX as demonstrated within this work. Thus, Cilia-APEX2 enabled to study time resolved remodeling of the cilia proteome during Sonic Hedgehog signaling for the first time (May *et al.*, 2021).

The Sonic Hedgehog signaling pathway is a fundamental signaling pathway of the embryonic development and depends in mammals strictly on primary cilia. Disruption of the Sonic Hedgehog signaling pathway leads to death at an early embryonic stage or to severe birth defects. Nevertheless, many of the underlying mechanisms remain poorly understood. Using Cilia-APEX2, new information on the mechanisms of Sonic Hedgehog signaling in Inner Medullary Collecting Duct 3 (IMCD3) cells were obtained e.g. the putative phosphatase Paladin (PALD1) was associated with Sonic Hedgehog signaling for the first time. Within this work, it was shown that PALD1 localizes to primary cilia after activation of Sonic Hedgehog Signaling *via* the Sonic Hedgehog receptor Protein patched homolog 1 (PTCH1). It was further shown, that when PTCH1 is bypassed in Sonic Hedgehog Signaling activation *via* use of the Smoothened Agonist (SAG), PALD1 still localizes to primary cilia. PALD1 does not complexate with the Sonic Hedgehog effector Smoothened (SMO) permanently but co-localized with SMO to primary cilia of IMCD3 cells after activation of Sonic Hedgehog signaling. Screening of different cell lines for PALD1 expression as well as a comparative phylogenetic analysis, revealed that PALD1 is conserved among species and present in different human and murine cell lines. To investigate the role of PALD1 further, different cell lines which lacked PALD1 were generated and analyzed such as IMCD3 cells, murine Fibroblasts and murine Myoblasts (May *et al.*, 2021).

Furthermore, it was shown that the here generated IMCD3 *Pald1*<sup>-/-</sup> cells are situated in a pre-activated Sonic Hedgehog signaling state. This was demonstrated by changes in two Sonic Hedgehog components, the G protein-coupled receptor GPR161 and the glioma-associated zinc finger 3 (GLI3) transcription factor, among others. Nevertheless, IMCD3 *Pald1*<sup>-/-</sup> cells can be further activated by addition of Sonic Hedgehog inducing reagents. Ciliary accumulation of PALD1 was shown to be dependent on both cAMP and the protein complex of intraflagellar transport proteins 27 and 25.

Furthermore, the accumulation of PALD1 is possibly influenced by the protein kinase A. Ciliary accumulation of PALD1 in dependence of active Sonic Hedgehog Signaling was also observed in Myoblasts within this work and it was shown that differentiation of Myoblasts into muscle cells was impaired after loss of PALD1. In Fibroblasts, even though no ciliary accumulation of PALD1 was detected, Sonic Hedgehog signaling pre-activation was also observed in a transcriptional analysis indicating specific but similar tissue specific functions for PALD1 among different cell lines. While the role of PALD1 in Fibroblasts and Myoblasts needs further research, it was demonstrated, that PALD1 controls Sonic Hedgehog dependent processes in different cell lines.

The identification of PALD1 as a previously unknown Sonic Hedgehog signaling component highlights the improved methodology of the Cilia APEX2 approach. Moreover, PALD1 was identified in this work as a novel negative mediator of the Sonic Hedgehog signaling pathway, and the underlying molecular mechanisms were studied in detail. The identification of such fine-regulatory components of the pathway has been tended to be neglected in the past and opens new opportunities for therapeutic regulation by fine-tuning the highly sensitive and tightly regulated Sonic Hedgehog pathway.

## 2. Zusammenfassung

### *Identifizierung und Charakterisierung der potenziellen Phosphatase PALD1 als bisher unbekanntes Komponente des Sonic Hedgehog Signalweges.*

In den letzten Jahrzehnten sind primäre Zilien in den Fokus der Forschung gerückt. Trotz des stark gestiegenen Interesses bleiben jedoch viele Fragen unbeantwortet. Der kleine Reaktionsraum des primären Ziliums ist mit sehr geringen Proteinmengen verbunden, was eine große Herausforderung bei der Untersuchung darstellt. Des Weiteren können primäre Zilien nicht wie vollständig membranumschlossene Organellen durch übliche Methoden isoliert werden, da sie zwar eine hochspezialisierte Membran besitzen, diese jedoch kontinuierlich mit der Plasmamembran verbunden ist. Basierend auf dem ersten methodischen Ansatz zur einfachen und zuverlässigen Untersuchung des Zilienproteoms mittels Proximity Labeling und massenspektrometrischer Analyse, wurde in dieser Arbeit eine neue Technik zur Untersuchung des Zilienproteoms unter Verwendung von Cilia-APEX2 etabliert. Das Cilia-APEX2-Konstrukt besteht aus einer verbesserten, in den Zilien lokalisierten Ascorbatperoxidase, APEX2, die eine höhere Markierungseffizienz bei geringerer Transgenexpression als das zuvor verwendete Cilia-APEX Konstrukt ermöglicht, wie in dieser Arbeit gezeigt wurde. Somit konnte durch Cilia-APEX2 zum ersten Mal der zeitlich aufgelöste Umbau des Zilienproteoms während der Sonic Hedgehog-Signalisierung untersucht werden (May *et al.*, 2021).

Der Sonic-Hedgehog-Signalweg ist ein grundlegender Signalweg der Embryonalentwicklung und hängt bei Säugetieren von primären Zilien ab. Eine Unterbrechung des Sonic-Hedgehog-Signalwegs führt zum Tod in einem frühen Embryonalstadium oder zu schweren Geburtsfehlern. Mit Hilfe von Cilia-APEX2 wurden neue Informationen über die Mechanismen der Sonic Hedgehog-Signalübertragung in Zellen des Inner Medullary Collecting Duct 3 (IMCD3) gewonnen, z. B. wurde die mutmaßliche Phosphatase Paladin 1 (PALD1) erstmals mit der Sonic Hedgehog-Signalübertragung in Verbindung gebracht. Im Rahmen dieser Arbeit konnte gezeigt werden, dass PALD1 nach der Aktivierung des Sonic-Hedgehog-Signalweges über das Rezeptor Patched Homolog 1 (PTCH1) in primäre Zilien lokalisiert. Bei einer Umgehung von PTCH1 über die Aktivierung des Signalweges durch den Smoothed Agonist (SAG) lokalisiert PALD1 ebenfalls in primäre Zilien. PALD1 komplexiert nicht permanent mit dem Sonic-Hedgehog-Effektor Smoothed (SMO), wird aber nach Aktivierung des Sonic-Hedgehog-Signalwegs zusammen mit SMO in primären Zilien von IMCD3-Zellen co-lokalisiert. Ein Screening verschiedener Zelllinien auf PALD1-Expression sowie eine vergleichende phylogenetische Analyse ergaben, dass PALD1 zwischen den Spezies konserviert und in verschiedenen menschlichen und murinen Zelllinien vorhanden ist. Um die Rolle von PALD1 weiter zu untersuchen, wurden Zelllinien generiert und analysiert, die kein PALD1 exprimierten. Dabei handelte es sich unter anderem um IMCD3-Zellen, aber auch um murine Fibroblasten und murine Myoblasten (May *et al.*, 2021).

Darüber hinaus konnte gezeigt werden, dass sich die hier erzeugten IMCD3 *PalD1*<sup>-/-</sup> Zellen in einem voraktivierten Sonic Hedgehog-Signalzustand befinden. Dies konnte unter anderem durch

Veränderungen zweier Sonic Hedgehog Komponenten, dem G-Protein gekoppelten Rezeptor GPR161 und dem Gliom assoziierten Zink Finger 3 (GLI3) Transkriptionsfaktor gezeigt werden. Dennoch können IMCD3 *Pald1*<sup>-/-</sup> Zellen durch Zugabe von Sonic Hedgehog induzierenden Reagenzien weiter aktiviert werden. Es konnte gezeigt werden, dass die ziliäre Akkumulation von PALD1 sowohl von cAMP als auch von dem Proteinkomplex der Intraflagellaren Transport Proteine 27 und 25 abhängig ist. Weiterhin wird die Akkumulation von PALD1 möglicherweise durch die Protein Kinase A beeinflusst. Die ziliäre Akkumulation von PALD1 in Abhängigkeit von aktivem Sonic Hedgehog-Signal wurde in dieser Arbeit auch in Myoblasten beobachtet und es wurde gezeigt, dass die Differenzierung von Myoblasten in Muskelzellen nach Verlust von PALD1 beeinträchtigt war. In Fibroblasten wurde keine ziliäre Akkumulation von PALD1 festgestellt, und es wurden keine Defekte bei der Zellmigration nach dem Verlust von PALD1 beobachtet. In einer transkriptionellen Analyse von Fibroblasten wurde jedoch eine Voraktivierung der Sonic-Hedgehog-Signalübertragung beobachtet, was auf spezifische, aber ähnliche Funktionen von PALD1 in verschiedenen Zelltypen hindeutet. Während die Rolle von PALD1 in Fibroblasten und Myoblasten noch weiter erforscht werden muss, konnte somit gezeigt werden, dass PALD1 Sonic-Hedgehog-abhängige Prozesse in verschiedenen Zelllinien kontrolliert.

Die Identifizierung von PALD1 als bisher unbekannte Sonic Hedgehog-Signalkomponente unterstreicht die verbesserte Methodik des Cilia-APEX2-Ansatzes. Darüber hinaus wurde PALD1 in dieser Arbeit als ein neuer, bisher unbekannter, negativer Mediator des Sonic Hedgehog-Signalwegs identifiziert und die molekularen Mechanismen wurden eingehend untersucht. Die Identifizierung solcher feinregulierenden Komponenten des Signalwegs wurde in der Vergangenheit eher vernachlässigt und eröffnet neue Möglichkeiten zur therapeutischen Regulierung über die Feinabstimmung des hochsensiblen und streng regulierten Sonic Hedgehog-Signalwegs.

### 3. Introduction

#### 3.1. A Brief History of Cilia.

Primary cilia are short cellular membrane protrusions that function as cellular antenna in the transmission and processing of extracellular signals (Anvarian *et al.*, 2019). The primary cilium is immotile and solitary for each cell (Satir & Christensen, 2007). Besides the primary cilium, there are other types of cilia that differ in function and appearance (Satir & Christensen, 2007). Motile cilia for example, possess the ability to move extracellular fluids or single cell organisms and can be present alone or in the hundreds on a single cell (Wanner *et al.*, 1996; Nonaka *et al.*, 1998, Bernabé-Rubio & Alonso, 2017). If these motile cilia are long, solitary and serve to propel a single, unicellular organism, they are often referred to as flagellum (Bernabé-Rubio & Alonso, 2017).

Historically, cilia have been classified as the first cellular organelles to ever be discovered (Harcourt *et al.*, 1932, Beales & Jackson, 2012). As early as 1675, advances in light microscopy enabled the Dutch scientist Antoni van Leeuwenhoek to observe thin, motile, cellular structures on protists for the first time. These structures, which reminded van Leeuwenhoek of small "legs," were the first sightings of motile cilia (Harcourt *et al.*, 1932, Beales & Jackson, 2012). However, the structurally distinct primary cilia were not discovered until 1898 when the swiss neuroscientist Karl Wilhelm Zimmermann observed the primary cilium on mammalian cells (Zimmermann, 1898; Bloodgood 2010; Yusifov *et al.*, 2021). Zimmermann had already suggested a possible sensory function for what he described as the central flagellum (Zimmermann, 1898). However, his discovery including the proposed function and nomenclature, was neglected for decades. In the second half of the 19<sup>th</sup> century, when electron microscopy had become more advanced, primary cilia research was stamped by Sergei Sorokin. Sorokin observed primary cilia as shortened, immotile cilia in electron microscopy (Sorokin, 1962). Since the function of this particular type of cilia was unknown, they were very ingloriously referred to as rudimentary and obsolete by Sorokin (Sorokin, 1962). Furthermore, it was suggested that primary cilia might be precursors of motile cilia (Sorokin, 1962). Although this assumption was later rejected, Sorokin's definition of "primary" cilia prevailed, instead of the nomenclature proposed by Zimmermann (Sorokin, 1962; Bloodgood 2010; Beales & Jackson, 2012). For decades, and even though sensory cilia were known from the model organism *Caenorhabditis elegans* as early as 1975, no conclusions about primary cilia in mammals were drawn from this observation (Ward *et al.*, 1975).

In 2000, the view of primary cilia finally changed. The reason for this change in perception was due to a landmark study by Gregory Pazour and his colleagues. It was found that the intraflagellar transport protein 88 (IFT88), whose defects in the model organism *Chlamydomonas* (green alga) lead to abnormally short flagella, is a homolog of the mouse gene *Tg737* (Pazour *et al.*, 2000). *Tg737*, when defective, can cause polycystic kidney disease in mice (Moyer *et al.*, 1994). Furthermore, mutations in *Tg737*, which is today commonly referred to as *Ift88* in mammals as well, causes severe liver and kidney damage associated with early infant death (Pazour *et al.*, 2000). This was the first time a link had been established between a flagellar protein and a mammalian disease. Additionally, the diseases observed in

mice due to defects in *Ift88* were similar to the symptoms seen in humans suffering from autosomal recessive polycystic kidney disease (ARPKD) (Moyer *et al.*, 1994). During this time, ARPKD was a poorly understood and severe disease associated with polycystic kidney and hepatic disease (PKHD) (Dalgaard *et al.*, 1971). The disease in humans is caused by a mutation of the gene named after its associated disease namely, *PKHD1* (Moyer *et al.*, 1994). ARPKD can lead to end-stage renal disease (ESRD) which is equivalent to renal failure, and occurs as early as the teenage years (Dalgaard *et al.*, 1971; Cole *et al.*, 1990;). The collecting tubules of the kidneys have a large number of primary cilia, the function of which was not clear at the time (Andrews & Porter, 1974). Based on this knowledge, Pazour *et al.* studied the primary cilia in the kidneys of mice with *Ift88* defects. It was shown that defects in *Ift88* correspond to shorter primary cilia in mouse kidneys. Subsequently, primary cilia were able to be linked to ARPKD (Pazour *et al.*, 2000). This landmark discovery suggested for the first time that primary cilia may have important unknown regulatory functions.

Only three years later, Kathryn Anderson's group was able to demonstrate a direct link between severe developmental disorders in mice and IFTs. This study suggested a function of primary cilia outside of the kidney (Huangfu *et al.*, 2003). Thus, it was observed for the first time that primary cilia could play important roles in the development of mammalian embryos (Huangfu *et al.*, 2003, Huangfu & Anderson, 2005). Due to this finding, the view of primary cilia and the consequent interest in them was about to change dramatically. The findings on the importance of primary cilia in the perception of extracellular stimuli also illuminated the study of motile cilia (Christensen *et al.*, 2007; Shah *et al.*, 2009; Jain *et al.*, 2012). The pure classification into motile and non-motile cilia is today partially obsolete, as both motile and primary cilia have been more and more associated with their sensory potential (Bloodgood, 2010). Today, numerous human diseases are known to be associated with primary cilia (Hildebrandt *et al.*, 2011). These diseases, so-called ciliopathies, are often characterized by a variety of symptoms due to the fact that primary cilia in particular are present on almost all cells of a mammalian organism (Hildebrandt *et al.*, 2011; Anvarian *et al.*, 2019). This underlines the physiological relevance of cilia, but often makes correct diagnosis and treatment difficult (Hildebrandt *et al.*, 2011).



### 3.2. Physiological Relevance of Cilia described by the Example of Selected Ciliopathies.

The term ciliopathies describes a group of rare diseases associated with ciliary defects. Ciliopathies are characterized by a variety of symptoms that affect multiple organs and tissues with often severe consequences (Hildebrandt *et al.*, 2011). Although ciliopathies are very rare, they generate a high level of suffering among affected individuals due to their multisystemic nature (Fliegauf *et al.*, 2007; Tobin & Beales 2009). This overlay of seemingly independent symptoms makes it difficult to classify and differentiate individual ciliopathies. Many ciliopathies are described as syndromic such as Meckel's Syndrome (Salonen & Paavola, 1998), Bardet Biedel Syndrome (Forsythe & Beales, 2013), Senior-Loken syndrome and Nephronophthisis (Ronquillo *et al.*, 2012). In addition, there are also some ciliopathies which are non-syndromic, e.g. autosomal dominant polycystic kidney disease (ADPKD) (Ong & Harris, 2005). In the following, some selected ciliopathies will be described to provide an overview of cilia-induced defects.

Meckel syndrome and Bardet-Biedl syndrome are two examples of syndromic ciliopathies. Meckel syndrome leads to perinatal death due to a combination of severe symptoms, including pulmonary hypoplasia (incomplete development of the lungs) (Erger *et al.*, 2017), polycystic kidneys and renal hypodysplasia (abnormally small kidneys) (Salonen *et al.*, 1984). However, Meckel's syndrome is also associated with malformations that are not necessarily life-threatening, such as situs inversus (Kyttälä *et al.*, 2006) and postaxial polydactyly (Mecke & Passarge, 1971). In contrast, life expectancy is not reduced in patients suffering from Bardet-Biedl syndrome (BBS), which affects ca. 1 out of 135, 000 – 160, 000 livebirths (Forsythe & Beales, 2013). BBS is characterized in particular by obesity, blindness and mental retardation. However, patients are not born with visual impairment. Instead, vision decreases systematically during childhood and results in blindness around the age of 15 (Tobin & Beales, 2007). This characteristic symptom usually leads to the diagnosis of BBS. BBS is caused by defects in genes coding for BBS proteins, which form a ciliary protein complex called the BBSome (Nachury *et al.*, 2007). The BBSome fulfills important functions within the cilium e.g., BBS proteins are involved in the ciliary signaling like Sonic Hedgehog (SHH) signaling (Tobin & Beales, 2007; Ye *et al.*, 2018; Shinde *et al.*, 2020).

Another syndromic ciliopathy is the Senior Loken syndrome. This disease is characterized by Nephronophthisis associated with retinal dystrophy (degenerative disease of the retina; Ronquillo *et al.*, 2012). Nephronophthisis is a renal ciliopathy associated with degenerative cystic kidneys (Salomon *et al.*, 2009). In fact, Nephronophthisis is the most common cause of kidney failure at a young age, on average at about 13 years. Unlike other kidney diseases such as ADPKD, which is associated with pathologically enlarged kidneys, in nephronophthisis, the size of the kidneys is unchanged or reduced (Salomon *et al.*, 2008). Mutations in the ciliary nephrocystin (*NPHP*) genes have been identified as the cause of this disease (Sang *et al.*, 2011). They encode several proteins associated with nephronophthisis, such as *NPHP3*, that localizes to the primary cilium due to an N-terminal myristoylation site and its coiled-coil domains (Nakata *et al.*, 2012). In nephronophthisis, a juvenile form and an infantile form can

be distinguished (Fanconi *et al.*, 1951; Gagnadoux *et al.*, 1989). While the juvenile form leads to ESRD in the second decade of life, this condition sets in before the age of 5 in the infantile form (Fanconi *et al.*, 1951; Gagnadoux *et al.*, 1989). Since renal failure is associated with anemia, hypertension and cardiac insufficiency, the state of renal failure is fatal without treatment by dialysis or kidney transplantation (Go *et al.*, 2006; Wali & Heinrich 2005). Besides Nephronophthisis, Senior-Loken Syndrome can be further associated with mental retardation, ataxia, polydactyly and breathing disorders (Ronquillo *et al.*, 2012). The relation between Senior Loken syndrome and Nephronophthisis vividly illustrates how difficult it is to differentiate individual ciliopathies not only from each other, but also from other non-cilia related diseases. For this reason, the number of people suffering from ciliopathies may be much higher than expected.

An example of a nonsyndromic ciliopathy is ADPKD. With an incidence of 1:500 – 1:1000 in Europe and the United States of America, ADPKD is one of the most common inherited disorders (Ong & Harris, 2005). As such, ADPKD is also the most common genetic kidney disease (Gabow, 1990). Defects of the *PKD1* and *PKD2* genes, are associated with a failure of renal tubule cell differentiation and maintenance (Cornec-Le Gall *et al.*, 2013). *PKD1* and *PKD2* encode polycystin-1 and polycystin-2 which are proteins that are highly enriched in the primary cilium (Nauli *et al.*, 2003) in addition to their presence in the Golgi apparatus (Su *et al.*, 2014) and endoplasmic reticulum (ER) (Nauli *et al.*, 2003). As a result of the defects in the polycystin proteins, lipid secretion is impaired and renal cysts form (Sutter & Germino, 2003). The first symptoms of ADPKD usually appear after the age of 20, where patients suffer from e.g. hypertension (Gabow *et al.*, 1990), abdominal pain (Sherstha *et al.*, 1997), hematuria (Gabow *et al.*, 1992), and urinary tract infections (Idrizi *et al.*, 2011; Bergmann *et al.*, 2018). However, about half of the patients do not experience symptoms, which complicates and delays the diagnosis of the disease. At a slightly older age, between 55 and 75 years, ESRD develops (Bergmann *et al.*, 2018).

The described diseases give only a small insight into the diversity of ciliopathies. It is due to the wide distribution in the organism on a multitude of cells in a multitude of tissues that the picture of cilia-dependent diseases is so diverse (Hildebrandt *et al.*, 2011; Chen *et al.*, 2019). Due to their physiological distribution, cilia fulfill numerous different functions within an organism and some of them are highly specialized (Bernabé-Rubio & Alonso, 2017).

### 3.3. Architecture and Function of Primary Cilia.

As already described, primary cilia are cellular membrane protrusions (Satir & Christensen, 2007). Primary cilia have an axonemal core and a specialized membrane that merges with the plasma membrane but differs from it in its composition (Fig. 1; Garcia *et al.*, 2018). The inner cilium is separated from the cellular cytoplasm by a so-called Transition Zone (TZ) that allows it to form a functional compartment with a specific proteome (Gonçalves & Pelletier, 2017). Distal to the TZ lies a specialized organelle, the basal body, which develops after cell division from the older (mother) of the two centrioles (Kobayashi & Dynlacht, 2011). The characteristic membrane invagination surrounding the base of some, but not all, ciliary types is called the ciliary pocket (Ghossoub *et al.*, 2011).

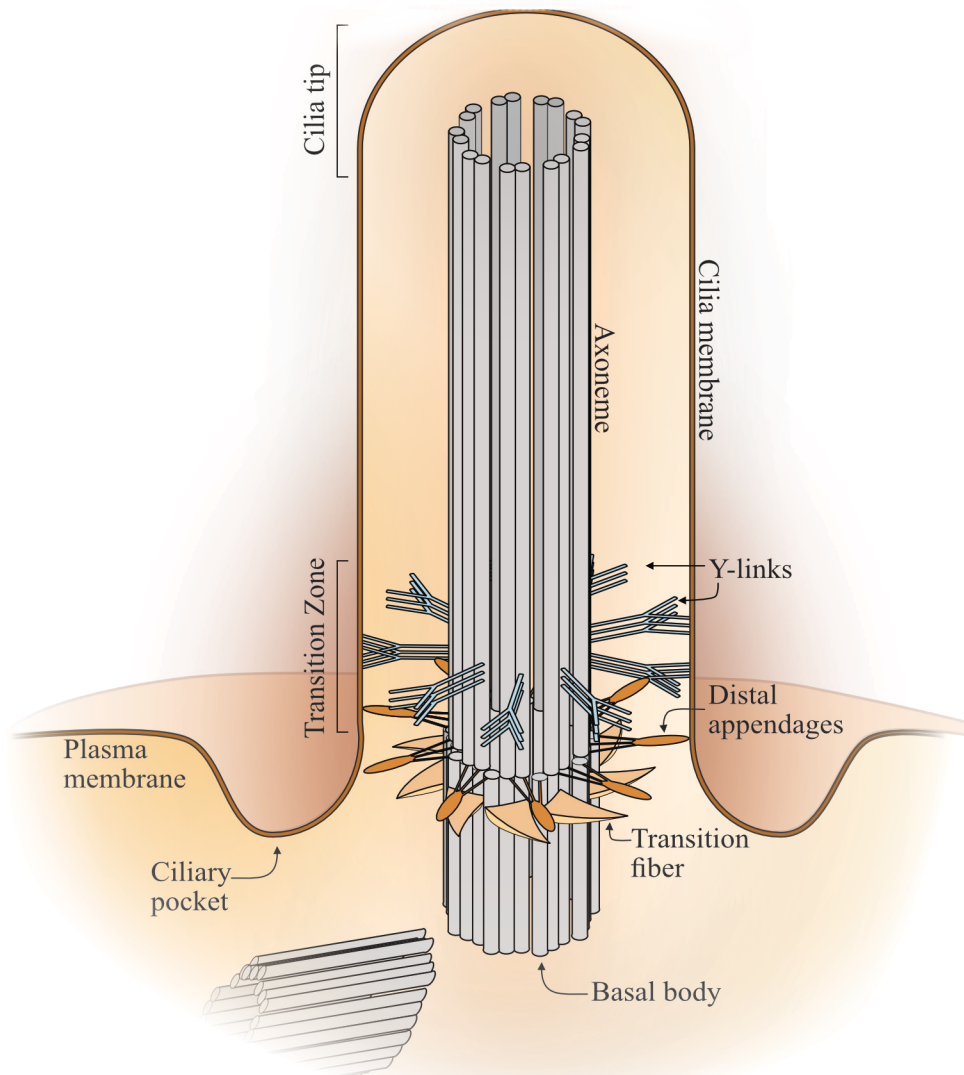


**Fig.1: The structure of a primary cilium.**

The axoneme forms the shaft of the cilium. It originates from the basal body, which in turn originates the transition fibers. The ciliary membrane surrounds the cilium and is anchored to the axoneme by the distal appendages and the Y-links, a characteristic protein structure of the transition zone. Where the ciliary membrane joins the plasma membrane, the membrane bulges into the ciliary pocket. The distal region of the cilium is called the ciliary tip.

The ninefold symmetrical axoneme of microtubule doublets forms the basic framework of all types of cilia (Bernabè-Rubio & Alonso, 2017). Depending on the presence or absence of an additional central pair of microtubule singlets, the axonemal structure is described as 9+2 or 9+0 (Bernabè-Rubio & Alonso, 2017). 9+2 motile cilia have an additional mechanoregulatory protein structure, the radial spokes, which other cilia types lack and serve to stabilize the cilium. These radial spokes are essential for cilia motility in 9+2 types of cilia (Gui *et al.*, 2021). Nodal cilia, that determine left-right symmetry during embryonic development, are the only known type of motile cilia that possess a 9+0 structure. In contrast, immotile cilia can be organized as either 9+2 or 9+0 (Gluenz *et al.*, 2010; Bernabè-Rubio & Alonso, 2017). Primary cilia are among others characterized by the fact that they cannot move independently i.e., they are immotile. Furthermore, they possess a 9+0 axonemal structure (Pazour & Witman 2003).

In both the ciliary membrane and the plasma membrane, phospholipids are the predominant component (Andrews & Nelson, 1979; Parks *et al.*, 1987). Still, the ciliary membrane differs from the plasma membrane in its protein and lipid composition, e.g., in its presence of various phosphatidylinositols (Garcia *et al.*, 2018). To date, the ciliary membrane is poorly characterized. Recent studies suggest a complex composition that could be differentiated in diverse domains within a single cilium, distinguished by the enrichment of certain proteins or lipids (Garcia *et al.*, 2018). An already known specialized ciliary membrane domain is the ciliary pocket, an invagination at the base of the ciliary membrane. This structure surrounds the entire ciliary base (Ghossoub *et al.*, 2011). Some studies propose that the ciliary pocket is enriched with receptors and may fulfill important signaling properties (Molla-Herman *et al.*, 2010). Still, due to the lack of specific markers and the inability to isolate the pocket specifically, the ciliary pocket remains poorly understood (Ghossoub *et al.*, 2011). The shape and general presence of the ciliary pocket may vary depending on the cell type, an observation that gives rise to further questions about its exact function (Molla-Herman *et al.*, 2010). Indeed, the presence of additional membrane domains could play an important role in the regulation of ciliary signaling since it is already known that the SHH signaling pathway is regulated, among other things, by small accessible fractions of lipids in the ciliary membrane (Garcia-Gonzalo *et al.*, 2015; Kinnebrew *et al.*, 2019; Radhakrishnan *et al.*, 2020).

The TZ is characterized by its champagne-glass-shaped protein structures, known as Y-links (Jensen *et al.*, 2015; Garcia-Gonzalo & Reiter, 2017). Furthermore, the TZ serves as a diffusion barrier that separates the inner cilium from the cytoplasm (Garcia-Gonzalo & Reiter, 2017). Proteins that enter the cilium move along the axoneme. As cilia do not possess a molecular machinery for protein translation, they depend on protein import from the cytoplasm (Rosenbaum & Child, 1967). These proteins need to be transported along the axoneme to reach their destination, which is mediated by the Intraflagellar Transport (IFT) system (Kozminski *et al.*, 1995). IFT not only refers to the system that mediates the transport of proteins but also to the class of proteins involved in it. As IFT proteins are essential for the formation and maintenance of cilia, they are conserved among all ciliated organisms (Pazour *et al.*, 2000; Pazour *et al.*, 2002). Another ciliary protein transport system relies on the BBSome. The BBSome

is a protein complex composed of eight stable subunit proteins associated with the Bardet-Biedel syndrome (see 3.3. Ciliopathies; Blacque & Leroux, 2006; Nachury *et al.*, 2007). This complex is specialized on the removal of membrane proteins and G-protein coupled receptors (GPCRs) from the primary cilium (Nachury *et al.*, 2007). Proximal to the TZ is the basal body, which emerges from the mother centriole after the cell cycle (Kobayashi & Dynlacht, 2011). The basal body also plays a potential role as a hub of ciliary signal transduction (Leitch *et al.*, 2014; Vertii *et al.*, 2016). From here, extends the axoneme, which templates the cilium. Specific protein structures connect the extending axoneme to the enclosing membrane. These connecting structures are called transition fibers (Garcia-Gonzalo & Reiter, 2017).

Although all cilia have a similar architecture, they differ according to their function, as described earlier (Fig. 2). As a result, different types of cilia are found in different species of organisms, e.g., the eukaryotic protozoa *Paramecium tetraurelia* forms hundreds of short cilia that beat in unison to enable locomotion (Brehm & Eckert, 1978). Motile cilia have additional dynein and kinesin arms that are lacked in primary cilia. Dynein and kinesin are motor proteins that bind microtubules and enable IFT mediated retrograde and anterograde transport of proteins in all types of cilia (Bernabé-Rubio & Alonso, 2017). Furthermore in motile cilia, dynein motor proteins bridge between two adjacent microtubules to allow their movement (Heuser *et al.*, 2009; Roberts *et al.*, 2013). The result is the characteristic ciliary beat. This property, found in complete groups of organisms, is therefore aptly names as ciliates (Parducz, 1967). Furthermore, there are the unicellular model organisms *Trypanosoma brucei* (parasite causing "sleeping sickness") and the model organism *Chlamydomonas reinhardtii* (green alga), which harbor one or two motile cilia (50 - 150  $\mu\text{m}$ ), also called flagellum, as mentioned above. Possession of a flagellum is also known in the *spermatozoa* in multicellular animals (Inaba, 2011). Interestingly, different types of cilia can also be found within a multicellular organism and at different developmental stages (Nonaka *et al.*, 1998; Veland *et al.*, 2009). However, the primary cilium is present on almost all cell types in all tissues of mammals (Venkatesh, 2017). Despite the large number of different cilia types with their different functions, many features are conserved among species (Pazour *et al.*, 2000; Essner *et al.*, 2002; Baker *et al.*, 2003; Morante *et al.*, 2020). For this reason, conclusions can be drawn about primary cilia and *vice versa* by studying motile cilia.

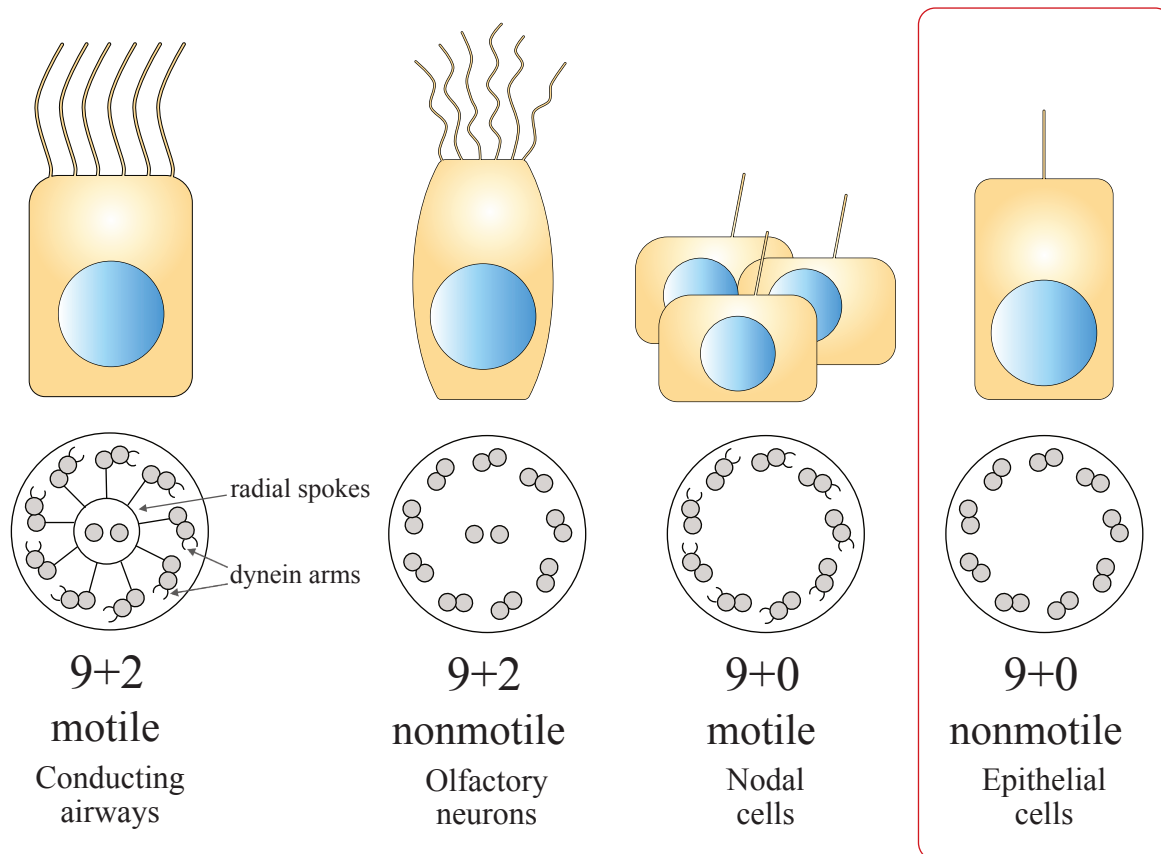


**Fig. 2: Different types of cilia, their structural differences and exemplary cell types.**

The shape and design of cilia depend strongly on their function. The two organization types 9+2 and 9+0 describe the structure of the axoneme. Both types exist for motile and immotile cilia. While motile cilia organized in a 9+2 structure have radial strokes, this structure is not found in any other type of organization. For example, the motile cilia found in the conducting airways (9+2) and nodal cells (9+0) have additional dynein arms for movement. These dynein arms are lacking in the immotile cilia found on olfactory neurons (9+2). Primary cilia, which have a 9+0 structure, also lack dynein arms. Primary cilia are found on almost all cell types of mammalian organisms and are shown here as an example on epithelial cells (modified after Bernabé-Rubio & Alonso, 2017).

Multiciliated tissues include, for example, the conducting airways of the lungs. The cilia in these tissues generate metachronous waves to remove pathogens and particles contained in the mucus (Bustamante-Marin & Ostrowski, 2017). As described earlier, there are also immotile cilia with a 9+2 structure that lack the additional dynein arms required for movement. Examples of these immotile 9+2 cilia are the sensory cilia of olfactory neurons in humans and other mammals, which harbor receptors for odor molecules. These neurons are located in the olfactory epithelium in the nasal mucosa near the nasal roof. Upon the binding of odor molecules to these receptors, ciliary G-proteins are activated. Activation of these G-proteins leads to an increase in cAMP levels and subsequent activation of ion channels and depolymerization of the membrane (Bear *et al.*, 2011). The rare 9+0 motile cilia occur in mammals only during embryonic development in the so-called nodal cells. These nodal cilia lack the radial spokes that are essential for 9+2 motile cilia (Gui *et al.*, 2021; Nonaka *et al.*, 1998). Photoreceptor cilia, which

mediate the transport of proteins from the outer to the inner segment of photoreceptor cells (Wensel *et al.*, 2016), are immotile as primary cilia and have a 9+0 structure (Abou Alaiwi *et al.*, 2009).

By far, the most abundant cilia on mammalian cells, are primary cilia. Primary cilia, which are always solitary for each cell, are relatively short compared to other cilia and have a length of about 3–10 $\mu$ m (Wann & Knight, 2012; Hernandez-Hernandez *et al.*, 2014; Bernabé-Rubio & Alonso, 2017). During the cell cycle, primary cilia are dynamically assembled and disassembled (Wang & Dynlacht, 2018). Their main function is to incorporate external stimuli into cellular responses. Besides that, they also regulate important cellular signaling pathways (Anvarian *et al.*, 2019). The best described signaling pathway that strictly depends on primary cilia in mammals is the SHH signaling pathway, which plays a crucial role in proper embryonic development. Furthermore, SHH signaling is essential for tissue homeostasis and maintenance in the adult organism (Gigante & Caspary, 2020).

### 3.4. Cilia-APEX - A Tool For Studying The Ciliary Proteome.

While interest in primary cilia is increasing and extensive research is being conducted, many questions still remain unanswered. Visualization of time-dependent changes in the cilia proteome and membrane could expand our understanding of how stimuli are transmitted, paving the way for e.g., the identification of new drug targets to treat ciliopathies. However, the inability to isolate non-membrane enclosed organelles is the hindering factor of investigation, posing a major challenge. Therefore, several approaches aim to overcome this difficulty and develop a better understanding of the primary cilium.

Some of the first attempts to better understand cilia were different genetic studies (Avidor-Reiss *et al.*, 2004; Sun *et al.*, 2004; Pazour, 2004). Comparing genes of cilia-containing organisms to those of non-cilia-containing organisms helped to identify cilia-specific sets of genes (Pazour, 2004). In 2005, in another approach to specifically study the ciliary proteome, *C. reinhardtii* were treated with the toxic reagent dibucaine (Pazour *et al.*, 2005). This treatment separated flagella of *C. reinhardtii* from the rest of the organism. Fractionation was then used to separate ciliary protein fractions from the cytosolic protein fractions for analysis by mass spectrometry (Pazour *et al.*, 2005; Craige *et al.*, 2013). In another hallmark study by Lechtreck *et al.* in 2009, the flagella of *C. reinhardtii* were successfully isolated by applying a pH shock. Subsequently, the conservation of the BBSome was confirmed and the BBSome was identified as an IFT cargo responsible for the specific export of certain proteins (Lechtreck *et al.*, 2009). A few years later, primary cilia were also successfully isolated from cells of the inner medullary collecting duct 3 (IMCD3) of mice using calcium shock (Ishikawa *et al.*, 2012). Subsequent mass spectrometric analysis was able to provide further information about the ciliary proteome (Ishikawa *et al.*, 2012). Even though all of these approaches brought us closer to understanding cilia, they were either too stenous or insensitive. Because of this, the application of the described methods were impractical for daily use.

Despite all of the successes and setbacks, the studies described shed light on the ciliary proteome. In 2015, Mick *et al.* combined ascorbate peroxidase-based proximity labeling (APEX labeling) of primary cilia with comparative mass spectrometric analysis. This study revealed proteins with previously unknown ciliary localization (Wright *et al.*, 2011). Proximity labeling had previously been used to identify non-ciliary protein-protein interactions with success (Firat-Karalar *et al.*, 2014; Lambert *et al.*, 2015; Roux *et al.*, 2012). The transfer of this technology to the isolation of ciliary proteins revolutionized cilia research. The cilia ascorbate peroxidase (cilia APEX) method was developed specifically for labeling ciliary proteins by Mick *et al.* In this method, the peroxidase used to label proteins (APEX) is specifically localized to primary cilia *via* a fragment of the ciliary protein nephrocystin 3 (NPHP3), specifically the amino acids 1 – 200 that encode the ciliary targeting sequence (Mick *et al.*, 2015). The correct localization of the cilia APEX construct can thereby be verified *via* a Green Fluorescent Protein (GFP)-tag. Cilia protein labeling is performed by the addition of biotin tyramide and H<sub>2</sub>O<sub>2</sub> to the Cilia-APEX expressing cell line (Mick *et al.*, 2015). After uptake of biotin tyramide by the cells, the Cilia-APEX fusion protein catalyzes the oxidation of biotin tyramide substrate



in the cilium in the presence of  $H_2O_2$ . Therefore, the corresponding labeling reaction is controlled and initiated by the addition of  $H_2O_2$ . APEX generates biotin tyramide radicals that react with exposed electron-rich amino acids on neighboring proteins and covalently bind biotin to them thereby labeling ciliary proteins with biotin (Rhee *et al.*, 2013). Subsequently, the biotinylated ciliary proteins can be isolated by streptavidin affinity chromatography, which allows subsequent analysis *via* mass spectrometry (MS).

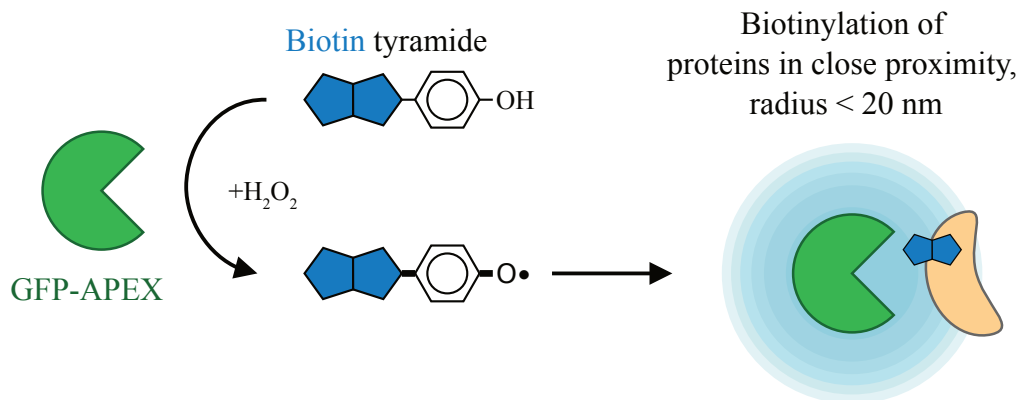


**Fig. 3: Overview of the APEX labeling reaction.**

In the presence of  $H_2O_2$ , APEX generates biotin tyramide radicals that react with exposed electron-rich amino acids on proteins in close proximity (radius < 20 nm). The proteins are biotinylated = labeling. Biotinylation allows isolation and detection by streptavidin (Mick *et al.*, 2015; figure modified after unpublished original from Tommy Sroka)

To ensure the accuracy of this method, a selected set of controls, including a cell line expressing a non-cilia localized peroxidase, is essential. Nevertheless, 162 category one candidate cilia proteins were identified in this study (Mick *et al.*, 2015). Thus, the developed APEX-labeling provides a simple and feasible approach for studying the ciliary proteome in future studies. However, the study was also subject to certain limitations: I.) membrane proteins with known ciliary localization and transition zone components were lacking from the list of identified proteins. Reasons for these difficulties could lie in the high hydrophobicity of these proteins and their hard accessibility in the ciliary membrane. Besides that, Cilia-APEX presumably localizes highly specific to the inner cilium and therefore could fail in labeling TZ proteins II.) low abundance proteins with known ciliary localization, e.g., the ciliary SHH signaling components GPR161 and PTCH1, could not be identified in this study (Mick *et al.*, 2015). Accordingly, increasing the sensitivity of ciliary labeling and subsequent proteomic studies to generate a more accurate picture of the ciliary proteome became a major priority to unravel the puzzle of ciliary signaling. Therefore, the first part of this work aimed to perform initial experiments to improve the sensitivity of APEX labeling and to investigate the SHH components localized in cilia.

### 3.5. Ciliary Signaling – the Sonic Hedgehog Signaling Pathway.

The Hedgehog signaling pathway is one of the most important signaling pathways in embryonic development, as it regulates numerous processes during this phase. The discovery of Hedgehog signaling which originally occurred in the fly model organism *Drosophila melanogaster* significantly improved our understanding of early embryonic development. For this reason, the discovery of the Hedgehog pathway was part of a work that was rewarded with a Nobel Prize in 1995 (Nüsslein–Volhard & Wieschaus, 1980). Disruption of Hedgehog signaling in humans and mammals can lead to early infant death and severe birth defects. These include, for example, neural tube defects such as holoprosencephaly (incomplete separation of the basal forebrain; Roessler *et al.*, 1996), spina bifida (open spine; Goodrich *et al.*, 1997), defective axis patterning and cyclopia (Chiang *et al.*, 1996). In addition, disruption of Hedgehog signaling has been associated with the development and progression of several cancers in adults, e.g., squamous cell carcinoma of the oral cavity (Takabatake *et al.*, 2019), ovarian cancer (Liao *et al.*, 2009), and pancreatic cancer (Feldmann *et al.*, 2008), as well as in children, e.g., medulloblastoma (most common malignant brain tumor in children; Roussel & Hatten, 2011). Today, three mammalian Hedgehog proteins are known, namely Sonic Hedgehog (SHH), Indian Hedgehog and Desert Hedgehog, which bind as ligands to a receptor and thus initiate activation of the signaling pathway. As a result, they form concentration gradients as morphogens that activate the Hedgehog signaling pathway to varying degrees. Although all three Hedgehog proteins are named after different Hedgehog species, they are by no means exclusive to this species. Instead, the three Hedgehog proteins serve as distinct and important functions during embryonic development (Gigante & Caspary 2020). SHH, for example, is essential for the organization of the nervous system (Li *et al.*, 2020). Neural ventral cell fates are determined by gradients of the Sonic morphogen that lead to altered ratios of transcription factors. In this way, SHH target genes are regulated (Niewiadomski *et al.*, 2019). The focus of this work will be on SHH signaling, which will be discussed below.

In *D. melanogaster*, but not in any known mammalian species, SHH signaling occurs independently of primary cilia. Consequently, the importance of the primary cilium for SHH signaling in mammals remained unknown for a long time. First associations between cilia and SHH signaling were established in the early 2000s. At that time, mice with defective IFT172 and IFT88 were studied and it was found that when IFT172 and IFT88 were missing, ventral neural cell fates were lost. Thus, these animals did not form a neural tube (Huangfu *et al.*, 2003). In 2005, Huangfu and Anderson demonstrated that primary cilia are essential for all SHH signaling-dependent actions downstream of the receptor Patched 1 (PTCH1) and the positive effector Smoothed (SMO), two of the major SHH effectors (Huangfu & Anderson, 2005). This confirmed for the first time the importance of primary cilia for SHH signaling in mammals.

SHH signaling is orchestrated by a precise and complex interplay of positive and negative regulators that eventually determine embryonic patterning (Gigante & Caspary 2020; May *et al.*, 2021). In the absence of the Hedgehog ligand Sonic (Fig. 3, left), the signaling pathway is inactive. In this state, the

12-transmembrane receptor PTCH1 localizes to the primary cilium (Rohatgi *et al.*, 2007). The presence of PTCH1 in cilia prevents accumulation of the major SHH effector and GPCR SMO. SMO shuttles in and out of cilia in the SHH inactive state without appreciable accumulation (Kim *et al.*, 2009; Goetz & Anderson, 2010). This prevents the activation of downstream components of the SHH signaling pathway (Gigante & Caspary, 2020). SMO that does not remain in primary cilia is post-translationally modified by addition of ubiquitins and subsequently degraded (Desai *et al.*, 2020). How PTCH1 prevents SMO from accumulating in cilia without interacting directly with it has long been an enigmatic question to answer. Today, it is now known that lipids in the ciliary membrane play a critical role in the regulation of SMO by PTCH1 (Byrne *et al.*, 2016; Luchetti *et al.*, 2016; Kinnebrew *et al.*, 2019). Another GPCR that localizes to primary cilia during non-active signaling is the orphan GPCR GPR161. GPR161 serves two known important functions: I) it serves as an A-kinase anchoring protein (AKAP) for cyclic adenosine monophosphate (cAMP)-dependent protein kinase A (PKA; Bachmann *et al.*, 2016), II) constitutively active GPR161 stimulates adenylyl cyclases (AC), resulting in increased cAMP levels in the cilium. PKA is activated by these elevated cAMP levels (Mukhopadhyay *et al.*, 2013). PKA is a holoenzyme consisting of complexes of the regulator (PKA-R) and catalytic subunits (PKA-C). These sub-complexes bind to each other to abolish kinase activity (Uhler *et al.*, 1986; Uhler *et al.*, 1986; Taylor *et al.*, 2004; Taylor *et al.*, 2005). However, the regulatory subunit  $\alpha$  of PKA (PKA-R $\alpha$ ) binds cAMP with a high affinity. cAMP allosterically inhibits PKA-R $\alpha$  binding to the catalytic subunit PKA-C. Subsequently, high levels of cAMP lead to the release of PKA-C and thus activate kinase activity (Taylor *et al.*, 2006). PKA-C then phosphorylates the transcription factor GLI3 which is a key step in the negative regulation of SHH signaling. Phosphorylation of GLI3 ultimately leads to its cleavage (Niewiadomski *et al.*, 2019). The proteolytic processing of GLI3 results in a truncated repressor (GLI3<sup>R</sup>) for SHH target genes (Niewiadomski *et al.*, 2019). Repression of SHH target genes suppresses ventral cell fates (Gigante & Caspary, 2020).

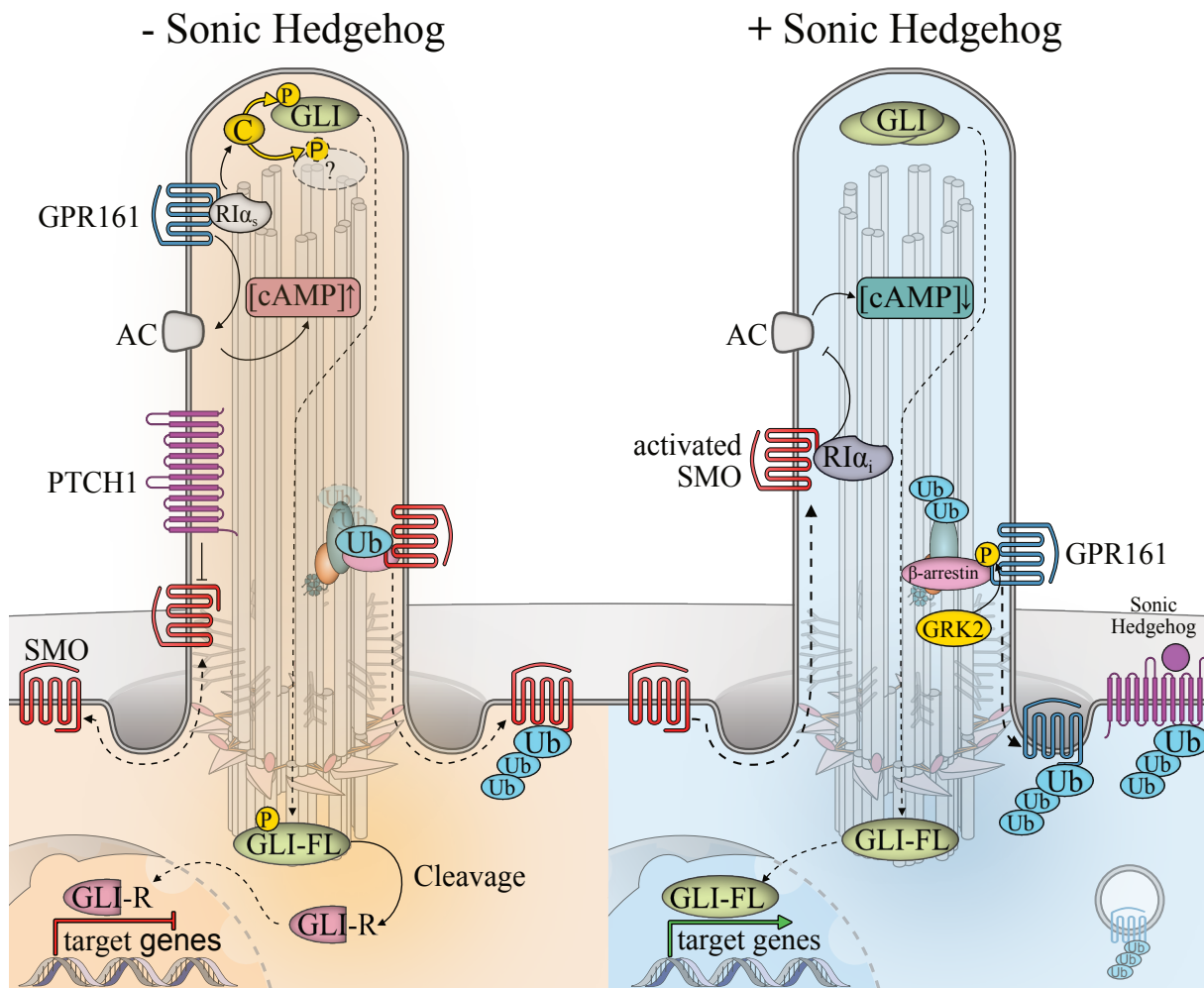


**Fig. 4: The Sonic Hedgehog Signaling Pathway in Mammalian Cells.**

Left side: In absence of the ligand, Sonic localizes the receptor PTCH1 to the primary cilium and prevents SMO accumulation. Active GPR161 induces AC via  $G\alpha_s$  which results in high cAMP levels, thus leading to the phosphorylation with subsequent cleavage of GLI3. SMO is degraded after the addition of ubiquitins.

Right side: In presence of Sonic, PTCH1 is activated through the binding of its ligand. PTCH1 subsequently exits the primary cilium resulting in SMO accumulation. Active SMO inhibits AC via  $G\alpha_i$  and cAMP levels drop. GPR161 is phosphorylated by GRK2, a modification that is sensed by  $\beta$ -arrestins which mediate GPR161 exit. High cAMP levels prevent GLI3 from processing. The GLI3<sup>FL</sup> is retained and activates target genes (modified from May *et al.*, 2021, the original figure was designed and conceptualized by Tommy Sroka).

The presence of the Hedgehog ligand, Sonic activates signal transduction through its initial binding to the receptor PTCH1 (Fig. 3, right panel). After binding, PTCH1 leaves the primary cilium, resulting in retention of SMO (Gigante & Caspary, 2020). GPCR kinase 2 (GRK2) then phosphorylates the C-tail of GPR161 (Bachmann *et al.*, 2016; Pal *et al.*, 2016). This modification is sensed by  $\beta$ -arrestins, particularly  $\beta$ -arrestin 2, which mediates the removal of GPR161 (Pal *et al.*, 2016). Interestingly, SMO and GPR161 are different types of GPCRs and differ in their specific function. While SMO activates  $G\alpha_i$ -proteins, GPR161 activates  $G\alpha_s$  proteins (Ayers & Thérond, 2010). Consequently, the tonically active GPR161 stimulates adenylyl cyclases, while these are inhibited when active SMO replaces

GPR161 in primary cilia. The change in the ciliary proteome results in a decrease in cAMP levels (Mukhopadhyay *et al.*, 2013). Although this mechanism of subsequent decrease in PKA activity is a compelling and logical idea, it needs further explanation. This is because PKA-C has not been yet detected in the cilium beyond doubt, and is usually localized at the base of the cilium (Barzi *et al.*, 2010). When PKA-dependent phosphorylation of GLI3 is abrogated, this leads to a termination of proteolytic processing. The transcription factor now acts as its full-length version (GLI3<sup>FL</sup>). This mechanism results in the activation of SHH target genes. Subsequently, other GLI transcription factors are activated and act on target genes. Upon active SHH signaling, ventral cell fates are induced (Niewiadomski *et al.*, 2019).

Understanding SHH signaling regulation has been, and continues to be, the subject of extensive research and the mechanisms described here only partially reveal the complexity of SHH signaling. For these reasons, many questions about the regulation of SHH signaling remain unanswered. For example, it remains unclear how the changes in the ciliary membrane that enable PTCH1 regulation of SMO are achieved. In addition, the regulation of PKA via GPR161 as its dynamics continue to raise questions. SHH signaling regulates highly complex mechanisms within embryonic development and needs to be regulated down to the finest differences. How exactly this essential fine-tuning takes place remains to be another unanswered question.

### 3.6. Objectives of this work

The existing cilia APEX approach provided novel information about the primary cilium proteome (Mick *et al.*, 2015). Despite the achieved results, the method contained some weaknesses which were discussed above. Improved sensitivity of Cilia-APEX could overcome the described limitations and enable the studying of unknown protein dynamics. Consequently, this work aimed to establish and apply the improved Cilia-APEX2 approach to enlighten our understanding of the ciliary proteome (May *et al.*, 2021). In this context, SHH signaling dynamics were investigated and the putative phosphatase Paladin 1 (PALD1) was linked to SHH signaling for the first time. PALD1 has not previously been associated with the SHH signaling pathway. Accordingly, the assumption that a fine regulator of the SHH signaling pathway had been identified was already made at the beginning. These fine regulators can control the precise tuning of the SHH signaling pathway and thus allow minute changes (Zhou *et al.*, 2006; Ma *et al.*, 2019). If these so-called mediators could be identified and understood, this would open up numerous possibilities for new therapeutic approaches that might reduce the danger of undesirable negative effects (Li *et al.*, 2012; Wu *et al.*, 2017; Bufalieri *et al.*, 2017). Consequently, the second aim of this work was to understand and describe the role of PALD1 in SHH signaling. The exact function of PALD1 should not only be investigated in the IMCD3 cell line in which the protein was identified. Instead, tissue and cell type specific influences were included in the analysis. This work further aimed to understand, the molecular mechanisms underlying the regulation of PALD1 and identify proteins that could be regulated by PALD1.

## 4. Material

### 4.1. Antibodies

**Tab. 1: Primary antibodies**

Anti-body	Manufacturer	Order number	Species	Dilution
anti-Ac-tub	Sigma Aldrich (Merck KgaA)	T7541	mouse	IF: 1:2000
anti-ARL13b	ProteinTech Group	17711-1-AP	rabbit	IF: 1:2000
anti-IFT88	ProteinTech Group	12967-1-AP	rabbit	IF: 200 WB: 1:1000
GFP anti-6His- tagged eGFP	Self-made	n.a.	rabbit	WB: 1:1000
anti-GPR161	gift from S. Mukhopadhyay	n.a.	rabbit	IF: 1:250
anti-GLI3	R&D Systems	AF3690	goat	WB: 1:1000
anti-Actin	Self-made	n.a.	rabbit	WB: 1:5000
anti-GAPDH	ProteinTech Group	60004-1-Ig	mouse	WB:1:3000
anti-PALD1	Sigma Aldrich (Merck KgaA)	HPA017343	rabbit	IF: 1:250 WB: 1:1000
anti-SMO	Santa Cruz Biotechnology	Sc-166685	mouse IgG2a	IF: 1:250
anti-SMO	Abcam	ab236456	mouse IgG2a	IF: 1:250
anti-PTCH1	Abcam	ab53715	rabbit	WB: 1:1000
anti-CEP164	gift from T. Stearns	n.a.	rabbit	1:6000
Streptavidin pHRP	Thermo Fisher Scientific Inc.	#21140	n.a.	WB: 1:1000
Streptavidin AF647	Invitrogen	S21374	n.a.	IF: 1:1000
anti-Myosin	Sigma Aldrich (Merck KgaA)	M1570	mouse IgG2b	WB:1:1000

**Tab. 2: Secondary antibodies & Dyes**

Anti-body	Manufacturer	Order number	Species	Dilution	Dye
anti-mouse IgG2a	Jackson ImmunoResearch	115-545-206	goat	IF: 1:500	AlexaFluor 488
anti-rabbit	Jackson ImmunoResearch	115-165-207	goat	IF: 1:500	Cy3
anti-mouse IgG2b	Jackson ImmunoResearch	115-547-287	goat	IF: 1:500	Cy5
anti-goat	Li-COR Biosciences GmbH	926-32214	donkey	WB: 1:15000	IRDye 800
anti-rabbit	Li-COR Biosciences GmbH	926-32213	donkey	WB: 1:20000	IRDye 800
anti-mouse	Li-COR Biosciences GmbH	926-32212	donkey	WB: 1:20000	IRDye 680

## 4.2. Bacteria

**Tab. 3: Bacterial strains**

Bacterial strain	Genotype	Reference
<i>Escherichia Coli</i> Mach1 T1r	F <sup>-</sup> $\phi$ 80lacZ $\Delta$ M15 $\Delta$ lacX74 <i>hsdR</i> (r <sub>k</sub> <sup>-</sup> , m <sub>k</sub> <sup>+</sup> ) $\Delta$ <i>recA</i> 1398 <i>endA</i> 1 <i>tonA</i>	Thermo Fisher Scientific

## 4.3. Buffer & Solutions

### Antibiotics

Ampicillin:

c<sub>final</sub>: 100  $\mu$ g/ml; Stock diluted in dH<sub>2</sub>O

Kanamycin:

c<sub>final</sub>: 50  $\mu$ g/ml; Stock diluted in dH<sub>2</sub>O



### *Bacterial cultivation*

Lysogeny Broth (LB)- Agar:	1.6% (w/v) LB-Agar in LB-Medium
LB- Media:	1% (w/v) Tryptone; 0.5% (w/v) Yeast extract; 0.5% (w/v) NaCl

### *Biotin*

Biotin-tyramide:	$c_{\text{final}}$ : 0.5mM, Stock diluted in DMSO
------------------	---

### *Bis-Tris Gels*

10% Separation gel:	10% (v/v) Acrylamide, 0.3M Bis Tris in dH <sub>2</sub> O
4.5% Stacking gel:	4.5% Acrylamide, 4.5% 1M Bis Tris in H <sub>2</sub> O dest.

### *Blocking Buffers*

Blocking Buffer Immunofluorescence:	5% (v/v) FBS, 3% (w/v) BSA in 1x PBS
Blocking Buffer Western Blot:	5% (w/v) milk Intercept in 1x PBS
Intercept LiCOR Blocking Solution:	100% or 50% (v/v) in TBS

### *Fixation*

Paraformaldehyde (PFA):	4% PFA (v/v) in 1x PBS
Methanol (MetOH):	100% (v/v) MetOH p.a.

### *Ligation*

10X T4 DNA ligase buffer:	
---------------------------	--

### *Membrane Stains*

Ponceau S:	0.5% (w/v) Ponceau S, 1% (v/v) Acetic acid in H <sub>2</sub> O dest.
------------	---

### *Phosphate buffered Saline (PBS)*

PBS (10x):	27mM KCl; 18mM KH <sub>2</sub> PO <sub>4</sub> ; 1369mM NaCl; 81mM Na <sub>2</sub> HPO <sub>4</sub> x 2 H <sub>2</sub> O; H <sub>2</sub> O dest.; pH <sub>final</sub> = 7.4
------------	---

*Protease inhibitors*

Complete EDTA-free Roche: 1 tablet in 1ml dH<sub>2</sub>O  
PMSF: 200mM PMSF in 100% (v/v) EtOH p.a.

*Running buffer*

3-MOPS Buffer: 0.5M MOPS, 0.05M Tris, 1% (w/v) SDS,  
10.25mM EDTA

Sample buffer: 4% (w/v) SDS; 20% (v/v) Glycerol;  
120mM Tris , 0.02% (v/v) Bromphenolblue  
100mM DTT

*Sample buffers*

Laemmli buffer: 10% (w/v) SDS; 300mM Tris-HCl pH = 6.8;  
50% (v/v) Glycerol;  
0.05% (w/v) Bromphenolblue

*Solubilization buffers*

Lysis buffer: 25mM Tris/HCl, 300mM CaCl,  
1mM EDTA, 10% (v/v) Glycerol,  
1% Triton X-100 (v/v),  
0.1 % SDS (w/v), 1mM PMSF, proteins  
inhibitors Complete EDTA-free Roche

Lysis buffer APEX: 600mM NaCl; 200mM Tris-HCl; 20mM  
Sodium ascorbate; 20mM sodium azide;  
10mM Trolox; 20% (v/v) Glycerol in  
H<sub>2</sub>O dest.

*Tris-buffered Saline (TBS)*

TBS (25x): 0.5M Tris-HCl; 3.12M NaCl;  
H<sub>2</sub>O dest. pH = 7.4

TBS-T: 0.05 % (v/v)Tween in 1 x TBS

*Transfer buffers*

Tank Blot buffer:

96mM Glycin; 12.4mM Tris; 10% (v/v) EtOH

*Quenching buffers*

APEX Labeling:

10mM Sodium Ascorbate;  
10mM Sodium Azide; 0.5mM Trolox  
in 1x PBS (sterile)

#### 4.4. Cells & Consumables

**Tab. 4: Cell lines**

Cell line	Parental	Species	Cell type	Reference
Cilia-PKI	IMCD3 FlipIN	mouse	Inner Medullary Collecting Duct	Mick <i>et al.</i> , 2015
Control-PKI	IMCD3 FlipIN	mouse	Inner Medullary Collecting Duct	Mick <i>et al.</i> , 2015
3T3	n.a.	mouse	Immortalized Embryonic Fibroblasts	Todaro & Green, 1963
C2C12	n.a.	mouse	Myoblasts	Blau <i>et al.</i> , 1985
Cilia-APEX	IMCD3 FlipIN	mouse	Inner Medullary Collecting Duct	Mick <i>et al.</i> , 2015
Cilia-APEX2	IMCD3 FlipIN	mouse	Inner Medullary Collecting Duct	May <i>et al.</i> , 2021
Control-APEX	IMCD3 FlipIN	mouse	Inner Medullary Collecting Duct	Mick <i>et al.</i> , 2015
Control-APEX2	IMCD3 FlipIN	mouse	Inner Medullary Collecting Duct	May <i>et al.</i> , 2021
EcR-ShhN	HEK	human	Human Embryonic Kidney	ATCC: JHU-65
HEK293T	n.a.	human	Human Embryonic Kidney	Stroud <i>et al.</i> , 2016
IMCD3 FlipIN	n.a.	mouse	Inner Medullary Collecting Duct	Rauchmann <i>et al.</i> , 1993; Mukhopadhyay <i>et al.</i> , 2013
IMCD3 <i>Ift27<sup>-/-</sup></i>	IMCD3 FlipIN	mouse	Inner Medullary Collecting Duct	Keady <i>et al.</i> , 2012
IMCD3 <i><math>\beta</math>-Arr1/2<sup>-/-</sup></i>	IMCD3 FlipIN	mouse	Inner Medullary Collecting Duct	Ye <i>et al.</i> , 2018
IMCD3 <i>Tulp3<sup>-/-</sup></i>	IMCD3 FlipIN	mouse	Inner Medullary Collecting Duct	Ye <i>et al.</i> , 2018
MIN6 $\beta$	n.a.	mouse	Pancreatic $\beta$ cell line	Poitout <i>et al.</i> , 1995
3T3 <i>Pald1<sup>-/-</sup></i>	3T3	mouse	Immortalized embryonic fibroblasts	May <i>et al.</i> , 2021, this work
C2C12 <i>Pald1<sup>-/-</sup></i>	C2C12	mouse	Myoblasts	This work
IMCD3 <i>Pald1<sup>-/-</sup></i>	IMCD3 FlipIN	mouse	Inner Medullary Collecting Duct	May <i>et al.</i> , 2021, this work
RPE1-hTERT	n.a.	human	Retinal Pigment Epithelium	Bodnar <i>et al.</i> , 1998
IMCD3 SStr3 <sup>NG</sup>	IMCD3 FlipIN	mouse	Inner Medullary Collecting Duct	Nager <i>et al.</i> , 2017

**Tab. 5: List of consumables**

Consumable	Manufacturer	Order/reference number
6-well plate	Greiner Bio-One International GmbH	657160
12-well plate	Greiner Bio-One International GmbH	665180
24-well plate	Greiner Bio-One International GmbH	662160
48-well plate	Greiner Bio-One International GmbH	677180
96-well plate	Greiner Bio-One International GmbH	10101852
10 cm dish	Greiner Bio-One International GmbH	628160
15 cm dish	Greiner Bio-One International GmbH	639160
Blotting Paper MN 218 B	Machery & Nagel	742111
Cover slips 12 mm #1.5	Thermo Fisher Scientific Inc.	11846933
Cryo tube	Greiner Bio-One International GmbH	122263
Disposable Cell Lifter	Fisherbrand /Thermo Fisher Scientific Inc.	08-100-240
FACS tube	Becton Dickinson GmbH	8003562
Falcon tube 15 ml	Greiner Bio-One International GmbH	10384601
Falcon tube 50 ml	Greiner Bio-One International GmbH	227261
Filter 0.22 µm	Sarstedt AG & Co. KG	83.1826.001
Inoculation loop	Sarstedt AG & Co. KG	86.1562.050
Serological pipette 50 ml	Brand GmbH + Co KG, Sarstedt AG & Co. KG	86.1256.001
Serological pipette 25 ml	Brand GmbH + Co KG, Sarstedt AG & Co. KG	86.1685.001
Serological pipette 10 ml	Brand GmbH + Co KG, Sarstedt AG & Co. KG	86.1254.001
Serological pipette 5 ml	Brand GmbH + Co KG, Sarstedt AG & Co. KG	86.1253.001
Leica Dmi8 with PlanApochromat objectives	Leica Microsystems AG	n.a.
Nitrocellulose membrane	GE Healthcare Amersham	15269794

## 4.5. Kits

**Tab. 6: Kits used within this work**

Kit name	Manufacturer	Order number
Gateway LR clonase II Enzyme mix	Thermo Fisher Scientific Inc.	11791100
Machery & Nagel NucleoBond Xtra Midi prep kit	Thermo Fisher Scientific Inc.	12798402
Monarch Plasmid MiniPrep Kit	New England Biolabs (NEB) GmbH	T1010L
RNeasy mini Kit	Qiagen N.V.	74104

#### 4.6. Culture media & media supplement

**Tab. 7: Culture media & media supplement**

Medium/supplement	Manufacturer	Order number	Application
Ampicillin sodium salt	Carl Roth GmbH + Co. KG	HP62.1	Bacterial cultivation
Bacto Agar	BD Biosciences	214010	Production of LB-Media, cultivation of bacteria
Bambanker	Fujifilm Wako Chemicals U.S.S. Cooperation	302-14681	Storage of mammalian cell lines at -80°C
Difco Yeast Nitrogen Base Amino Acids	BD Biosciences	291920	Production of LB-Media, cultivation of bacteria
Differentiation Medium	Thermo Fisher Scientific Inc.	11594486	Differentiation of myoblasts into muscle cells, DMEM containing 0.2% (v/v) horse serum
Dulbecco's Modified Eagle Medium (DMEM)	Thermo Fisher Scientific Inc.	11594486	Cultivation of all cell lines except IMCD3s
Dulbecco's Modified Eagle Medium Nutrient Mixture F-12 (DMEM F-12)	Thermo Fisher Scientific Inc.	11594426	Cultivation of IMCD3 cell lines
Fetal Bovine Calf Serum (FBS)	Thermo Fisher Scientific Inc.	11573397	Supplement for cell culture medium
Gibco Horse Serum (HS), New Zealand origin	Thermo Fisher Scientific Inc.	11520516	Supplement for cell differentiation medium
Growth Medium	Thermo Fisher Scientific Inc.	n.a.	For all HEK, 3T3 or C2C12 derived cell lines DMEM + 10% (v/v) FBS; for all IMCD3 derived cell lines DMEM F-12 + 10% (v/v) FBS
Kanamycin sulfate	Thermo Fisher Scientific Inc.	11578676	Cultivation of cells during and after FACS sorting
LB-Medium	Self-made	n.a.	Culture of bacterial cells
Opti-MEM Reduced Serum Medium	Thermo Fisher Scientific Inc.	31985062	Transfection of cells
Penicillin -Streptomycin (Pen-Strep)	Thermo Fisher Scientific Inc.	11528876	Cultivation of cells during and after FACS sorting
Starvation Medium	Thermo Fisher Scientific Inc.	n.a.	DMEM or DMEM-F12 containing 0.2% (v/v) FBS

## 4.7. Laboratory equipment

**Tab. 8: List of equipment**

Equipment	Manufacturer
Bacterial incubator Exotron	Infors HT AG
CellXpert C170 cell incubator	Eppendorf AG
Cell incubator Heracell 150i	Thermo Fisher Scientific Inc.
Centrifuge 5424 R	Eppendorf AG
Centrifuge 5427 R	Eppendorf AG
Centrifuge 5804 R	Eppendorf AG
Centrifuge Heraeus Megafuge 16R	Thermo Fisher Scientific Inc.
Centrifuge MySPIN12	Thermo Fisher Scientific Inc.
Clean bench	Heraeus Instruments
Clean bench SAFE 2020	Thermo Fisher Scientific Inc.
Counting chamber acc. to Neubauer	Hirschmann Laborgeräte GmbH & Co. KG
Electrophoresis Mini-PROTEAN Tetra Vertical Electrophoresis Cell Gel chamber	Bio-Rad Laboratories, Inc.
Foam Pad	Sigma Aldrich (Merck KgaA)
Gel imager 600	GE Healthcare
Leica Dmi8 Plan Apochromat oil objective 63x 1.4. NA	Leica Microsystems
LI-COR Odyssey laser scanner	LI-COR Biosciences
Light Microscope Leica DMIL	Leica Microsystems
Microscope slides	Rogo-Sampiac France - matériel de laboratoire
Magnetic stirrer	Thermo Fisher Scientific Inc.
neoVAQ-Maxi suction device adjustable with filling level control	Neolab Migge GmbH
Tecan Reader SPARK 10M	Tecan Group AG
Thermo Mixer HC	Starlab International GmbH
Roller RS-TR05	Phoenix Instruments GmbH
VortexGenie2	Scientific Industries
Water bath Isotemp GPD 20	Thermo Fisher Scientific Inc.



## 4.8. Cloning

**Tab. 9: Oligonucleotides**

Name	Sequence
oPald1_gRNA_fw	CACCGGGTCCTGCAGAACTCCAGA
oPald1_gRNA_rev	AAACTCTGGAGTTTCTGCAGGACCC
oPald1_gSeq_fw	GTCAGGATCCCATCACCGAGAAGATGGACATA
oPald1_gSeq_rev	GTCAAAGCTTTTTCTGTTCTGAAGTTCCAGGC

**Tab. 10: Plasmids**

Name	Application	Reference
pCRISPR-Pald1-GFP	Generation of <i>Pald1</i> knock-out cell lines	May <i>et al.</i> , 2021
pDaM181	Cilia-APEX2	May <i>et al.</i> , 2021
pSPCas9(BB)-2A-GFP	CRISPR Cas9 + GFP encoding plasmid	Ran <i>et al.</i> , 2017

## 4.11. Reagents

**Tab. 11: List of reagents**

Reagent	Manufacturer	Order/reference number
2-Mercaptoethanol	Sigma Aldrich (Merck KgaA)	M-6250
2-Propanol	Sigma Aldrich (Merck KgaA)	34863-2.5L
Acrylamid	Carl Roth GmbH + Co. KG	7906.2
Ammoniumperoxodisulfat (APS)	Grüssing GmbH	700478
Biotin tyramide	Iris Biotech	LS-3500.1000
Bis-Tris	Carl Roth GmbH + Co. KG	9140.3
Bradford Reagent ROTIQuant	Carl Roth GmbH + Co. KG	K015.1
Bromphenol blue	Carl Roth GmbH + Co. KG	B5525-10G
Bovine Serumalbumin (BSA)	Sigma Aldrich (Merck KgaA)	3737.3
Complete EDTA-free	F. Hoffmann-La Roche AG	5056489001
Coomassie-Brillant Blue G	Carl Roth GmbH + Co. KG	17524.02
Cyclopamine	Merck Millipore (Merck KgaA)	#239806
Difco Yeast Nitrogen Base Amino Acids	BD Biosciences	291920
Dimethylsulfoxid	Carl Roth GmbH + Co. KG	A994.2
Ethylendiametetraacetic acid (EDTA)	Carl Roth GmbH + Co. KG	8043.2
Ethanol	Biesterfeld Spezialchemie	702543
Ethanol absolute	Thermo Fisher Scientific Inc.	UN1170
Fluoromount G	Electron Microscopy Sciences	15586276
FuGene HD Transfection Reagent	Promega	E2691
Formaldehyde, methanol-free ultra pure	Polysciences, Inc.	18814-20
Glycerol	Sigma Aldrich (Merck KgaA)	67757-1L
HEPES	Carl Roth GmbH + Co. KG	9105.3
Hoechst 33342. trihydrochloride	Invitrogen AG	1154876
Hydrogen peroxide	Sigma Aldrich (Merck KgaA)	H1009-100ML

Reagent	Manufacturer	Order/reference number
Intercept TBS Protein free blocking buffer	Li-COR Biosciences	927-80003
Lipofectamine 3000	Thermo Fisher Scientific Inc.	15212475
Milk powder	Sucofin	n.a.
Methanol	Biesterfeld Spezialchemie	701224
MOPS	Carl Roth GmbH + Co. KG	69+9.3
Sodium chloride	Grüssing GmbH	703009
Gibco PBS (cell culture), pH 7.2	Thermo Fisher Scientific Inc.	11530546
Page ruler plus	Thermo Fisher Scientific Inc.	815-968-0747
peqGOLD Universal Agarose	PEQLAB Biotechnologie GmbH	35-1020
Ponceau S	Serva Electrophoresis GmbH	33429
Potassiumhydrogenphosphate	Carl Roth GmbH + Co. KG	7758-11-4
Proteaseinhibitor PMSF	Carl Roth GmbH + Co. KG	6367.2
Protein standard	Bio-Rad Laboratories, Inc	500005
Roti-Mount FluorCare DAPI	Carl Roth GmbH + Co. KG	HP20.1
Roti-Quant	Carl Roth GmbH + Co. KG	K015.1
Sodium dodecyl sulfate	Central chemical storage Uds	80294
Sonic conditioned cell medium, N-terminus of Shh-N	Self-made	n.a.
Somatostatin	Alfa Aesar	J66168
TEMED	Sigma Aldrich Corp.	2367.1
Trypsin-EDTA (0.25%) phenol red	Thermo Fisher Scientific Inc.	25200056
Triton X-100	Sigma Aldrich Corp.	X100-500ML
Tween-20	Carl Roth GmbH + Co. KG	9127.2

## 4.12. Software & clouds

**Tab. 12: List of used software & cloud systems**

Name	Manufacturer/ reference	Version	Application
Affinity Designer	Serif Ltd	1.9.2.	Conceptualization and design of all figures
Affinity Publisher	Serif Ltd	1.9.2.	Writing and design of this thesis
Benchling [Biology Software]	Benchling	2021 retrieved from <a href="https://benchling.com">https://benchling.com</a>	Design of plasmids
Chopchop	Labun <i>et al.</i> , 2019, Labun <i>et al.</i> , 2016, Montague <i>et al.</i> , 2014	2018 retrieved from <a href="https://chopchop.cbu.uib.no">https://chopchop.cbu.uib.no</a>	Design of sgRNA for CRISPR knock outa
Fiji (ImageJ)	Open source	2.1.0/1.53c	Preparation of IF & WB images, quantification of IFs
GraphPad Prism	GraphPad Software Inc.	9.1.0 (216)	Statistics
InterPro	Blum <i>et al.</i> , 2020	83.0	Protein predictions
Image Studio Lite	Li-COR Biosciences	5.2.5	Quantification of WB
Leica Camera System	Leica Microsystems	DFC3000	Documentation of fixed images
Leica Application Suite	Leica Microsystems	3.7.0.20979	Imaging of microscope slides
Microsoft Office	2018 Microsoft	16.16.5	Calculation, data organization (Excel), writing of text passages (word), communication (outlook, teams)
NMT predictors	Bologna <i>et al.</i> , 2004	2021 retrieved from <a href="https://mendel.imp.ac.at/myristate/SUPLpredictor.htm">https://mendel.imp.ac.at/myristate/SUPLpredictor.htm</a>	Protein predictions

## 5. Methods

### 5.1. Sequence analysis

To predict PALD1 domains, the sequence was analyzed using the InterPro 83.9 tool available online and N-terminal myristoylation (NMT) sites predictors (Bologna *et al.*, 2004; Maurer-Stroh *et al.*, 2002). Based on these predictions, a possible domain map of PALD1 was designed.

### 5.2. Phylogenetic Analysis via Gene Clime

Phylogenetic analysis of *Pald1* was performed using the Gene Clime analysis tool available online (derived from gene-clime.org). The algorithm, Gene Clime, analyzes gene sequences and clusters them into evolutionary conserved modules (ECMs), based on homologies according to the bayesian hidden Markov tree model (Li *et al.*, 2018). Based on this analysis, a phylogenetic tree was created (Li *et al.*, 2014; Li *et al.*, 2018). For this purpose, in addition to the analysis with Gene Clime, for the species *Batrachochytrium dendrobatididis*, *Chlorella spirulina* and *Emiliana huxleyi*, nucleotide blasts were performed. Hits with an E-value of less than or equal to  $10^{-25}$  were considered hits.

### 5.3. Bacterial transformation

For transformation of DNA in *E. coli*, 50µl of the chemically competent *E. coli* strain Mach1 T1r was thawed on ice. Then 1 – 5µl DNA were added to the bacteria and the mix was incubated on ice for 30min. Bacterial cells were subjected to a heat shock at 42° C for 45s and incubated again on ice for 10min. After subsequent addition of 500µl of LB-medium without antibiotics, the cells were grown for 1h at 37° C and 800RPM in a thermo mix. LB Plates containing the appropriate antibiotics were dried at 37° C during bacterial transformation. After 1h of growth of bacterial cells, they were seeded on the prepared Agar plates using a Drigalski-spatula and incubated over night at 37° C.

### 5.4. Bacterial overnight cultures

To amplify the generated plasmids in *E. coli*, overnight cultures were prepared. For this purpose, the target plasmid was first transformed in *E. coli* (see 5.3. Bacterial transformation). Then, a clone was picked using an inoculation loop and transferred into 5ml LB medium containing appropriate antibiotics. The bacteria was incubated overnight at 37° C and 250RPM to allow for optimal growth. After 8 – 12h, during the end of the exponential growth phase, cells were harvested for plasmid preparation. The Monarch Plasmid MiniPrep Kit was used for this purpose and the preparation was carried out according to the corresponding user manual. For Midi-Preps, pre-cultures were generated in 5ml LB medium with respective antibiotics as described. After 8h, 1ml of the pre-culture was transferred into 100ml LB-Medium and incubated overnight as described above for 5ml bacterial cultures. Midi-preps were performed using the Machery & Nagel NucleoBond Xtra Midi prep kit. DNA preparation was performed according to the corresponding the user manual.

## 5.5. Cell lines

### 5.5.1. Inner Medullary Collecting Duct 3 (IMCD3) cells

In 1993, cells from an SV40 (large T antigen) carrying transgenic mouse were isolated. Isolation was performed from the terminal third of the collecting tube of the murine kidney. The cells obtained were successfully cultured and named after their origin from the Inner Medullary Collecting Tube (IMCD3), where 3 indicates the clone number. The cell line exhibits some characteristic features of a renal epithelial cells such as high transepithelial resistance and survival in highly osmotic environments, as found physiological in the kidney (Rauchman *et al.*, 1993). Within this IMCD3 cell line, an FRT site was introduced, in which specific gene sequences could be inserted. Accordingly, the cell line used in the following experiments and all IMCD3 derived cell lines are IMCD3 FlipIN cells, which will be referred to as IMCD3 for simplicity in the following text (Mukhopadhyay *et al.*, 2010).

### 5.5.2. 3T3 Immortalized Fibroblasts

As early as 1963, the first 3T3 cell line was established, in which 17 to 19 day old Swiss mouse embryonic fibroblasts were isolated and cultured. As part of their establishment, the cells were subjected to a strict transfer protocol in which they were transferred every 3 days and seeded at the same cell density (Todaro & Green, 1963). This immortalization procedure is eponymous for the 3T3 cell line, which is widely used in experimental research today. In particular, studies investigating SHH signaling are often performed on 3T3 cells (Breslow *et al.*, 2018; Pusapati *et al.*, 2018).

### 5.5.3. C2C12 Myoblasts

Myoblasts have the ability to recognize other myoblasts. As a result, they can spontaneously fuse with each other to form a myotube. The formed differentiated myotube possess multiple nuclei, and is subsequently called a heterokaryon. Differentiated myoblasts lose the ability to divide or synthesize DNA. Instead, the resulting heterokarya produce large amounts of muscle proteins (Blau *et al.*, 1968). The C2C12 myoblast is a diploid subclone originally obtained by Yaffe (Yaffe, 1968). After karyotyping, the cells were selected for their ability to rapidly differentiate into myotubes and for expressing the characteristic muscle proteins. In 1968, the C2C12 subclone was analyzed and established by Helen Blau (Blau *et al.*, 1968). The C2C12 cell line used within this work was kindly provided by Prof. Dr. Dagmar Wachten from the Institute of Innate Immunity from the University of Bonn.

## 5.6. Cell culture

All cell lines were cultivated in cell incubators with 5% CO<sub>2</sub> at 37°C. Depending on the cell line, cultivation was performed using DMEM with 10% FBS or DMEM F-12 with 10% FBS for all IMCD3 derived cell lines. 10cm cell culture plastic dishes were used for culturing the respective cell lines. Unless otherwise indicated, all cells were cultured in the absence of antibiotics. For experiments, cells were counted using a Neubauer counting chamber, fixed cell numbers were seeded as indicated in the description of the corresponding experiments. To induce ciliation, growth medium was removed, cells

were washed with 1 x cell culture PBS, and growth factor reduced culture medium (DMEM containing 0.2% FBS or DMEM-F12 containing 0.2% FBS) was added. For some experiments, cell seeding and division of cells was carried out with technical support by Nicola Byers according to the instructions described above. For long term-storage, cell lines were pelleted and resuspended in bambanker storage medium. The corresponding cell aliquots were frozen at -80° C until use.

### **5.7. APEX Labeling**

Ciliary APEX labeling was established in 2015 to study the proteome of the primary cilium (Mick *et al.*, 2015). Within this work, an IMCD3 cell line was used in which either the ascorbate peroxidase (APEX) or the improved ascorbate peroxidase (APEX2) were targeted to the primary cilium (Cilia-APEX/Cilia-APEX2). The respective cell line was incubated in presence of 0.5mM biotin tyramide for 30min in a cell incubator at 37°C and 5% CO<sub>2</sub>. Thereafter, the cells were labeled by the presence of 1mM H<sub>2</sub>O<sub>2</sub> for 2min at room temperature (RT). Due to cell toxicity of H<sub>2</sub>O<sub>2</sub>, timing of labeling is essential for this experimental approach. After incubation, the medium was quickly aspirated and the cells were quickly washed with APEX quenching buffer (see 4.3. buffers & solutions). Washing was repeated three times with two wash steps of approximately 5min each. Cells can then either be fixed with 4% PFA and MetOH for Immunofluorescence (IF) experiments or processed into lysates for subsequent Western Blot (WB) analysis. As a labeling control, the parental cell line, without the Cilia-APEX/Cilia-APEX2 construct was used.

### **5.8. Sonic conditioned-medium**

Different approaches can be chosen for hedgehog signaling assays, as described (see 5.9. Sonic Hedgehog Signaling Assay) e.g. induction can be executed with the ligand of PTCH1, Sonic. To induce cells with Sonic, Sonic Conditioned Medium was prepared. This Sonic conditioned medium consists of cell supernatant that contains the N-terminus of Sonic (Shh-N) which is secreted in the medium by a specialized HEK derived cell line (EcR-ShhN). The conditioned medium can be harvested and used to stimulate the cells to elicit the desired SHH response. After recovery from thawing (one week or longer), the EcR-ShhN cells were split in a 15cm cell culture dish. EcR-ShhN cells were maintained at approximately 80% confluency throughout the process. From 80% confluency, cells were split into five new plates and left at 37° C and 5% CO<sub>2</sub> for two days. Cell density was checked each day to prevent cells from growing too densely, which leads to detachment from the surface. On the third day, the growth medium was carefully changed to DMEM containing 2% FBS. Since the cells detached easily, no PBS washing step was performed. After 48h of incubation at 37° C and 5% CO<sub>2</sub>, the medium was harvested, filtered through 0.22µm and stored at -20° C until use. Each batch of Shh-N conditioned medium must be tested to determine the concentration sufficient to induce a significant SHH response (usually 10 – 16% v/v Shh-N per culture medium). This concentration was determined by IF microscopy by observing SMO accumulation in primary cilia. In parallel with the production of Shh-N, HEK293T cells were treated accordingly to produce control medium, as HEK293T cells do not secrete Shh-N in the surrounding medium.

### **5.9. Sonic Hedgehog Signaling Assays**

Cells were seeded at the desired format two days prior to the experiment (see 5.10. Immunofluorescence (IF) Microscopy or 5.13. Quantitative Fluorescence Western Blot (qWB) Analysis). After 24h, ciliation was induced as described above (see 5.6. Cell culture). When cilia formation was induced, cells were also treated with SHH inducing, or blocking, reagents or vehicle. For induction with Shh-N, the starvation medium was supplemented with 10 % – 16 % Shh-N or control medium. For induction with SMO Antagonist (SAG), cells were treated with 200nM SAG or vehicle DMSO. To block the signaling pathway, cells were treated with 10 $\mu$ M cyclopamine (CYC) or vehicle MetOH. Treatments were performed for 24h or at the indicated time points. After the subsequent time, cells were either fixed for immunofluorescence microscopy (see 5.10. Immunofluorescence (IF) Microscopy) or harvested as lysates for quantitative fluorescence Western blot analysis (see 5.13. Quantitative Fluorescence Western Blot Analysis).

### **5.10. Immunofluorescence (IF) Microscopy**

Immunofluorescence (IF) microscopy was performed to examine the localization of target proteins, ciliation rates, cilia length and shape. For this purpose, 50,000 cells were seeded on 12mm #1.5 coverslips two days prior to the experiment. After 24h of growth phase, ciliation was induced and cells were grown for an additional 24h as described (see 5.6. Cell culture). In addition, cells were treated with additional reagents during starvation, if necessary (see 5.9. Sonic Hedgehog Signaling Assays and 5.7. APEX Labeling). Subsequently, cells were fixed with 4% PFA for 10 – 15min. For APEX labeling experiments, cells were additionally fixed with MetOH for 5min at -20° C. After fixation, cells were either stored in 1 x PBS at 4° C until experimentation or processed directly for IF. After MetOH fixation, cells were washed extensively with 1 x PBS for at least 30min to rehydrate coverslips and allow antibody binding. On the day of the experiment, cells fixed exclusively with 4% PFA were also treated with 0.2% Triton-X 100 (TrX-100) for 15 – 20min to permeabilize them. Regardless of the fixation method, all coverslips were blocked with 100 $\mu$ l IF blocking buffer for 20 – 30min (see 4. Materials). This reduced non-specific binding of the antibodies. This was followed first by three washing steps with PBS (2 – 5min) and then antibody staining. The corresponding antibodies were diluted in blocking buffer. Incubation with the primary antibodies was performed for approximately 1h at RT or overnight at 4° C. Washing steps with PBS were then performed again as described above. Cells were then incubated in a dilution of dye-conjugated secondary antibodies. The dilution was also prepared in blocking buffer and incubated for 30min on the coverslips. Finally, all coverslips were stained for 15min with 40 $\mu$ l of Hoechst 33342 trihydrochloride (1:40,000) and mounted with Fluoromount G without dye. The samples were dried for 24h, after which they were imaged on a Leica Dmi8 microscope with a 64 x 1.4 NA oil objective.

### **5.11. Cilia Quantification**

Primary cilia immunofluorescence signals were assessed from immunofluorescence images using the open-source ImageJ software (Fiji). A 3 pixel-wide line was drawn along the cilium using the Fiji program. Here, the cilium was defined by the ciliary marker, whereas all other channels, especially those



with proteins of interest, were masked out to blind the analysis. The fluorescent signals of several randomly selected cilia (at least 30 per condition, exact n indicated in the figure legend) from multiple images were measured. Images were acquired from different locations of the coverslips (6 or more images), and of these, at least four were randomly selected for quantification. First assessments of the measurements were made using Microsoft Excel where values were sorted by channel so that all signals were assigned to the corresponding protein. Then, the background of each image was quantified using ImageJ. For this purpose, a square as large as possible was placed over an area without cilia but with cell background signal. In this area, the signals for each channel's were measured and then subtracted from the signals of the respective target protein recorded from the same image. This process was repeated for all cilia and all channels and will be referred to as background correction. The resulting values were normalized by dividing the background subtracted mean fluorescence values by the background subtracted mean cilia marker fluorescence signals. All calculations were performed in Microsoft Excel. The resulting intensity values were transferred to GraphPad Prism 8 for statistical analysis (see 5.21. Statistics). Negative values were set to zero and considered as signals below background. Statistical analyses were performed as described (see 5.21. Statistics).

### **5.12. Bradford Assay**

Bradford assay is a commonly used method to determine protein concentrations down to the  $\mu\text{g}$  range. The assay is based on the binding of the dye Coomassie brilliant blue G-250 to proteins, resulting in a shift of absorption maximum of this dye from 465nm to 595nm. The change in absorption can be measured and used to determine protein concentrations using a calibration curve (Bradford, 1976; Compton & Jones, 1985). To perform this assay, 50 $\mu\text{l}$  of a protein standard solution BioRad IgG with a known concentration of 1.47 $\mu\text{g}/\mu\text{l}$  was diluted with 50 $\mu\text{l}$  of  $\text{dH}_2\text{O}$  (solution 1). A dilution series was prepared from this solution 1, using 50 $\mu\text{l}$   $\text{dH}_2\text{O}$  each for a total of five dilutions. In addition, a sample of pure  $\text{dH}_2\text{O}$  was used to measure the zero value in absence of any protein. For each sample to be determined, 2 $\mu\text{l}$  of each was diluted in 48 $\mu\text{l}$   $\text{dH}_2\text{O}$ . This step was performed in a triplicate for each sample. To determine the protein concentration of the lysates, all prepared dilutions were mixed by pipetting with 700 $\mu\text{l}$  Roti-Quant 1:5 Bradford Reagent. The absorbance of all samples was measured in a clear 48-well plate using the Tecan Plate Reader. Based on the known calibration curve concentrations of 36.75 $\mu\text{g}$ , 18.375 $\mu\text{g}$ , 9.1875 $\mu\text{g}$ , 4.59 $\mu\text{g}$ , 2.295 $\mu\text{g}$  and 0 $\mu\text{g}$ , protein concentrations were calculated using Microsoft Excel and GraphPad Prism 8.

### **5.13. Quantitative Fluorescence Western Blot (WB) Analysis**

Quantitative fluorescence Western blots were performed to determine protein steady-state levels. At the beginning of each experiment, cell lysates were prepared for this purpose. After aspiration of the medium (careful removal with a pipette in the case of HEK293T and other easily detachable cell lines), a wash step with cell culture PBS was performed. Cells were then placed on ice, PBS was removed, and solubilization buffer was added to the cells (800 $\mu\text{l}$  for 15cm dish, 180 $\mu\text{l}$  for 10cm dish and 80 $\mu\text{l}$  for 6 well). The cells were detached by scraping with a cell scraper. The resulting cell solution was transferred into a 1.5 ml reaction tube and incubated on ice for 10 – 30 min; the cells were exposed to a velocity of

20,000g for 45min at 4°C. The supernatant was collected, and pellets were discarded. Fresh lysates were kept on ice throughout the process. Protein concentration was determined by Bradford assay (see 5.12. Bradford Assay) and samples were diluted to a concentration of 2.5µg/µl or 5µg/µl with Laemmli sample buffer (see 4. Material). Residues were shock frozen in liquid nitrogen for storage, and diluted samples were heated to 95° C for 5min and stored at -20° C until the experiment. 25µg of protein was separated by SDS gel electrophoresis with 10% Bis-Tris polyacrylamide gels and transferred to a nitrocellulose membrane by wet transfer at 100V for 1h for proteins less than 100kDa and 1h 15min for proteins greater than 100kDa. The protein transfer was performed on ice, for the transfer buffer used (see 4.3. Buffer & Solutions). Membranes were either stained with Ponceau to assess transfer and blocked after destaining or blocked immediately after blotting with Intercept TBS protein free Blocking Buffer (LI-COR) for 1 1/2h or longer. After blocking, the membrane was washed three times with TBS-T for approximately 15min and decorated with primary antibodies, diluted in either 5% milk or 1% BSA. The primary antibodies were incubated overnight at 4° C with shaking. After TBS-T washing, a second primary antibody from a different species was decorated as a loading control. If no loading control was decorated, washing was performed immediately before the addition of secondary antibodies. Primary antibodies used to determine proper loading (house-keeping proteins, loading controls) were incubated for 45 min to 1h and the membrane was then washed with TBS-T. Secondary antibodies conjugated with fluorescent dye were freshly diluted in TBS and the membrane was incubated for 30min under light protection. Finally, the membrane was washed extensively, twice with TBS-T for 10min or longer and twice with TBS for 10min or longer. Membranes were scanned using a Li-COR Odyssey laser scanner and quantification of the bands was performed using the Image Studio Lite program.

#### **5.14. Ponceau Stain**

To assess blotting efficiency and uniformity after WB, various staining procedures can be performed. However, not all staining methods are suitable for LI-COR scanning as some generate high background Fluorescence signals that can hinder the sensitive fluorescence scanning instrument. Nitrocellulose membranes, in particular, can be reversibly stained at RT with Ponceau S, a red dye. The staining was performed for approximately 5min. Subsequently, the membrane was washed twice with TBS. After assessing the band patterns, the membrane was decolorized with H<sub>2</sub>O. After complete destaining of the membrane, the membrane was blocked and processed as described (see 5.13. Quantitative Fluorescence Western Blot (WB) Analysis).

#### **5.15. CRISPR-Cas9 based Genome Editing**

The Clustered Regularly Interspaced Short Palindromic Repeats (CRISPR)-CRISPR associate endonuclease 9 (Cas9) system was originally discovered in bacteria, where it is dedicated to repelling bacteriophages. Today, CRISPR-Cas9 is widely used in scientific research to generate gene knock-outs. The general principle of CRISPR-Cas9 is based on a single guide RNA (sgRNA) that encodes a palindromic sequence of a target gene. Binding of the sgRNA to the target gene marks the DNA sequence for restriction by the endonuclease Cas9. Although cellular reparative mechanisms occur, consistent restriction of the DNA sequence can lead to mutagenesis and subsequently defective proteins

or early transcriptional silencing. Knock-outs can be efficiently generated by transfecting cells with a plasmid encoding a specific sgRNA, the Cas9 enzyme, and a selection marker.

Sequences for sgRNAs targeting a specific exon were designed using the online tool chopchop (<https://chopchop.cbu.uib.no>). Chopchop generates multiple suggestions (CRISPR hits) for sgRNA target sequences. Based on the position in the target gene (early exon, splice site, conserved region), predicted restriction efficiency (as high as possible), and predicted off-target effects (as low as possible), a target sequence matching the described criteria was selected, which is located in the exon 4 of *Pald1*. The designed oligonucleotides can be found under 4.9. Oligonucleotides. They have a 5-base pair long overhang for recombination with the target plasmid. First, an initial phosphorylation and annealing step was performed in PCR tubes as follows:

TOP OLIGO 100 $\mu$ M	1 $\mu$ l
Bottom OLIGO 100 $\mu$ M	1 $\mu$ l
H <sub>2</sub> O	6 $\mu$ l
10X T4 DNA ligase buffer	1 $\mu$ l
T4 Polynukleotidkinase (PNK)	1 $\mu$ l

This mix was incubated at 37° C for 30min, then heated to 95° C for PNK inactivation. The temperature is then gradually decreased until it reaches 25° C. The decrease is performed at 1°C/min to allow annealing. Afterwards, the oligonucleotides are stored at 4° C until further processing. Finally, 40 $\mu$ l dH<sub>2</sub>O are added to the oligonucleotides and the ligation with the target plasmid, BbsI pre-digested pSpCas9 (BB)-1A-GFP encoding a GFP tagged version of Cas9, is performed. The ligation was performed as follows

Annealed oligos	7 $\mu$ l
BbsI pre-digested plasmid 10 ng/ $\mu$ l	1 $\mu$ l
10 x T4 Ligase buffer	1 $\mu$ l
T4 DNA ligase	1 $\mu$ l

Subsequently, the mix was incubated for one hour at room temperature and transformed into *E. coli* as described (see 5.3. Bacterial Transformation). The constructs can be transfected into the target cell line after a DNA prep. Transfected clones of this cell line are then selected and cultured *via* fluorescence activated cell sorting (see 5.17. Fluorescence Activated Cell Sorting (FACS)).

## 5.16. Mammalian Cell Transfection

Transfection describes the introduction of foreign DNA or RNA into an eukaryotic target cell line. Transfections can be either temporary (transient) or permanent (stable). In this work, transient and stable transfections were conducted. Subsequently, transfection conditions for the different cell lines in our laboratory were tested and established. These processes included testing different transfection reagents

and different dilutions of transfection reagents, varying transfection times and conditions. Here, the final protocols for transient transfections and generation of cell lines are described. All transfections were carried out in a six well format.

#### *Stable transfection of IMCD3 cells*

For the generation of a stable *Pald1* knockout cell line in IMCD3 cells, the cells were transfected with the lipid-based, non-liposomal transfection reagent FuGene *via* modified reverse transfections. That is, a transfection mix of 100µl Opti-MEM and 5µl FuGene was prepared in a FACS tube. This mix was gently mixed by swirling the FACS tube. After incubating the mix for five minutes, 1.2µg of DNA or control plasmid was added. The complete mix was incubated for 30 – 45min at RT. During this time, IMCD3 cells were harvested and counted as described (see 5.6. Cell culture) and 300,000 cells were seeded per well. Cells were directly transfected dropwise with the transfection mix and then gently mixed by sliding the plate back and forth. A total volume of 100µl of transfection mix was added per well in a six wells. Cells were incubated with the transfection mix for approximately 20h before growth factor deprivation was performed. After approximately 24h, cells were prepared for FACS sorting as described (see 5.17. Fluorescence Activated Cell Sorting (FACS)).

#### *Stable transfection of 3T3 and C2C12 cells*

To generate a stable *Pald1* knockout cell line in 3T3 and C2C12 cells, a modified reverse transfection was performed using the lipid-based transfection reagent Lipofectamine 3000. For this purpose, 6µl Lipofectamine 3000 was diluted in 100µl Opti-MEM, mixed by vortexing for 1s, briefly spun, and incubated for 2 – 5 min. In parallel, 500ng of DNA was diluted in 4µl of P3000 and also mixed by vortexing for 1s, briefly spun, and incubated for 2 – 5min. After incubation, the Opti-MEM/ Lipofectamine dilution was added to the P3000/DNA dilution, mixed by gently tapping the tube, and incubated for approximately 30min at room temperature. During incubation, cells, which were to be transfected were harvested as described in (see 5.6. Cell culture). 210,000 cells were seeded and 100µl of transfection mix was added directly dropwise onto the cells. After 4h of incubation, the medium was replaced with fresh DMEM + 10% FBS and the cells were incubated for approximately 20h until growth factors were withdrawn. After approximately 24h, cells were prepared for FACS sorting (see 5.17. Fluorescence Activated Cell Sorting (FACS)). For both approaches, pipetting was kept to an absolute minimum to avoid deposits of the reagent in the pipette tip.

#### *Transient transfection of IMCD3 cells*

For transient transfections, IMCD3 cells were transfected with the polymer-based transfection reagent JetPrime in a forward transfection. For this purpose, 250,000 IMCD3 cells were seeded in a six-well plate one day before transfection. On the day of transfection, a mix of the following components, pipetted in the order indicated, was prepared: 200µl JetPrime buffer, 2µg DNA and 4µl JetPrime reagent. After addition of the JetPrime buffer, the mix was vortexed for 10s and spun down. Immediately after, the JetPRIME reagent was added and the mix was vortexed again for 1s, spun down and incubated for 10min at RT. After the incubation period, the complete mix was added dropwise onto the cells, and

the cells were gently mixed by sliding the plate back and forth and incubated overnight. After 24h, the medium was changed to starvation medium, DMEM-F12 containing 0.2% FBS, and the cells were incubated for an additional 24h. 48h after transfection, cells were fixed with 4% PFA or imaged directly under the microscope.

#### *Transient transfection of C2C12 and 3T3 cells*

Transient transfections of C2C12s and 3T3s were conducted as the described transfection for production of a *Pald1* knock-out cell line.

### **5.17. Fluorescence Activated Cell Sorting (FACS)**

FACS is a special form of flow cytometry. In this technical approach, the characteristic light scatter of different cells is used to determine cell populations. In addition, fluorescent markers are used to sort a defined number of cells into, for example, a 96-well plate to select transfected clones. In this work, FACS was used to separate cell clones that were successfully transfected with the CRISPR-Cas9 encoding plasmid (pSPCas9(BB)-2A-GFP). Transfected cells could be sorted based on their GFP expression. For FACS sorting, cells were harvested by detachment using 500µl trypsin (see 5.6. Cell culture). Cells were then sedimented by spinning for 3min at 500RPM and resuspended in 1ml medium containing 10% FBS, 20mM HEPES and 1% Pen-Strep. FACS sorting was kindly performed by PD Dr. Elmar Krauß from the Center for Integrative Physiology and Molecular Medicine of UdS. Cells were sorted into 96-well plates and incubated at 37° C and 5% CO<sub>2</sub> for approximately two weeks before splitting into new wells in a 48-well plate followed by a 24-well plate. After transferring the cells into 6-well plates, WB analysis was performed confirming the loss of PALD1.

### **5.18. Muscle differentiation assay**

C2C12 myoblasts have the ability to recognize each other and differentiate into myotubes, which express characteristic muscle proteins, by undergoing cell fusion. Through this property, the characteristics of muscle cells could be studied in a cell culture model (Blau *et al.*, 1968). Furthermore, the ability to differentiate, which depends on different factors such as SHH signaling, can be studied (Elia *et al.*, 2007). In the following, 60,000 C2C12 cells were seeded per well in a six well plate. These cells were cultured for 72h in DMEM medium containing 10% FBS at 37° C and 5% CO<sub>2</sub>. After that, the growth medium was removed and the cells were washed once with PBS. Furthermore, the cells were cultivated in differentiation medium which consists of DMEM containing 2% HS. Samples corresponding to time point T<sub>0</sub> were taken immediately after the first medium change. Next, medium was changed daily for a total of four more days in which cells were washed with PBS before the medium change. One sample was taken on each day. The last well of cells was incubated for 72h at 37° C and 5% CO<sub>2</sub> without medium change before the last sample was taken. Lysates were generated from all samples and analyzed by quantitative WB as described (see 5.13. Quantitative Fluorescence Western Blot (WB) Analysis).

### 5.19. Scratch Assay

For the scratch assay, 200,000 3T3 WT and 3T3 *Pald1*<sup>-/-</sup> cells per well were seeded per well in growth medium in a 6-well plate. Cells were incubated for 24h in 2ml medium at 37° C and 5% CO<sub>2</sub>. Then scratches were applied to the monolayer using a 5ml pipette. Immediately after adding the scratches, the cells were analyzed under the light microscope and the imaged area was marked on the plate. After that, an image was taken every day from the same spot until the scratch in the 3T3 WT cells was overgrown. Then, the cell borders of the scratch in Fiji were determined and the distance between the cell borders was measured. Each measured distance was then normalized to the maximum distance of the respective cell line. Values were analyzed as described (see 5.21. Statistic and respective figure legend).

### 5.20. Reverse transcription Quantitative real-time Polymerase Chain Reaction (qRT-PCR)

By means of quantitative real-time PCR, cellular RNA can be isolated, reverse transcribed in cDNA and thereby quantified by interaction with a specific dye. In this way, conclusions can be drawn about the expression of certain genes. In this work, qRT-PCR was used to compare the transcriptional SHH response of different cell lines. For this purpose, 150,000 cells per well were cultured in a 12-well plate in the presence of the respective cultivation medium for 24h at 37° C and 5% CO<sub>2</sub>. This was followed by deprivation of growth factors (see 5.6. Cell culture) and induction of the SHH signaling pathway using Shh-N or the respective control (see 5.9. Sonic Hedgehog Signaling Assays). After 24h of incubation at 37° C and 5% CO<sub>2</sub>, cellular RNA was then purified using the miRNeasy mini kit according to the manufacturer's protocol. Further steps were kindly performed by Dr. Nicole Ludwig and Esther Maldener from the Department of Human Genetics in Homburg. In this process, the RNA was first purified by ethanol precipitation. Subsequently, 200ng of RNA was converted into cDNA using the QuantiTect reverse transcription kit. After reverse transcription, qRT-PCR was performed with 4ng of cDNA per batch using the StepOnePlus Real-Time PCR system with SybrGreen dye. Specific primers for the *Gli1* and *Gapdh* were used to amplify the constructs as previously described, *Gapdh* was used as a reference (Everson *et al.*, 2018).

### 5.21. Statistics

All statistical analyses were performed using GraphPad Prism. For immunofluorescence microscopy, at least 30 cilia per experiment were analyzed (exact n indicated in the figure legend). To compare biological replicates, relative fluorescence values (RFU) were normalized to WT cells treated with vehicle or control medium, as described (see 5.11. Cilia Quantification and 5.9. Sonic Hedgehog Signaling Assay). Statistical significance was tested by t-test for comparison of two groups or by two-way ANOVA for comparison of more than two groups. The two-way ANOVA was followed by one of two post hoc tests; Holm-Sidak's test or Tukey's tests. The applied test and exact p-value is stated in the respective figure legend. For quantitative WB analysis of GLI3 forms, the means of three biological replicate experiments were calculated. For each replicate, the FL/R ratio was normalized to FL/R of WT cells in the absence of the inducing reagents. Two-way ANOVA was then performed and  $p < 0.05$  was considered statistically significant.

## 6. Results

### 6.1. Improved Cilia-APEX2 expressing cell line enables proteomic screen to investigate the remodeling of the primary cilium proteome in response to SHH signaling

Some of the following experiments were previously published in May *et al.*, 2021 in the Journal of Cellular Biology (JCB) and have been cited accordingly.

Prior to this work, an IMCD3 cell line expressing an enhanced, cilia localized APEX construct was generated. This cell line will be referred to as IMCD3 Cilia-APEX2 hereafter. IMCD3 Cilia-APEX2 was generated by David Mick, based on his previous study in which he established the predecessor cell line, IMCD3 Cilia-APEX (Mick *et al.*, 2015). For the transgene encoding the APEX2 enzyme and its targeting sequence, the general structure of the first APEX transgene sequence was maintained. The Cilia-APEX2 transgene encodes the amino acids 1 – 200 of NPHP3, which contain the ciliary targeting sequence (Bergmann *et al.*, 2008). This is followed by a sequence encoding a green fluorescent protein (GFP) which can be used for the subsequent detection of the construct *in vivo* and *in vitro* (Zimmer, 2002). At the end of the construct lies the sequence encoding APEX, the ascorbate peroxidase for proximity labeling. However, instead of APEX, APEX2, an improved peroxidase with higher labeling efficiency, was used here (Lam *et al.*, 2015). As a high transgene expression could result in non-physiological changes in the cell, a considerably weaker promoter was used to generate Cilia-APEX2. The possibility of using a weaker promoter was opened up by the use of the APEX2 enzyme, so that labeling capacity could be maintained while exchanging the pEF1 $\alpha$  with a pCMV $\Delta$ 6 promoter (Morita *et al.*, 2012; Ye *et al.*, 2018; Fig. 5).

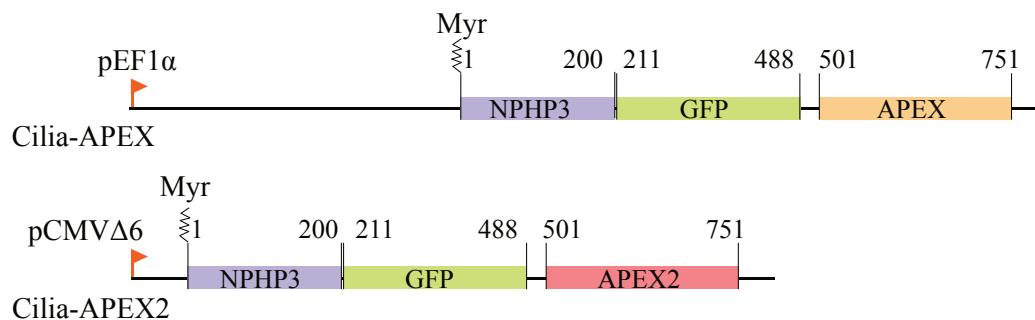


**Fig. 5: The Cilia-APEX construct vs. the improved Cilia-APEX2 construct.**

Cilia-APEX (top) encodes NPHP3 for cilia targeting, GFP for detection and APEX, an ascorbate peroxidase, for specific labeling in presence of hydrogen peroxide under the control of a pEF1 $\alpha$  promoter. The improved Cilia-APEX2 construct (bottom) encodes NPHP3, GFP and the improved APEX2 enzyme. The construct is expressed under the control of the weaker pCMV $\Delta$ 6 promoter (modified from May *et al.*, 2021)

In the first experiments of this work, the IMCD3 Cilia-APEX2 cell line was analyzed in comparative assays with the predecessor IMCD3 Cilia-APEX and the parental IMCD3 (WT) cell lines. Quantitative WB and IF microscopy assays were thus used to obtain information on the expression levels of the

transgenes, their correct localization in the primary cilium, and their labeling capacities. Quantitative fluorescence WB analysis demonstrated that the steady-state expression levels of IFT88 showed no differences between IMCD3 Cilia-APEX2 and the reference cell lines IMCD3 Cilia-APEX and WT (Fig. 6A). The expression of IFT88 in IMCD3 Cilia-APEX2 alternates around 100% of the expression in Cilia-APEX expressing cells (Fig. 6B). These observations indicated that ciliary proteins are generally unaffected by ectopic expression of the transgene. Furthermore, GFP expression levels of the two APEX cell lines were compared to the WT. As expected, no transgene could be detected in the WT cells (Fig. 6A). However, GFP detection showed that the steady-state expression levels of the Cilia-APEX2 transgene decreased approximately 4-fold compared to the Cilia-APEX transgene (Fig. 6B).

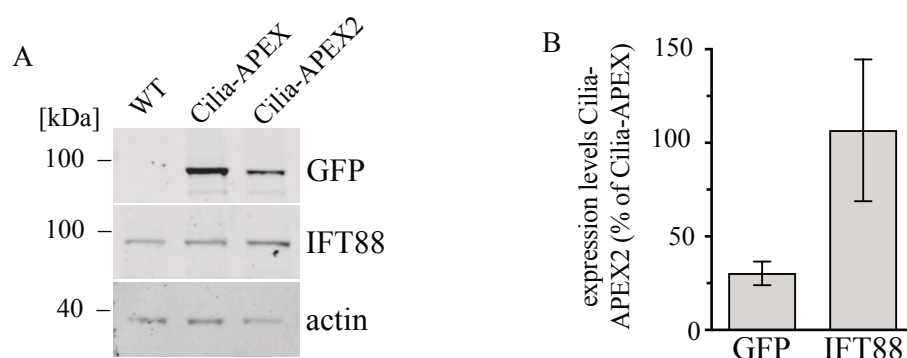


**Fig. 6: Cilia-APEX2 exhibits weaker transgene expression.**

(A) Representative image of a quantitative WB of IMCD3 Cilia-APEX, IMCD3 Cilia-APEX2 and WT cell lysates. IFT88, GFP and actin were detected with specific antibodies. GFP detection was used to assess steady state expression levels of the Cilia-APEX and the Cilia-APEX2 transgenes. Actin was used to ensure equal loading of protein. (B) Quantification of three biological replicates ( $n = 3$ ) of (A) shows protein steady state expression levels of GFP and IFT88 of Cilia-APEX2 in percentage of cilia-APEX expressing cells. Signals were assessed relative to their respective actin signals. Bar graphs indicate mean values with SD (modified from May *et al.*, 2021).

To assess the labeling capacity, further comparative IF microscopy was performed on WT, Cilia-APEX, and Cilia-APEX2 expressing cells. Here, after APEX labeling was performed, labeling efficiency was checked by staining biotinylated proteins using fluorescently labeled streptavidin on fixed cells. Transgene expression was detected by GFP fluorescence and cilia were stained using an antibody against a cilia marker protein (ARL13B). GFP fluorescence demonstrated that Cilia-APEX2 signals are significantly reduced by approximately 4-fold (Fig. 7A and B). In contrast, ciliary biotin signals nearly doubled after labeling (Fig. 7A and C). This indicated that increased labeling capacity was achieved at lower transgene expression. Consequently, proteins that were below the detection limit in previous experiments could be identified in future screenings using IMCD3 Cilia-APEX2 (May *et al.*, 2021). Furthermore, cilia length from the parental, Cilia-APEX, and Cilia-APEX2 expressing cell lines was analyzed based on IF microscopy to assess if cilia formation and maintenance were affected. The length analysis showed no significant changes in ciliary length between the three cell lines (Fig. 7D). Nevertheless, cilia length for IMCD3 Cilia-APEX2 could be distinguished into two different



populations, whereas for the WT cell line the length is homogeneously distributed. For IMCD3 Cilia-APEX, cilia length seemed to vary more, but did not lead to significant differences on average.

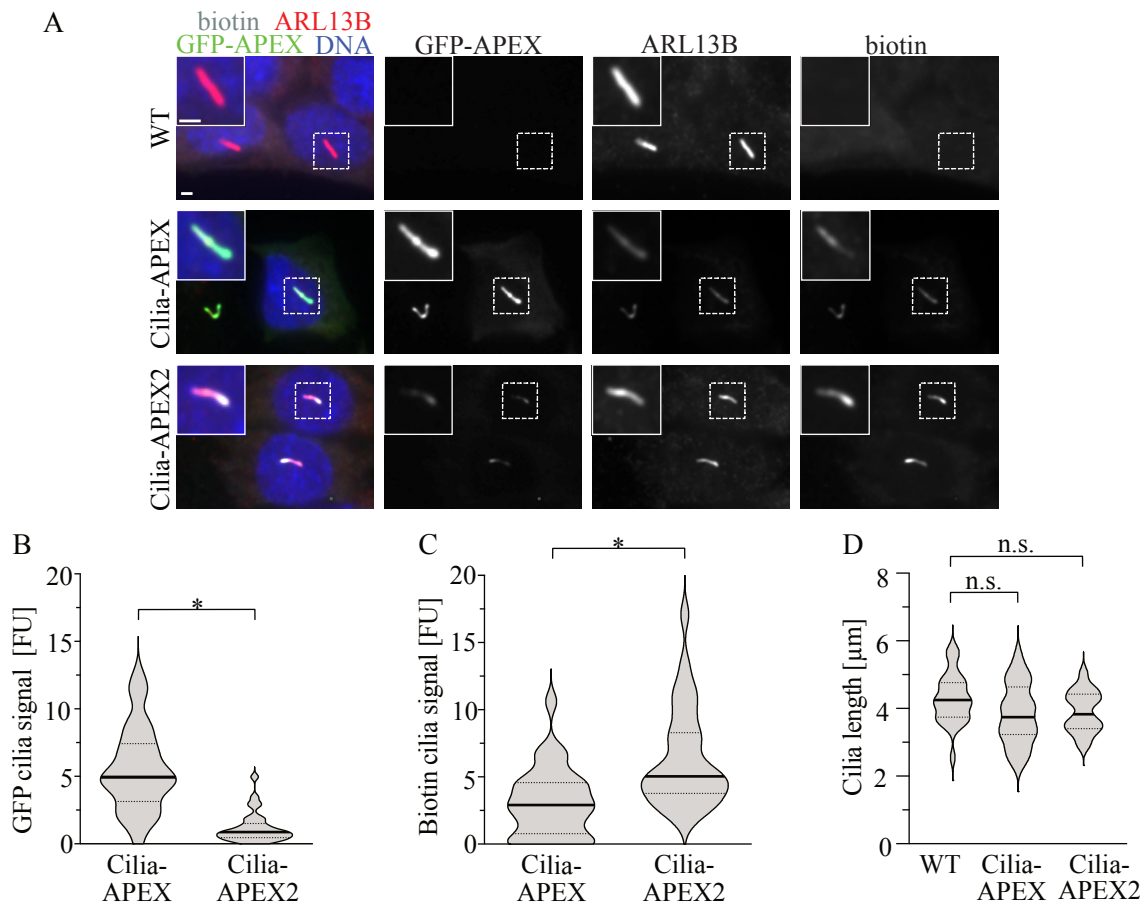


**Fig. 7: Cilia-APEX2 labels ciliary proteins with a higher efficiency than Cilia-APEX at lower transgene expression.**

(A) IF micrographs of representative images, scale bar shows  $2\mu\text{m}$ . WT, Cilia-APEX and Cilia-APEX2 expressing cells were fixed after APEX labeling and stained with an antibody against ARL13b and fluorescently labeled streptavidin. (B) Quantification of absolute ciliary GFP fluorescence signals in FU. Violin plots are shown. The dotted lines show the quartiles, the thick black continuous line shows the median. Statistic significance was assessed with an unpaired, two-tailed t-test;  $p < 0.0001$ . (C) Quantification of absolute cilia biotin signals in FU in IMCD3 Cilia-APEX vs. IMCD3 Cilia-APEX2 shown as violin plot. Statistic significance was assessed with an unpaired, two-tailed t-test;  $p < 0.0001$  (A-C was modified from May *et al.*, 2021). (D) Quantification of cilia length in WT, Cilia-APEX and Cilia-APEX2 expressing cells. Shown are violin plots. Statistic significance was assessed with a Dunnett's T3 multiple comparisons test;  $p < 0.01$ .

In previous studies, Cilia-APEX was limited to recognizing cilia-localized, low-abundance membrane proteins (Mick *et al.*, 2015). One example was the cilia-localized GPCR GPR161, which plays a critical role in SHH signaling. This transmembrane protein was barely detectable in the cilia of Cilia-APEX expressing cells in previous studies (Mick *et al.*, 2015). In this work, GPR161 localization was determined by IF microscopy in WT, IMCD3 Cilia-APEX and IMCD3 Cilia-APEX2 cells. Here, GPR161 was detected by antibody staining and ciliary signals were assessed relative to acetylated-tubulin (ac-tub). The relative ciliary GPR161 signals in IMCD3 Cilia-APEX2 cells were comparable to those of the WT cell line, whereas the signals in IMCD3 Cilia-APEX cells were significantly reduced and almost below the detection limit (Fig. 8A). After induction of SHH signaling, GPR161 exit from the primary cilium was detectable in Cilia-APEX2 expressing and the WT cells, whereas no significant changes in ciliary GPR161 signals were observed for IMCD3 Cilia-APEX cells (Fig. 8B).

These initial experiments indicated that in IMCD3 Cilia-APEX2 cells, ciliary proteins were labeled with higher efficiency at lower transgene expression compared to IMCD3 Cilia-APEX cells. In addition, the IMCD3 Cilia-APEX2 cell line proves to be a model with higher similarity to the WT cells, as low-expressed membrane proteins were detectable well above the detection limit of IF assays. The fact that these proteins were hardly detectable in IMCD3 Cilia-APEX cells limited the sensitivity of previous proteomic screens using APEX (Mick *et al.*, 2015). Subsequently, the IMCD3 Cilia-APEX2 cell line was selected as a new cell line for a potentially more precise proteomic analysis of the ciliary proteome. In addition, the ability to detect low-expressed SHH components allowed for the investigation of time dependent proteome changes in response to SHH signaling for the first time.

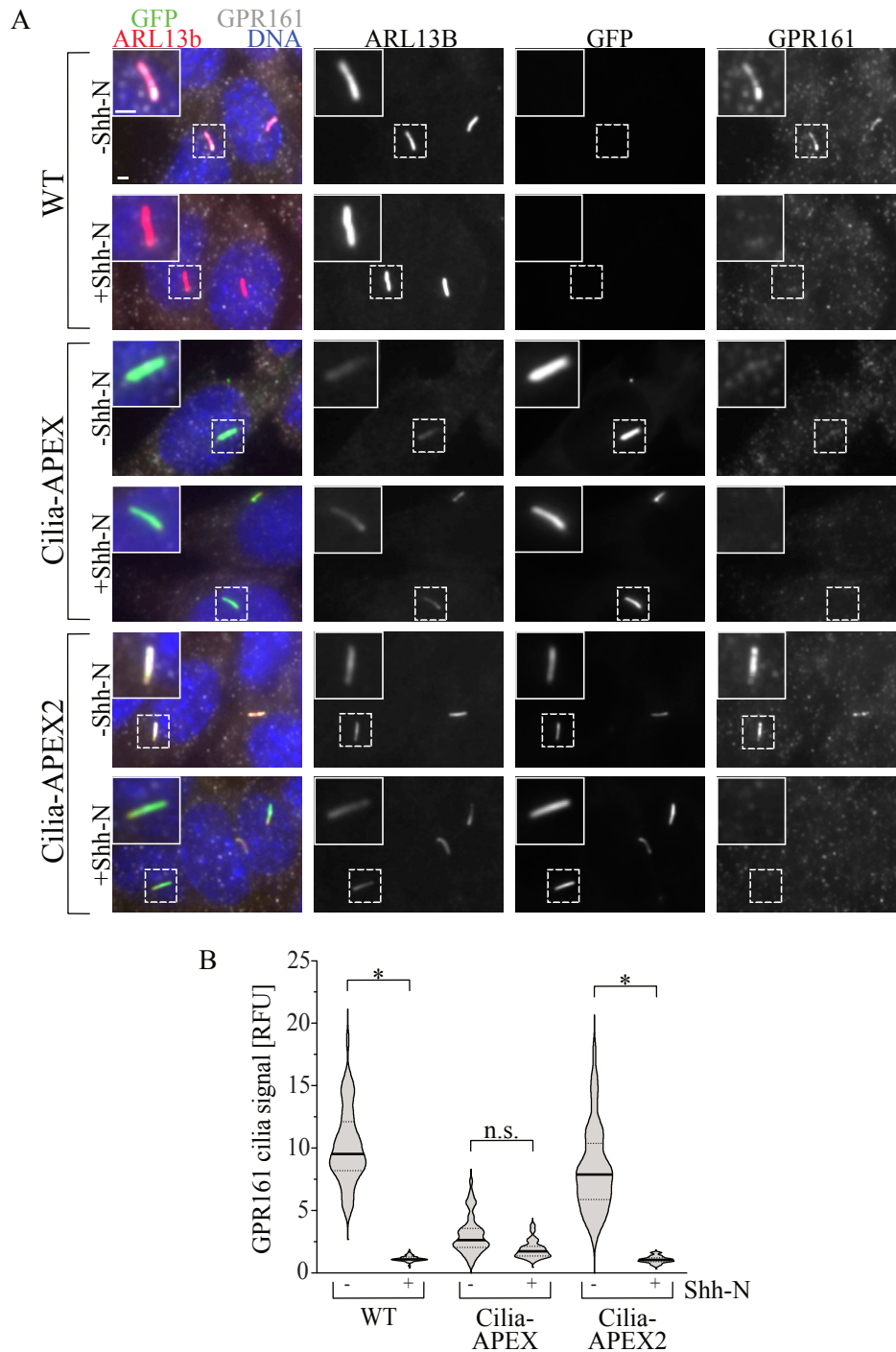


**Fig. 8: Detection of GPR161 in WT, Cilia-APEX and Cilia-APEX2 expressing cells.**

(A) Representative IF micrographs of fixed WT, Cilia-APEX and Cilia-APEX2 expressing cells in the presence and absence of Shh-N stained with antibodies against ARL13B and GPR161 with a scale bar showing 2µm. (B) Quantification of ciliary GPR161 signals relative to ARL13B in RFU from 30 cilia (n = 30) showed significant reduction of GPR161 ciliary signals in WT and IMCD3 Cilia-APEX2 cells after treatment with Shh-N. Shown are violin plots, the dotted lines show the quartiles, the thick black continuous line shows the median. Statistic significance was assessed with 2-way ANOVA and Sidak's multiple comparison test;  $p < 0.0001$  (modified from May *et al.*, 2021).

## 6.2. Improved proteomic screen identifies a new potential SHH Signaling component

The Cilia-APEX2 cell line was used with appropriate controls for a comparative proximity labeling. This approach was combined with quantitative mass spectrometric (MS) analysis. Proximity labeling experiments for MS were performed by David Mick and the MS analysis was kindly performed by Marian Kalocsay at Harvard Medical School (for details on the proteomic study please see May *et al.*, 2021). The study, on which this work is based, represents the first temporally resolved proteomic screen of the primary cilium proteome remodeling during the SHH response. It was demonstrated that upon stimulation with SHH inducing reagents, the regulatory subunit of PKA, PKA-R1 $\alpha$ , co-exits the cilium in a regulated manner together with GPR161. In addition, a new potential SHH signaling component was identified. The putative phosphatase Paladin (PALD1) was the only component of the ciliary proteome that was undergoing kinetics similar to the SHH effector SMO. Both proteins accumulated in the primary cilium after stimulation of the SHH signaling pathway in a specific kinetic (May *et al.*, 2021). Although numerous screens for SHH components have been performed, PALD1 had never been identified as a potential SHH signaling component. Instead, PALD1 has been linked to insulin signaling and neural crest migration in the past (Huang *et al.*, 2009; Roffers-Agarwal *et al.*, 2012). These facts raised many interesting questions about the role and function of PALD1 and its possible cell type specificity. In the following, these aspects will be discussed. The following chapters of this work will focus on the biochemical and molecular biological analysis of PALD1 with respect to ciliary signaling. Some results of this work are published in May *et al.*, 2021 as indicated in the respective figures.

### 6.3. The role of PALD1 in ciliary signaling in IMCD3 cells

As mentioned earlier, PALD1 possesses features indicative of its function as a potential protein-tyrosine phosphatase. Specifically, this involves four predicted minimal catalytic site motifs (CX5R) for phosphatase activity. These motifs indicate that the protein consists of at least one or two potential protein tyrosine phosphatase domains. However, despite the structural similarities, no protein-tyrosine phosphatase catalytic activity has yet been shown for PALD1. Also, no potential protein substrates of PALD1 had yet been identified. A recent preprinted study suggested that PALD1 functions as a Phosphatidylinositol (PIP) phosphatase targeting PI(4,5)P2 (Nitzsche *et al.*, 2020). Furthermore, PALD1 possesses the amino acid Glycine at position two, a property that scores high for a predicted myristoylation (Myr) (Fig. 9). The Myr at position two is a specific lipid modification that can be found on many ciliary proteins and oftentimes functions as a ciliary targeting signal (Roy & Marin, 2019).

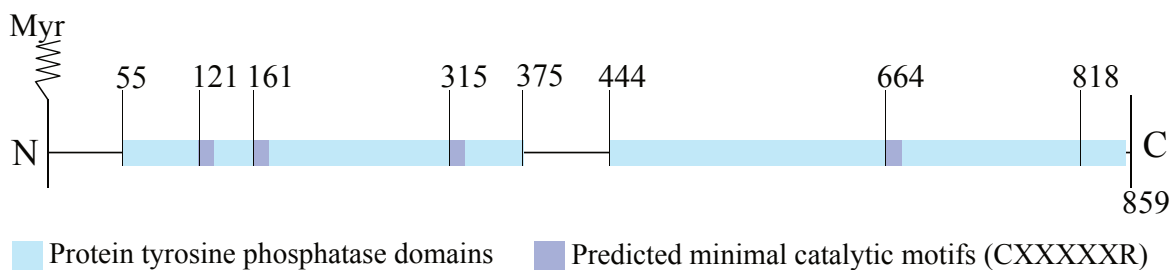


**Fig. 9: Domain structure of PALD1.**

PALD1, a 859 kDa in size protein, harbors two predicted protein tyrosine (PT) phosphatase domains with respective three and one minimal catalytic motifs consisting of CX5R. These motifs allow for the conclusion of a PT-phosphatase activity that had not yet been experimentally confirmed (modified from May *et al.*, 2021).

To confirm the PALD1 accumulation observed in the proteomic screen, an independent IF microscopy assay was performed. For this purpose, IMCD3 cells were treated with the SHH-inducing reagents Shh-N or SAG for 24 hours (Fig. 10). While Shh-N activates SHH via binding to the SHH receptor PTCH1, the Smoothened agonist (SAG) bypasses the receptor PTCH1 and activates the SHH pathway by directly interacting with SMO (Gigante & Caspary, 2020). Accordingly, activation with Shh-N is more similar to activation in living organisms in that the protein Sonic also binds directly to PTCH1. After treatment, cells were fixed. PALD1 and SMO were stained with the corresponding antibodies. In addition, to determine the respective localization of PALD1 and SMO, ac-tub was stained as a cilia marker. The inducing reagents Shh-N and SAG are commonly used for SHH assays and the question arises whether both will induce protein accumulation of PALD1.

It was shown that in response to both stimuli, SMO and PALD1 co-accumulate in the primary cilium (Fig. 10). To gain a better understanding of the underlying protein kinetics, Shh-N was also titrated to test whether a critical concentration could be identified. At this critical concentration, only SMO or PALD1 alone could accumulate in each case under certain circumstances, but not both. This could provide insight into whether a specific strength of SHH response underlies the respective accumulation. As a result, the co-accumulation of SMO and PALD1 observed in the MS analysis after treatment with SHH stimulating reagents could be confirmed; however, in the experiment, such a critical concentration could not be identified (Fig. 10). Thus, the type of induction seems to play a rather minor, or no role at all, in PALD1 accumulation. Because no critical concentration was observed at which only one of the two proteins accumulated, this raised the question whether PALD1 forms a complex with SMO and co-localizes solely because of direct interaction with it. That PALD1 and SMO further undergo a very similar time-dependent kinetic has not only been shown via MS analysis, but has also been confirmed in an IF assay by Inès Galtier D'Auriac from the University of San Francisco (UCSF; May *et al.*, 2021).

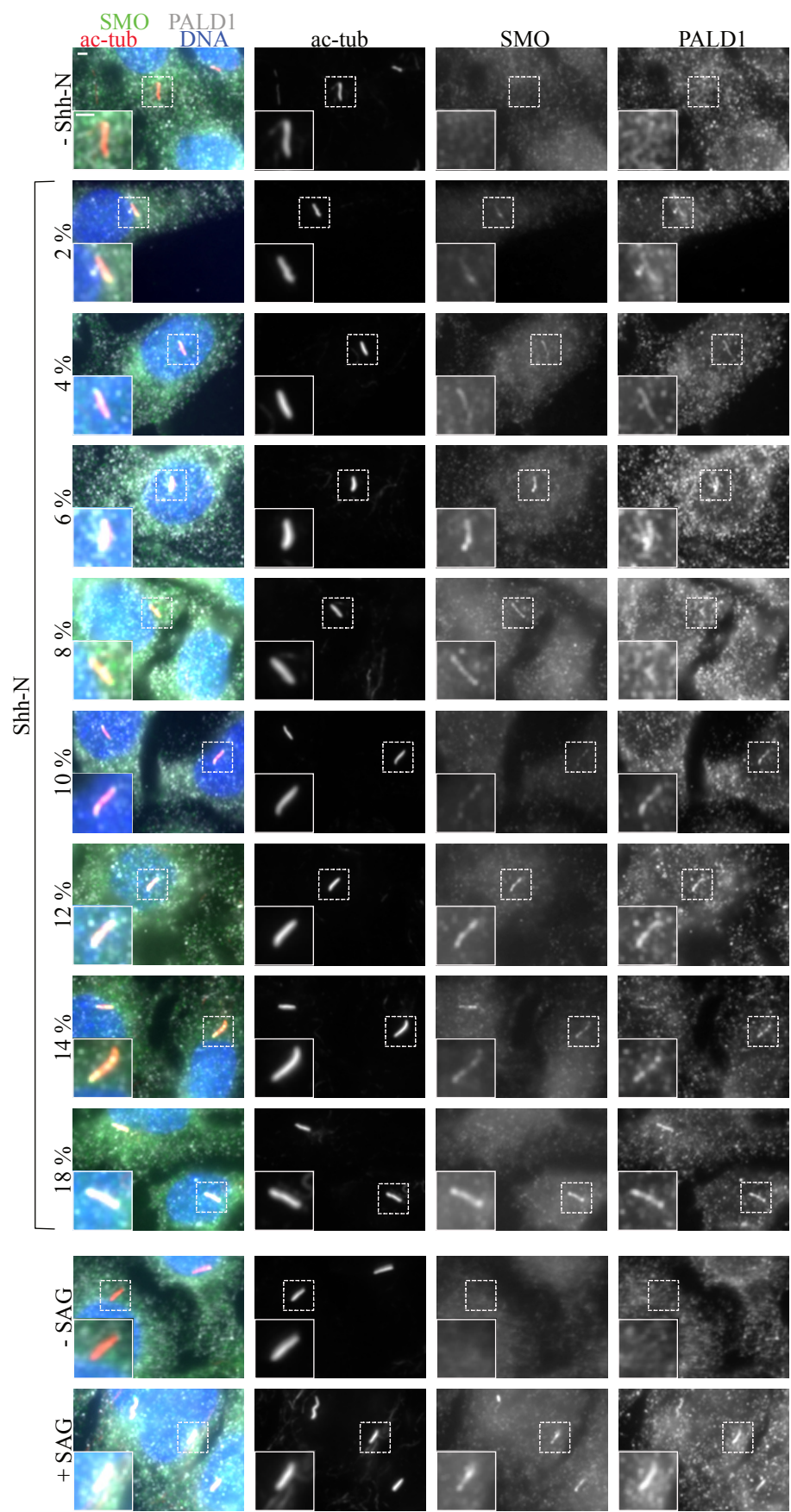


**Fig. 10: PALD1 and SMO after treatment with different concentrations of Shh-N or SAG.**

Representative IF micrographs of fixed IMCD3 cells stained with antibodies against SMO, PALD1 and the ciliary marker protein ac-tub. The scale shows 2 $\mu$ m. 24h prior to the experiment, the cells were treated either with titrated concentrations of Shh-N, SAG or respective controls. In the absence of Shh-N or SAG no accumulation of either PALD1 or SMO was observed. Clear and reliable accumulation of PALD1 and SMO was observed starting from a concentration of 10-12 % Shh-N per total medium volume.

To address the question regarding the complex formation of SMO and PALD1, IMCD3 cells were treated with the SHH-blocking reagent cyclopamine (CYC). CYC is a SMO antagonist that occurs naturally in *Veratrum californicum* (corn lily; Chen *et al.*, 2002). Although studies indicate its potential as an anti-cancer agent for the medical treatment of patients with SHH-dependent tumors (Bar *et al.*, 2007), CYC is not currently approved by the FDA or any other drug agency. Unlike other SHH inhibitors, CYC has the unique property of blocking SHH-induced signaling while leading to ciliary accumulation of SMO. On this account, IMCD3 cells were treated with CYC and the fixed cells were analyzed *via* IF microscopy using indicated antibodies against SMO, PALD1 and ac-tub. Treated cells display unambiguous SMO accumulation with cocomitant absence of PALD1 from primary cilia. Cells seeded the same day were treated with SAG as a control and displayed ciliary SMO and PALD1 accumulation (Fig. 11A). Quantification of the ciliary signals confirmed the absence of PALD1 from cilia in CYC-treated cells and time dependent accumulation of SMO (Fig. 11B and C).

These results confirm that PALD1 could fulfill a role in SHH signaling without permanent protein complexation with SMO as a pure cause of co-localization. Based on the fact that PALD1 changes its localization after SAG induction as well as after Shh-N induction, it could be suspected that PALD1 might function downstream from SMO in SHH signaling.



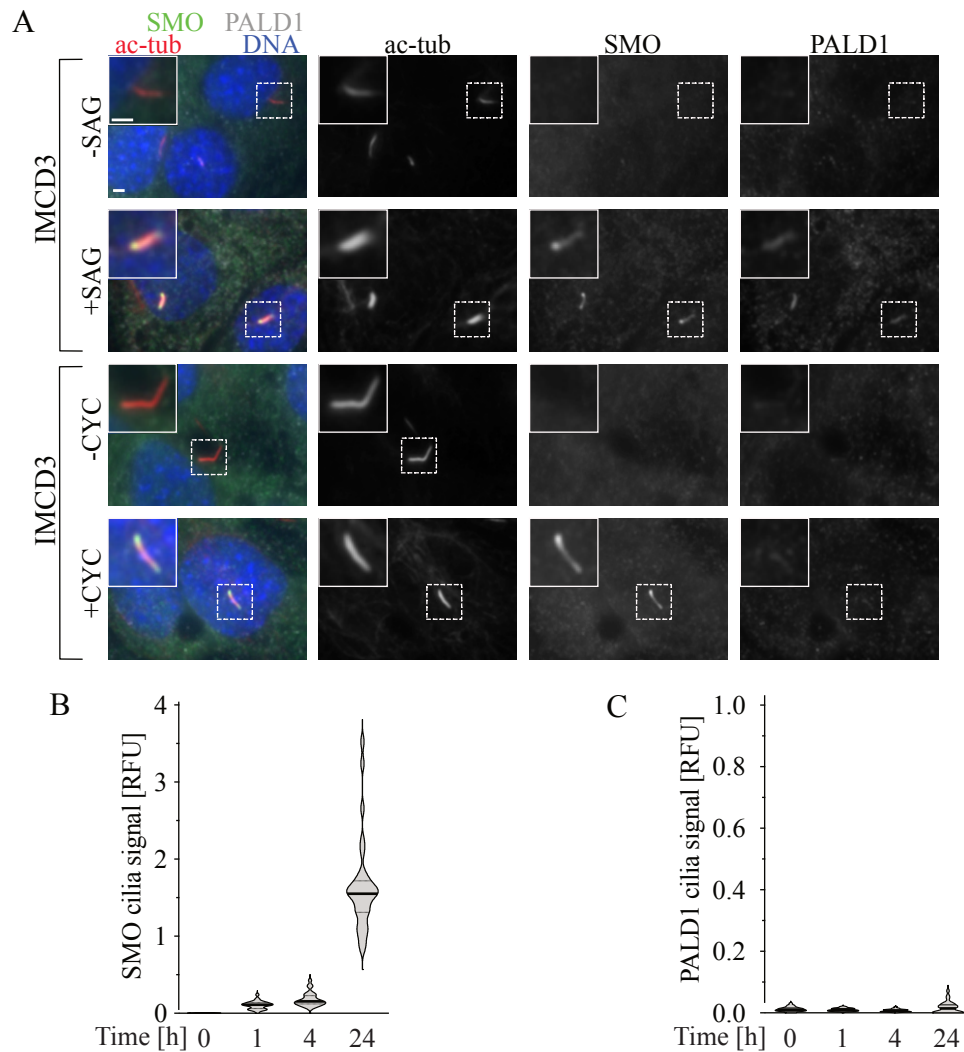


**Fig. 11: CYC-treated IMCD3 cells show ciliary SMO but not PALD1 accumulation.**

(A) IMCD3 cells were treated with SAG or CYC 24h before the experiment, fixed and stained with specific antibodies against PALD1, SMO and ac-tub. The scale bar shows a distance of  $2\mu\text{m}$ . (B) Quantification of ciliary SMO signals in IMCD3 cells after treatment with CYC in a time course over 24h (images not shown). The SMO signals relative to ac-tub in RFU were quantified with 30 cilia per condition ( $n = 30$ ). Shown are violin plots, the dotted lines show the quartiles, the thick black continuous line shows the median. (C) Quantification of ciliary PALD1 signals in IMCD3 cells after treatment with CYC in a time course over 24h (images not shown). PALD1 signals were quantified as described in (B; the figure was partially modified from May *et al.*, 2021).

#### 6.4. PALD1 is a cell type specific factor conserved among species.

Although numerous SHH screens have been performed, PALD1 was not identified as a potential pathway component. One could speculate that the choice of cell line might be the reason for this. Whereas 3T3 cells are commonly used as a model for SHH signaling studies because of their strong SHH response (Breslow *et al.*, 2018, Pusapati *et al.*, 2018), the proteomic screens of our laboratory were performed in IMCD3 cells (Mick *et al.*, 2015, May *et al.*, 2021). Thus, one possible hypothesis was that PALD1 is a cell type-specific factor. In this context, PALD1 might even be exclusive for the weakly SHH-responsive IMCD3 cells which will be illuminated below.

Several ciliated murine and human cell lines were examined by quantitative WB assay to perform a screen for PALD1 expression. Because some SHH signaling components change their steady-state expression levels according to active SHH signaling, such as the receptor PTCH1, cells were treated with SAG or the respective control 24h before lysate preparation (Cohen *et al.*, 2015). Cells selected for the experiment included 3T3 cells, murine, immortalized, embryonic fibroblasts (Todaro & Green, 1963) and myoblasts (C2C12 cells) which were chosen due to their proliferation and differentiation into muscle protein expressing myotubes under the influence of SHH signaling (Elia *et al.*, 2007). In previous studies, it has been demonstrated that PALD1 plays a role in insulin signaling and therefore may also be responsible for SHH independent ciliary signaling (Huang *et al.*, 2009). Because of this, MIN6 $\beta$  cells were also analyzed in terms of their steady state expression of PALD1. Two human cell lines were also included in the analysis because of the possibility that PALD1 exhibits specificity for certain organisms as well as cell type specificity. The used human cell lines were RPE cells, as they are frequently used as a model in cilia research (Phua *et al.*, 2017; Huang *et al.*, 2018; Alsolami *et al.*, 2019) and HEK cells, as they are a common model for biochemical approaches (Liu *et al.*, 2007; He *et al.*, 2018). Quantitative analysis of two to three experiments per cell line demonstrated and IMCD3 and MIN6 $\beta$  cells displayed the highest PALD1 steady state expression levels relative to a loading control. C2C12, 3T3 and HEK cells show lower PALD1 steady-state expression levels relative to a loading control whereas no PALD1 was detected in RPE cells. The expression levels of PALD1 remained independent of SHH pathway activation by SAG (Fig. 12).

These initial results suggested a cell-type specific role for PALD1, but it does not appear to be exclusive for IMCD3s. To follow up on these observations, the screened cell lines were analyzed by IF microscopy. The IF microscopy aimed to investigate if PALD1 accumulates in the primary cilia of any of the positively screened cell lines. As an additional control and to completely rule out a possible function of PALD1 in these cells, RPE cells were included in the analysis, although they did not show PALD1 steady state expression in WB.

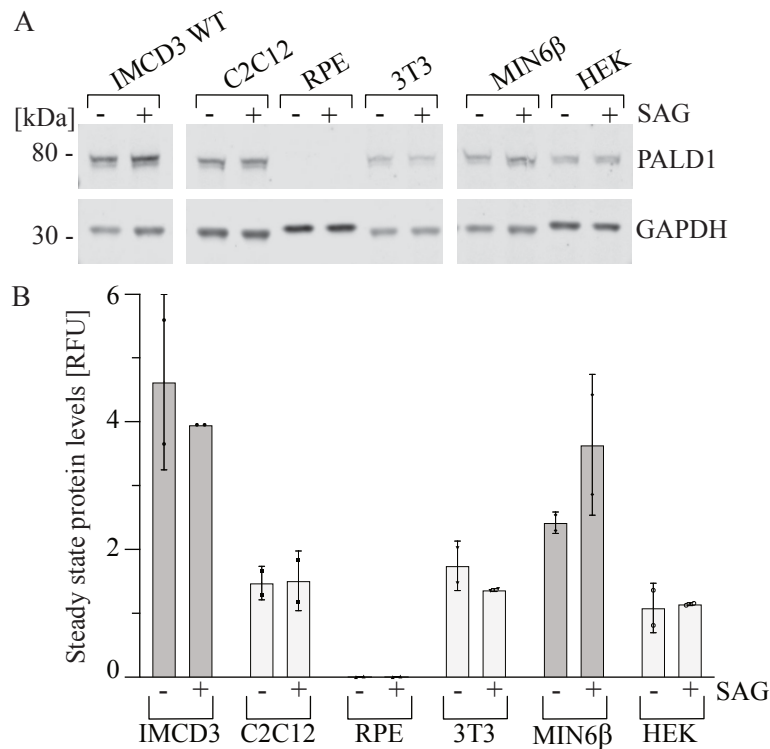


**Fig. 12: Steady state protein expression levels of PALD1 vary in dependence of the cell line.**

(A) Cell lysates of IMCD3, C2C12, RPE, 3T3, MIN6 $\beta$  and HEK cells were separated *via* SDS PAGE and analyzed in a quantitative WB. PALD1 and GAPDH were detected with specific antibodies. GAPDH was used to ensure equal loading of protein. (B) Quantification of PALD1 relative to GAPDH in RFU of 2 – 3 biological independent experiments ( $n = 2 - 3$ ) from (A). Shown are mean values in a bar diagram. Dots show individual values and error bars show SD (reanalyzed after May *et al.*, 2021).

As expected, there was no ciliary accumulation of PALD1 detected in RPE cells after activation of SHH signaling (Fig. 13 A). In C2C12 cells, PALD1 accumulated in primary cilia after treatment with SAG (Fig. 13 B). Consequently, quantification of ciliary signals for PALD1 relative to ac-tub at different time points after treatment with SAG was performed for C2C12 cells and showed a significant increase in signal (Fig. 13 C). However, the observed time dependent kinetics differed from the previously reported kinetics for PALD1 accumulation in IMCD3 cells (May *et al.*, 2021). This observation could have technical reasons or indicate differences within the exact molecular mechanisms. Despite successful SHH activation detected by accumulation of SMO *via* antibody staining, no ciliary PALD1 accumulation was observed in 3T3 cells (Fig. 13 D). For MIN6 $\beta$ , neither ciliary PALD1 nor SMO accumulation was detected in primary cilia. This lack of accumulation of both investigated SHH components may indicate an inability to respond to SHH signals for MIN6 $\beta$  cells. To investigate this theory, cells were stimulated with both SAG and Shh-N, neither of which produced a measurable SHH response (Fig. 13 E). Whereas previous studies successfully examined the cilia of HEK cells (Vien *et al.*, 2020), the attempt made in this work to elicit sufficient ciliation in HEK cells failed. Thus, the responsiveness of HEK cells to SHH signals as well as possible accumulation of PALD1, could not be conclusively assessed (data not shown).

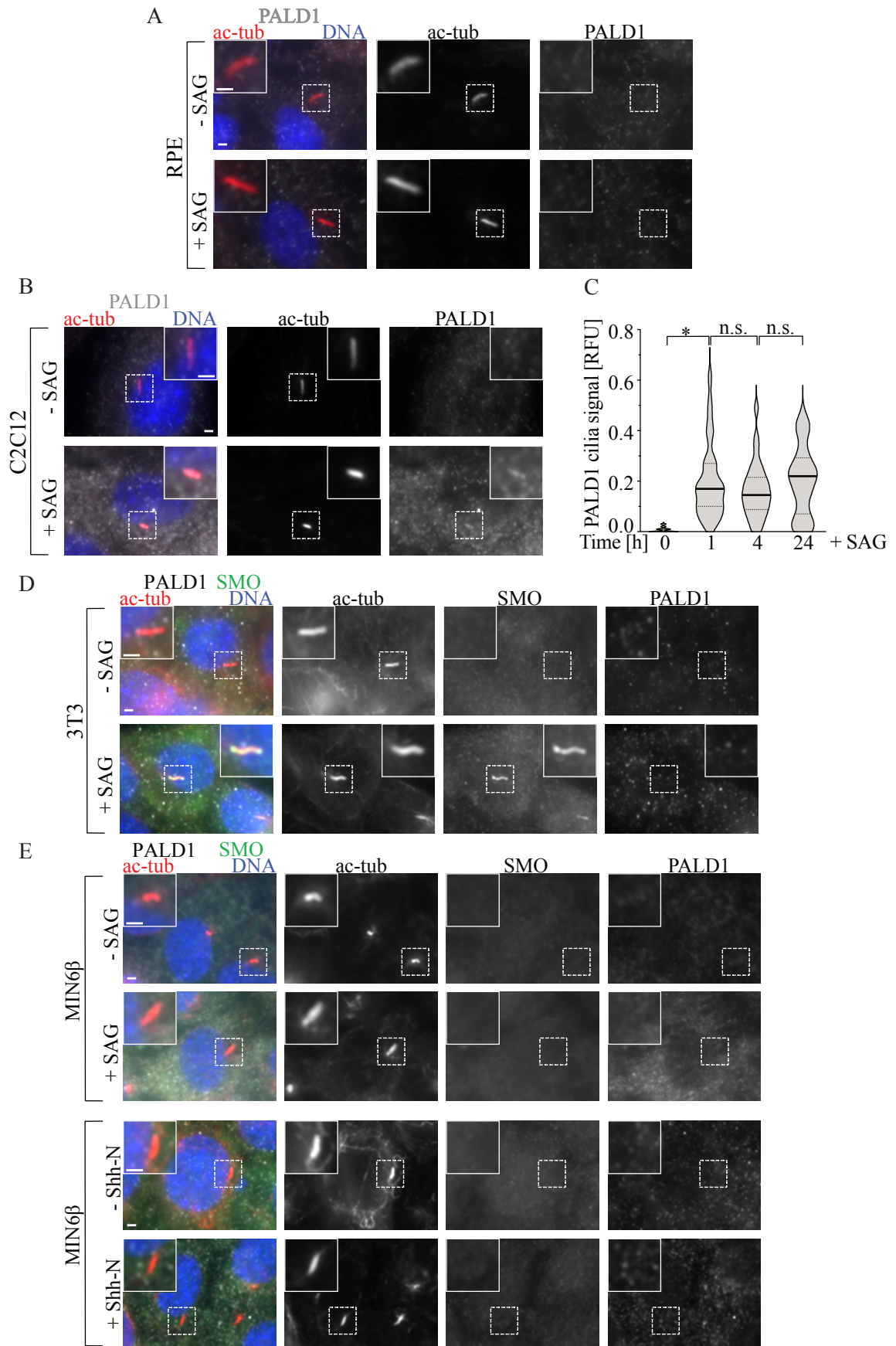


**Fig. 13: Accumulation of PALD1 was observed in primary cilia of C2C12 cells but in no other cell line.**

(A) Representative IF micrographs of RPE cells treated with SAG 24h prior to IF microscopy. After fixation, cells were stained with antibodies against PALD1 and ac-tub. (B) Representative IF micrographs of C2C12 cells. The experiment was performed as described in (A). (C) Primary cilia of C2C12 cells were analyzed for different time points after the addition of SAG. Ciliary PALD1 signals of 30 cilia per condition (n = 30) relative to ac-tub were analyzed in RFU. Statistic significance was assessed by one-way-ANOVA and Tukey's multiple comparisons test. Shown are violin plots, the dotted lines show the quartiles, the thick black continuous line shows the median (B and C were modified from May *et al.*, 2021). (D) 3T3 cells were fixed and stained with antibodies against PALD1 and SMO 24h after treatment with SAG. Shown are representative IF micrographs. (E) Representative IF micrographs of MIN6 $\beta$  cells treated with SAG, Shh-N or respective controls. 24h after treatment MIN6 $\beta$  cells were fixed and stained with antibodies against SMO and PALD1. All scale bars show 2 $\mu$ m.

These results suggested that PALD1 is not exclusive for IMCD3 cells which raised the question whether PALD1 is conserved between species. This was tested in a comparative analysis using the online available algorithm CLIME (Clustering by Inferred Models of Evolution). In a first step, CLIME clusters genes in evolutionarily conserved modules (ECM) based on a combination of statistic models and algorithms (Li *et al.*, 2018). Next, CLIME performs an expansion step in which the algorithm evaluates and ranks other genes that might have co-evolved with the gene of interest (Li *et al.*, 2014). This expansion is based on a log-likelihood ratio test, a test that compares the fit of two models to reduce errors based on uncertainties of the evolutionary tree structure (Li *et al.*, 2014, Li *et al.*, 2018). Genes with similar functions are often gained or lost at similar time points of evolution (Pellegrini *et al.*, 1999, Kensche *et al.*, 2008). Identifying co-evolution of genes is therefore an important tool to predict possible functions of unknown genes.

PALD1 is conserved between organisms. The corresponding gene is present in species that possess both primary cilia and motile cilia e.g. *Homo sapiens*. It is therefore striking that *C. elegans*, which have only primary cilia, do not have a PALD1 gene whereas species such as *Nematostella vectensis*, which possess exclusively motile cilia, do have a PALD1 gene. Interestingly, PALD1 was clustered with the intraflagellar transport component IFT25, which is conserved between some but not all species. Individual IFT proteins can be assigned to one of two defined protein complexes that differ not only in composition but also in their function. In the past, IFT-A and IFT-B were differentiated mainly on their function in retrograde and anterograde transport or in the import and export of cargoes, respectively. However, since there are some exceptions to these rules, the characterization cannot be done entirely on this basis (Nakayama & Katoh, 2020). IFT25 is assigned to the IFT-B complex and is not essential for cilia formation, however is involved in SHH signaling (Eguether *et al.*, 2018). Other cilia-associated proteins clustered with PALD1 were the cilia- and flagella-associated protein 54 (CFAP54), the tubulin detyrosinases vasohibin-1 and -2 (VASH1/2), the dihydroxylase OFD1 the centriolar protein (CEP19) and the Phosphatases PHOSPHO1 and PHOSPHO2 (Roberts *et al.*, 2004; Fig. 14). CFAP54 is a ciliary protein that has previously been associated with motility defects of cilia in mice (McKenzie *et al.*, 2015). VASH1/2 are tubuliny1-tyr-carboxypeptidases (Nieuwenhuis *et al.*, 2017) whereas PHOSPHO1/2 are members of the haloacid dehalogenase phosphatase superfamily that has no resemblance with protein-

tyrosine phosphatases and thus are independent of PALD1 (Baldwin *et al.*, 2001; Roberts *et al.*, 2004). CEP19 is a cilia-associated protein that plays a role in cilia assembly, where it recruits RAB GTPases and binds IFT-B complexes to initiate ciliation (Kanie *et al.*, 2017; Nishijima *et al.*, 2017). Surprisingly, no co-clustering with SMO could be observed in the analysis, suggesting a function of PALD1 that is distinct from that of SMO.

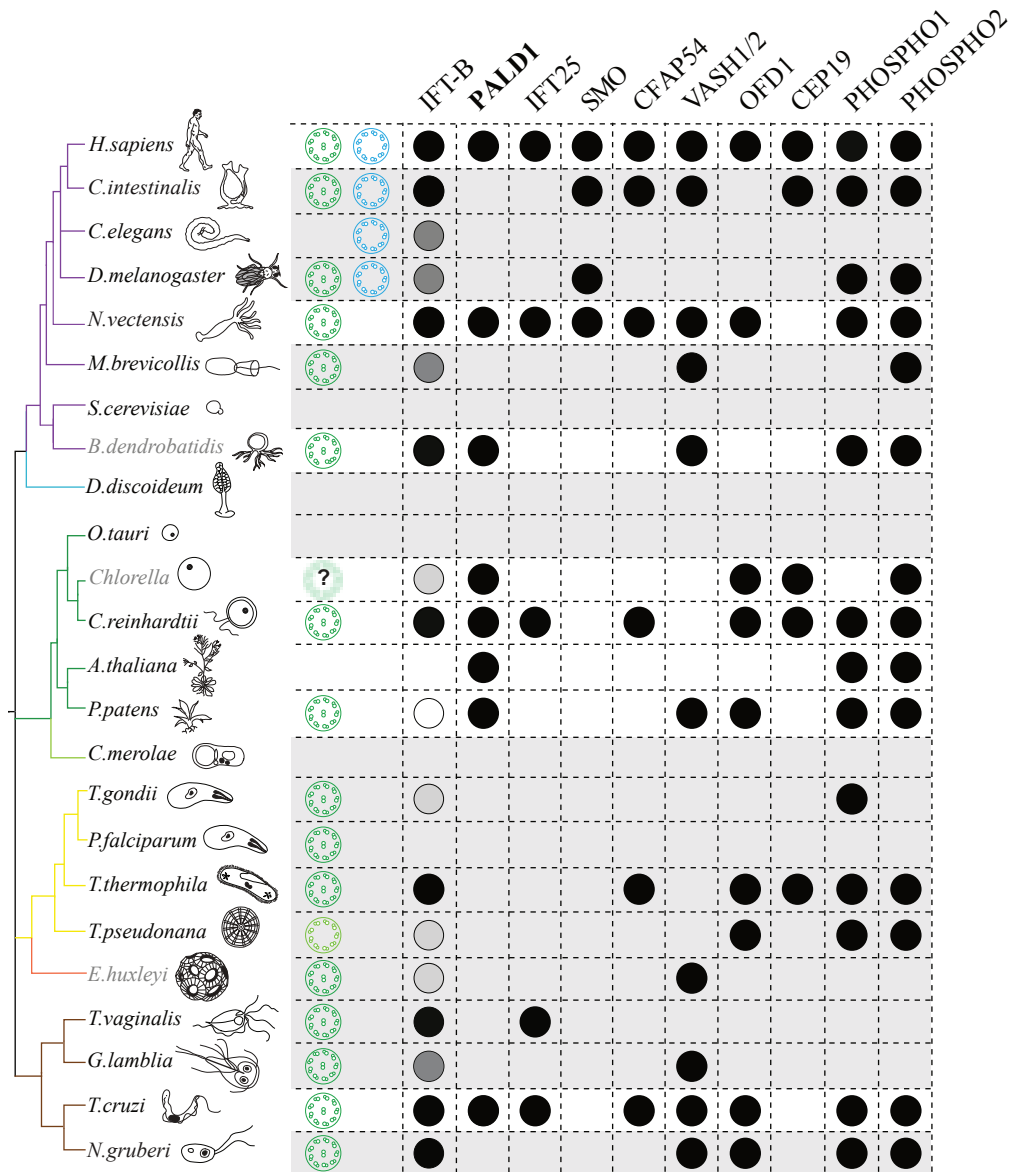


**Fig. 14: Co-evolutionary analysis of PALD1.**

Species from all clades of life were analyzed using gene CLIME (Li *et al.*, 2014, Li *et al.*, 2018). The simplified phylogenetic tree shows different groups of eukaryotic organisms in different colors (purple: *Ophisthokonts*, blue: *Amoebozoa*, green: plants, yellow: *Alveolates* and *Heterokonts*, orange: *Haptophytes*, brown: *Excavates*; modified from Carcalho-Sanots *et al.*, 2010). Primary cilia are shown in blue, motile cilia are shown in green. Organisms written in grey font were analyzed via NCBI gene blast. Proteins with E-values above  $10^{-25}$  were scored as co-clustering hits. The black circles indicate hits while IFT-B complex subunits are indicated by different shades of gray (black 100 %; dark gray < 100 %; light gray < 60 %, white < 30 %; modified from May *et al.*, 2021, figure after Carvalho-Santos *et al.*, 2010; Shida *et al.*, 2010).

The CLIME analysis confirmed that PALD1 is conserved among of all life clades. Nevertheless, the function and the role of PALD1 continued to remain enigmatic. PALD1 was clustered with intraflagellar transport components and other ciliary proteins that perform essential functions within the cilium but initially show little functional similarity to PALD1. As the clustered phosphatases show no similarity to PT phosphatases, the question arises whether PALD1 fulfills its role in SHH signaling independent of its potential phosphatase function. In addition, it remains unclear in which form PALD1 and IFT25 might interplay. To investigate these questions, an IMCD3 *Ift27*<sup>-/-</sup> cell line (Liew *et al.*, 2014) was tested for PALD1 and SMO accumulation. This cell line was chosen because PALD1 clustered in the gene CLIME analysis most strongly with IFT25 which forms a complex with IFT27. Upon loss of IFT27, IFT25 is also degraded, which is why both components, IFT25 and IFT27, are absent in a corresponding IMCD3 *Ift27*<sup>-/-</sup> cell line. (Keady *et al.*, 2012).

In previous studies, IFT27 was shown to mediate export of SMO from the primary cilium (Eugether *et al.*, 2018) which is consistent with the observation made here. Comparisons between IMCD3 cells (WT) and IMCD3 *Ift27*<sup>-/-</sup> cells were made, and each cell line was treated with SAG to induce SHH signaling and stained with antibodies against PALD1 and SMO 24h after treatment. It was evident that SMO accumulation was significantly increased in the cilia of IMCD3 *Ift27*<sup>-/-</sup> cells as compared to WT cells. This was true in both absence and presence of the SHH stimulating reagent SAG, which leads to further enhancement of ciliary SMO accumulation (Fig. 15A and B). In contrast, no significant accumulation of PALD1 was observable in either the presence or absence of SAG, suggesting that SHH-mediated accumulation of PALD1 is dependent of IFT27 and consequently IFT25 (Fig. 15A and C). These interesting first insights on the molecular mechanism of PALD1 accumulation raises the question whether PALD1 has a functionally similar role to IFT25/IFT27.

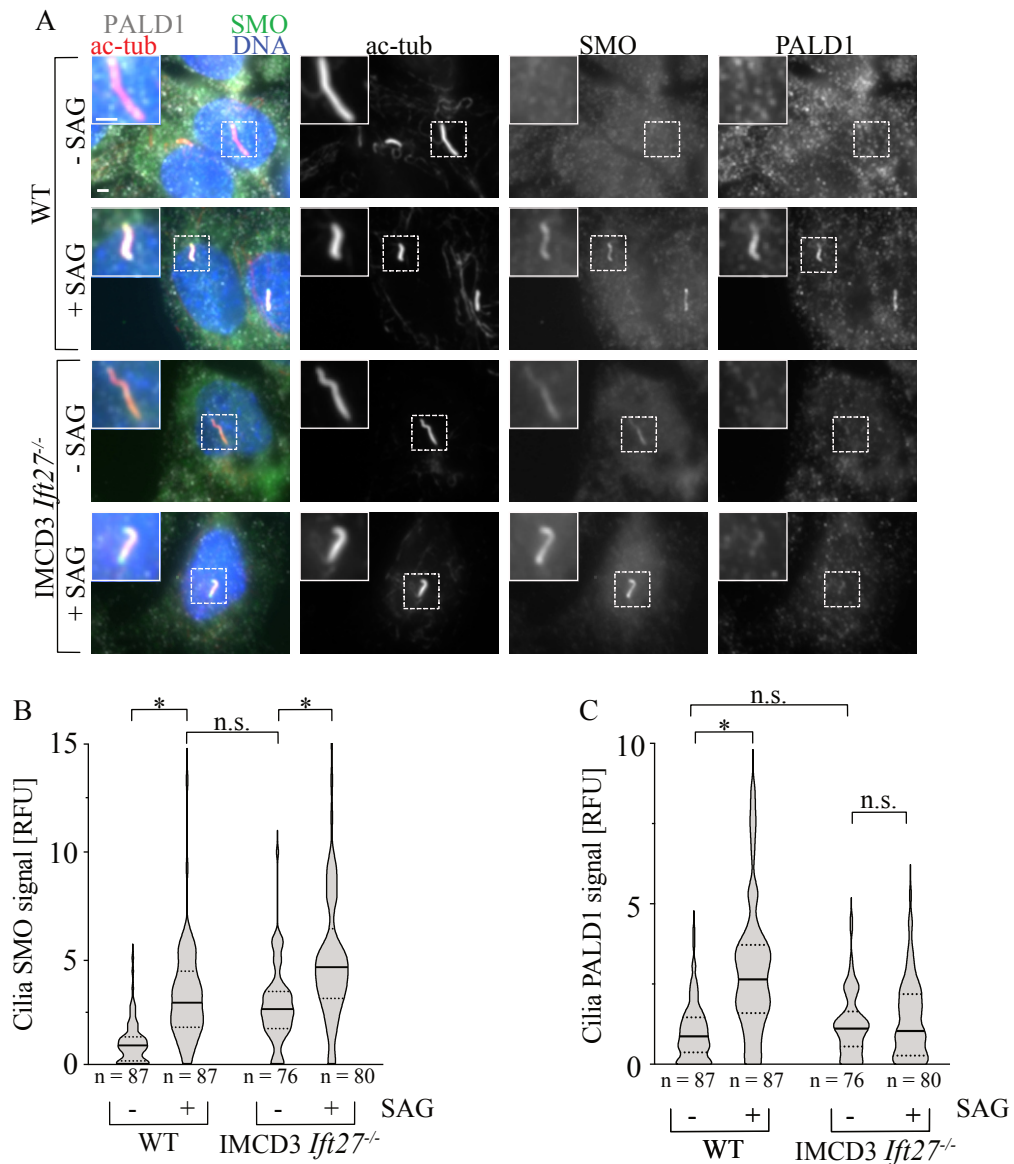


**Fig. 15: PALD1 accumulation is impaired in the IMCD3 *Ifi27*<sup>-/-</sup> cell line.**

(A) Representative IF micrographs of WT and IMCD3 *Ifi27*<sup>-/-</sup> cells treated with SAG or vehicle 24h before IF microscopy. After fixation, cells were stained with antibodies against PALD1, SMO and ac-tub. (B) Cilia signals of SMO were quantified from three independent replicates, 20 – 30 cilia per condition and per experiment relative to ac-tub in RFUs from WT and IMCD3 *Ifi27*<sup>-/-</sup> cells ( $n_{\text{Total}} = 76 - 87$ ). Shown are violin plots, the dotted lines show the quartiles, the thick black continuous line shows the median. Statistic significance was assessed by two-way ANOVA and Tukey's multiple comparison test. (C) PALD1 cilia signals of WT and IMCD3 *Ifi27*<sup>-/-</sup> cells were quantified and analyzed as described in (B).



### 6.5. IMCD3 *Pald1*<sup>-/-</sup> cells show mild pre-activation phenotype.

To obtain information on the physiological function of PALD1, a *Pald1* knockout cell line was generated in IMCD3 cells using the CRISPR-Cas9 system. The exon 4 was targeted for appropriate DNA editing *via* CRISPR-Cas9, which induces an early termination of translation. The cDNA of the resulting cell clones was sequenced and they were further examined for complete knockout of *Pald1* based on detection of PALD1 in quantitative fluorescence WB analysis. Sequencing confirmed early protein ablation due to a nonsense mutation while WB analysis confirmed loss of PALD1 (Fig. 16A and B). The cell line generated will be referred to as IMCD3 *Pald1*<sup>-/-</sup> in the following.

Further, the expression of IFT88 and PTCH1 in the presence and absence of Shh-N was examined in steady state by antibody detection in the quantitative fluorescence WB analysis (Fig. 16 B). No significant changes were detected in IMCD3 *Pald1*<sup>-/-</sup> cells for IFT88 or PTCH1 compared to the parental cell line (WT). Also, the correct localization of IFT88 was examined with IF microscopy and no differences were detected in IMCD3 *Pald1*<sup>-/-</sup> when compared with the WT cells (Fig. 16 C). In addition, cilia length was analyzed and showed a significant reduction by approximately 15%. Strikingly, the cilia length of the *Pald1* knockout cell line was not only shorter on average, but also the lengths were more homogeneously distributed than those of the WT cells (Fig. 16 D).

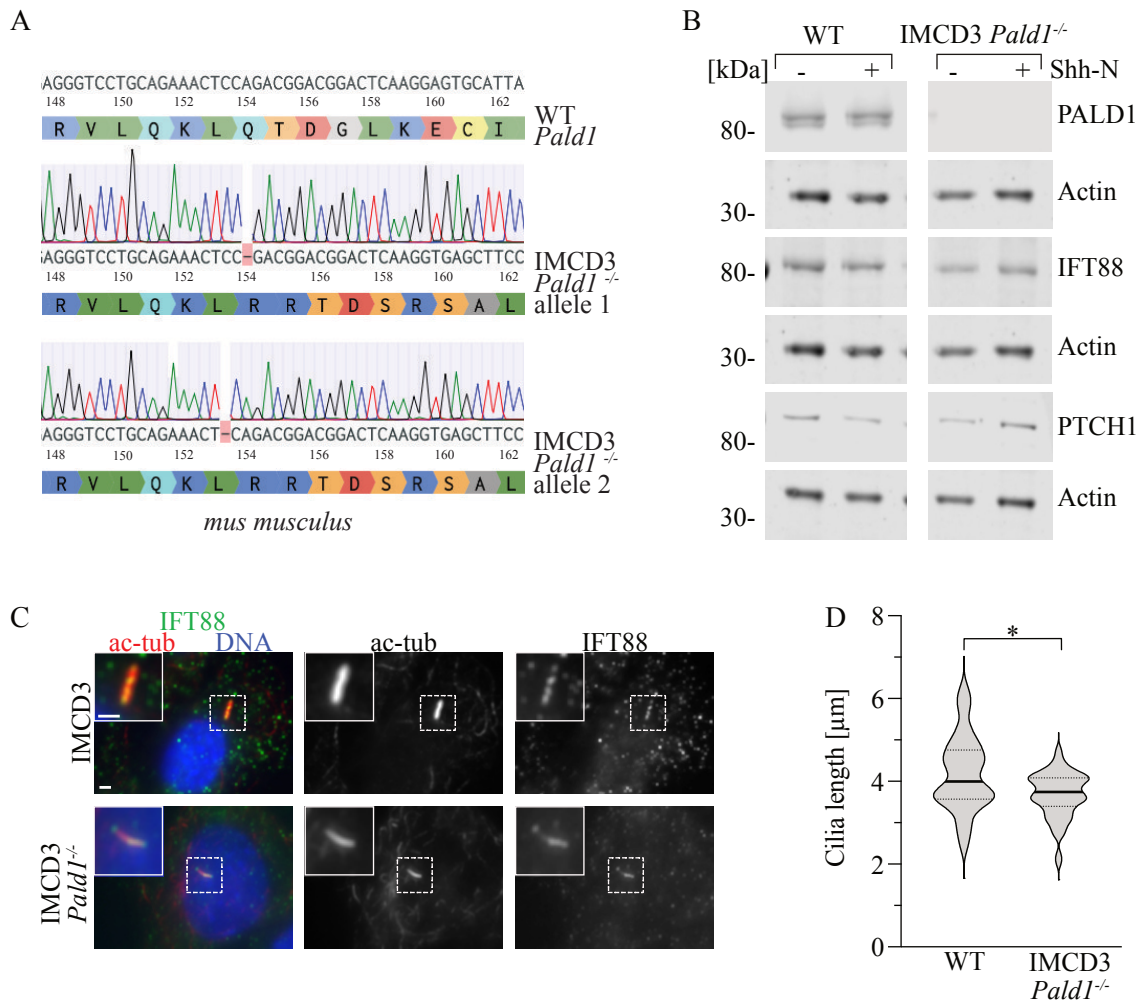


**Fig. 16: Generation of a IMCD3 *Pald1*<sup>-/-</sup> cell line and analysis in comparison to WT cells.**

(A) Sequencing of the cDNA from the generated IMCD3 *Pald1*<sup>-/-</sup> cell line confirmed early protein ablation due to a nonsense mutation. (B) Cell lysates were separated *via* SDS-PAGE and transferred in a quantitative fluorescence WB. PALD1, IFT88, PTCH1 and Actin were detected with specific antibodies. Actin was detected to ensure equal loading of protein. (C) WT and IMCD3 *Pald1*<sup>-/-</sup> cells were fixed and stained with antibodies against IFT88 and the cilia marker ac-tub. Localization of the ciliary protein IFT88 remained unaffected in IMCD3 *Pald1*<sup>-/-</sup> compared to WT cells. The scale bar shows 2μm (D) Cilia length of WT and IMCD3 *Pald1*<sup>-/-</sup> cells was assessed based on (B). Shown are violin plots, the dotted lines show the quartiles, the thick black continuous line shows the median. Statistic significance was assessed by an unpaired t-test,  $p < 0.0002$  (modified from May *et al.*, 2021).

During embryonic development, cell fates such as ventralization or dorsalization in the neural tube are determined by specific signaling pathways. SHH signaling, when activated, determines the ventralization of cells (Gigante & Caspar, 2020). This is designated by ratios of certain transcription factors, called glioma-associated oncogene (GLI) (Niewiadomski *et al.*, 2019). In the absence of SHH-stimulating signal, the GLI3 transcription factor is post-translationally modified and proteolytically cleaved into a repressor form (GLI<sup>R</sup>). Upon induction of SHH signaling, e.g. by Shh-N, the modifying enzymes are inhibited, leading to disruption of proteolytic cleavage and consequent increase in GLI3 full-length (GLI3<sup>FL</sup>). The repression of SHH target genes by GLI3<sup>R</sup>, such as the additional GLI

transcription factor GLI1, is thus stopped, and the signaling pathway is activated (Niewiadomski *et al.*, 2019; Gigante & Caspary, 2020).

Based on the mechanisms described, the ratio of GLI3<sup>FL</sup>/GLI3<sup>R</sup> can be used as an indicator of active SHH signaling. In this case, high values for the GLI3<sup>FL</sup>/GLI3<sup>R</sup> ratio indicate an active SHH signaling pathway, whereas low ratios indicate an inhibition of signaling (Niewiadomski *et al.*, 2019; Gigante & Caspary, 2020). For each cell line, these values must be considered in relation to corresponding controls to make a conclusive statement. In the following experiment, the GLI3<sup>FL</sup>/GLI3<sup>R</sup> ratio was assessed by quantitative WB analysis using an antibody that detects the GLI3<sup>FL</sup> and the GLI3<sup>R</sup> forms (Fig. 17 A). Quantification of three independent experiments and consideration of the respective ratios relative to the WT control of each experiment showed that IMCD3 *Pald1*<sup>-/-</sup> has significantly increased GLI<sup>FL</sup>/GLI<sup>R</sup> ratios compared to the WT. Effectively, GLI<sup>FL</sup>/GLI<sup>R</sup> in +Shh-N WT is not significantly different from IMCD3 *Pald1*<sup>-/-</sup> -Shh-N. This indicates that untreated IMCD3 *Pald1*<sup>-/-</sup> exhibits a state of active SHH signaling without induction. After addition of Shh-N, the GLI<sup>FL</sup>/GLI<sup>R</sup> ratio in WT and IMCD3 *Pald1*<sup>-/-</sup> increases significantly (Fig. 17 B). This suggests that although IMCD3 *Pald1*<sup>-/-</sup> is pre-activated in absence of signal, further activation can still occur after treatment with SHH inducing reagents. These experiments provide a first indication of the function of PALD1 as a negative regulator or attenuator of SHH signaling.

The described observations and conjectures raise the question whether other SHH signaling components that function upstream of GLI proteins might be altered by the loss of PALD1. The orphan receptor GPR161 is a major SHH signaling negative regulator that accumulates in the primary cilia of unstimulated cells. By activating Gα<sub>s</sub>-proteins, GPR161 stimulates adenylyl cyclases (Mukhopadhyay *et al.*, 2013). Thus, the increased cAMP level contributes to the modification and processing of GLI3 by activating PKA (Tschaikner *et al.*, 2020). SMO, the main SHH positive effector, accumulates in the primary cilia of stimulated cells upon signaling pathway activation. As it has previously been shown, SMO also co-accumulates with PALD1 and belongs to a different class of GPCRs than GPR161 (Tschaikner *et al.*, 2020; May *et al.*, 2021). SMO activates a Gα<sub>i</sub>-protein which results in the inhibition of adenylyl cyclases (Tschaikner *et al.*, 2020). Subsequently, cAMP levels decrease which results in inhibition of GLI3 processing. Decreasing cAMP inhibits PKA, which phosphorylates GLI3 modification and results in processing of GLI3<sup>FL</sup> and consequent transformation to GLI3<sup>R</sup> (Niewiadomski *et al.*, 2019). To examine a possible effect of PALD1 on the distribution of SHH dependent GPCRs such as SMO and GPR161, WT and IMCD3 *Pald1*<sup>-/-</sup> cells were analyzed *via* IF microscopy.

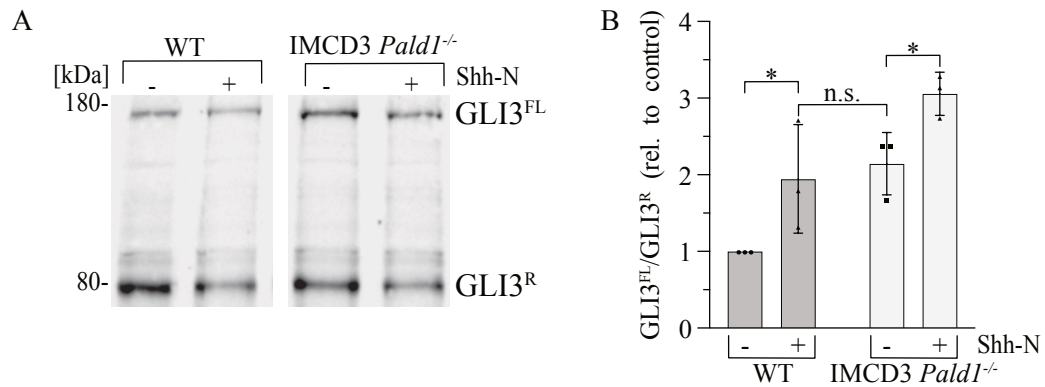


**Fig. 17: GLI3<sup>FL</sup>/GLI3<sup>R</sup> in IMCD3 *Pald1*<sup>-/-</sup> cells indicates pre-activation of SHH signaling after loss of PALD1.**

(A) WT and IMCD3 *Pald1*<sup>-/-</sup> cells were treated for 24h with Shh-N. Lysates were separated via SDS-PAGE and analyzed in a quantitative fluorescence WB assay. GLI3<sup>FL</sup> and GLI3<sup>R</sup> were detected by staining with one specific antibody against both versions GLI3. (B) Quantification of the GLI3<sup>FL</sup> and GLI3<sup>R</sup> bands from three independent experiments (n = 3) confirms pre-activation of IMCD3 *Pald1*<sup>-/-</sup> cells. GLI3<sup>FL</sup>/GLI3<sup>R</sup> ratios were calculated and internally normalized to the respective untreated WT for each experiment (WT - Shh-N = 1). Statistic significance was assessed by two-way-ANOVA with Tukey's multiple comparison test, p < 0.05. Shown are mean values with SD, dots indicate single values (modified from May *et al.*, 2021).

The two SHH effectors GPR161 and SMO principally show a normal localization in IMCD3 *Pald1*<sup>-/-</sup> that is comparable to WT cells. While GPR161 is depleted from the cilium after induction with SAG, SMO accumulates in IMCD3 *Pald1*<sup>-/-</sup> similar to WT primary cilia (Fig. 18 A). Quantification of the ciliary signals displays no significant changes in SMO accumulation between WT and IMCD3 *Pald1*<sup>-/-</sup> cells (Fig. 18 B). However, GPR161 quantification of three biologically independent experiments reveals that ciliary GPR161 signals are reduced in unstimulated IMCD3 *Pald1*<sup>-/-</sup> cells compared to unstimulated WT cells by approximately 30 – 40 % (Fig. 18 C). Because GPR161 is a negative regulator of SHH signaling, these results agree with the previous observation that IMCD3 *Pald1*<sup>-/-</sup> cells show a SHH signaling pre-activated phenotype. Moreover, reduced ciliary GPR161 levels could be the cause of the observed pre-activation in IMCD3 *Pald1*<sup>-/-</sup> cells.

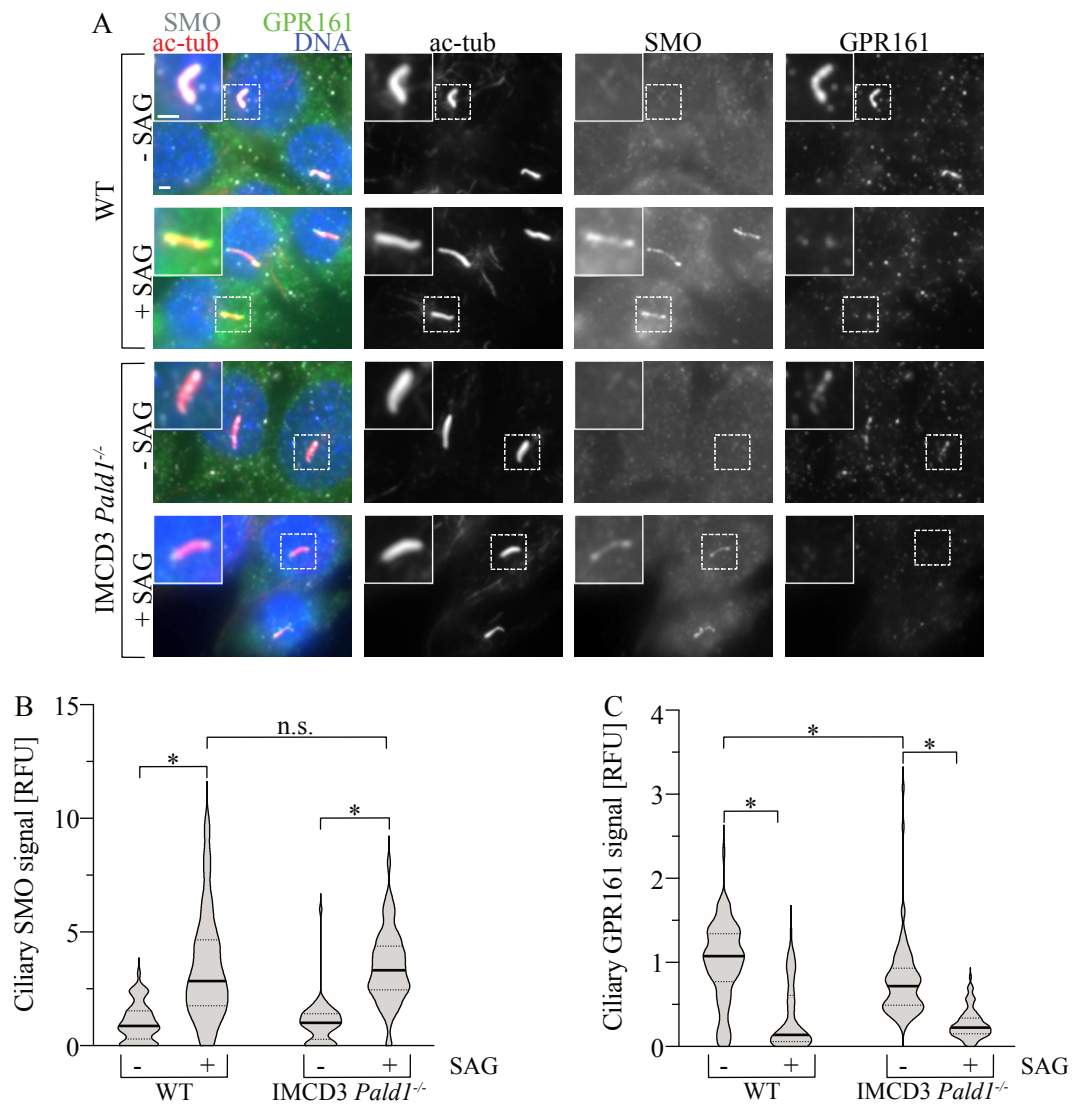


**Fig. 18: Ciliary GPR161 signals in IMCD3 *PalD1*<sup>-/-</sup> are decreased in unstimulated cells compared to WT cells.**

(A) Representative IF micrographs of fixed WT and IMCD3 *PalD1*<sup>-/-</sup> cells stained with antibodies against GPR161, SMO and ac-tub. Cells were treated with SAG for 24h. The scale bar shows a distance of 2 $\mu$ m. (B) Quantification of cilia signals of SMO relative to ac-tub in RFU. 30 ciliary signals were quantified per condition from a total of 2 biologically independent experiments ( $n_{\text{Total}} = 60$ ). Shown are violin plots, the dotted lines show the quartiles, the thick black continuous line shows the median. Statistic significance was assessed by two-way ANOVA with Tukey's multiple comparison test. (C) Quantification was done for GPR161 as described in (B) for SMO cilia signals. Statistic significance was assessed by two-way ANOVA with Tukey's multiple comparison test from 30 cilia quantified per condition for three independent experiments ( $n_{\text{Total}} = 90$ ). GPR161 signals were significantly reduced in unstimulated IMCD3 *PalD1*<sup>-/-</sup> cells. Statistic significance was assessed by two-way ANOVA with Tukey's multiple comparison test (reanalyzed after May *et al.*, 2021).

With respect to SMO, induction with SAG most probably bypasses effects by the loss of PALD1 on SMO by direct binding of SAG to SMO. For this reason the experiment was repeated by treating cells with Shh-N instead of SAG. When the experiment was repeated upon treatment with Shh-N, a

significant reduction in GPR161 was again observed in unstimulated WT cells as compared to unstimulated IMCD3 *Pald1*<sup>-/-</sup> cells (Fig. 19 B). In addition, the accumulation of SMO in the cilium was significantly increased for IMCD3 *Pald1*<sup>-/-</sup> cells after stimulation (Fig. 19 C), suggesting a stronger SHH signaling activation of the IMCD3 *Pald1*<sup>-/-</sup> cell lines compared to WT cells.

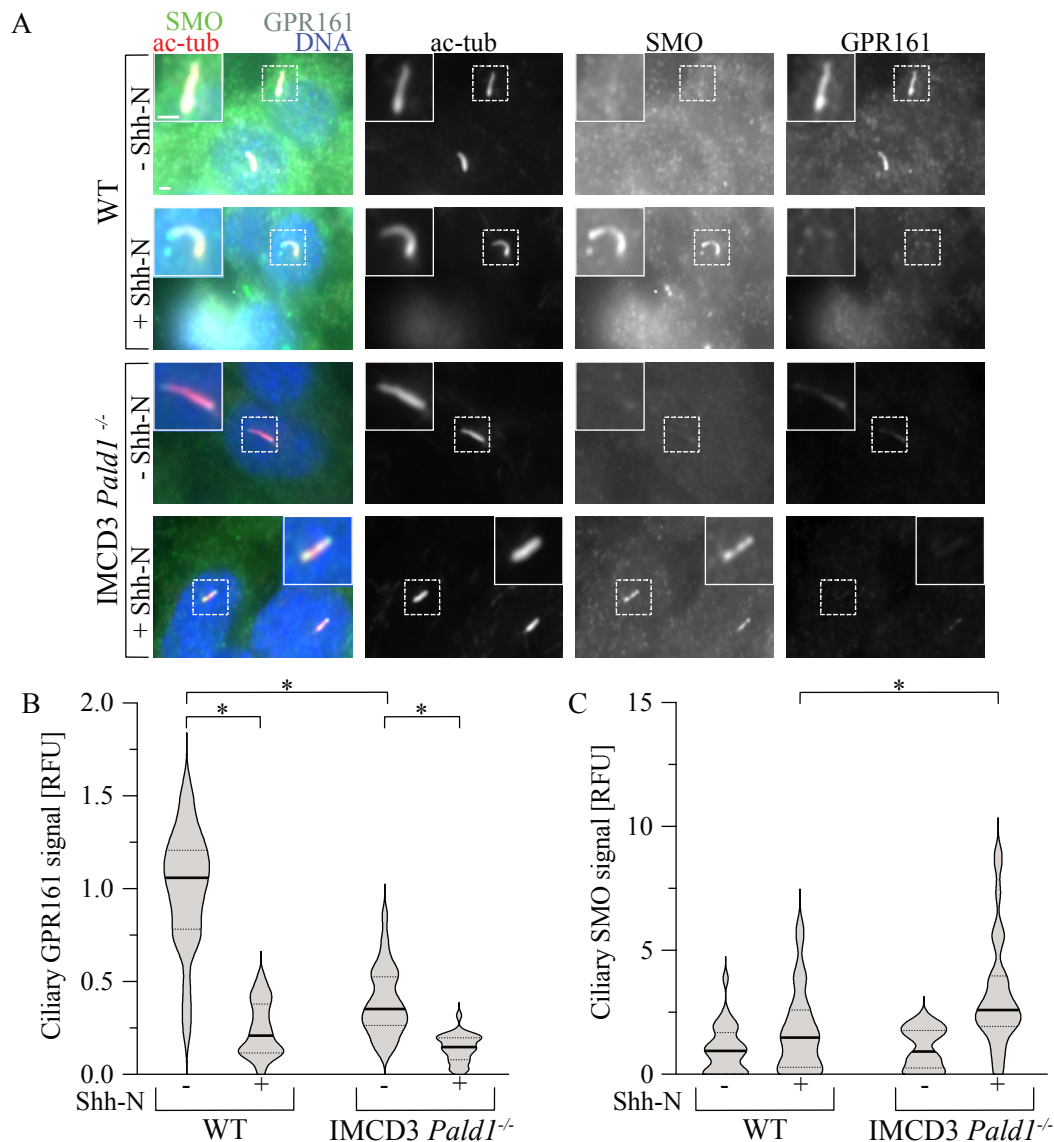


**Fig. 19: SMO accumulation is increased in IMCD3 *Pald1*<sup>-/-</sup> cells compared to WT cells after induction with Shh-N.**

(A) Representative IF micrographs of fixed WT and IMCD3 *Pald1*<sup>-/-</sup> cells stained with antibodies against GPR161, SMO and ac-tub. Cells were treated with Shh-N for 24h before fixation. The scale bar shows 2 μm. (B) Quantification of cilia signals of GPR161 relative to ac-tub in RFU of 30 cilia per condition from two independent experiments ( $n_{\text{Total}} = 60$  cilia) in WT and IMCD3 *Pald1*<sup>-/-</sup> cells. Shown are violin plots, the dotted lines show the quartiles, the thick black continuous line shows the median. Statistic significance was assessed by two-way-ANOVA with Tukey's multiple comparison test. (C) Quantification and analysis of ciliary SMO signals was done as described in (B).

All in all, these findings further suggest a negative regulating role of PALD1 in SHH signaling. The phenotypes observed after loss of PALD1, however, are much milder than those observed after the loss of other proteins that negatively regulate SHH signaling e.g. PTCH1 and SUFU. In the absence of these key negative regulators, SHH signaling is fully activated to a degree that cells are not responsive to SHH signaling activating reagents (Pusapati *et al.*, 2018). Consequently, PALD1 is suspected to possess a mediating role in SHH signaling. In that case, PALD1 may function as an attenuator of the SHH pathway. The fine modulating role of PALD1 in the SHH signaling pathway could be an additional explanation why PALD1 was not detected in previous SHH screens. Additionally, proteins positively interfering with SHH signaling are easier to identify than those that negatively regulate the signaling pathway (Breslow *et al.*, 2018).

## 6.6. Molecular mechanisms of PALD1 accumulation.

Having obtained initial information on the possible role of PALD1, the next question was how PALD1 mediates SHH signaling. PALD1 appears to be an SHH signaling attenuator that affects GPCR trafficking, as concluded from the decreased ciliary GPR161 levels. Therefore, a link to other components of the SHH pathway that also affect GPCR trafficking is possible. An important negative SHH signaling regulator is the Tubby-related protein (TULP3). TULP3 recruits the GPCR GPR161 to the cilium and in this way, inhibits SHH signaling. A functional antagonist of TULP3 when SHH signaling is activated is  $\beta$ -arrestin. This protein mediates the BBSome-dependent exit of GPR161 from the cilium, by recognizing phosphorylation of GPR161 and initiating exit (Nachury, 2018). To investigate a possible link between PALD1 and these two components of GPCR trafficking, IMCD3 *Tulp3*<sup>-/-</sup> and IMCD3  *$\beta$ -Arrestin1/2*<sup>-/-</sup> ( *$\beta$ -Arr1/2*<sup>-/-</sup>) cells were treated with SAG for 24h before being examined by IF microscopy.

SMO accumulation was not affected in IMCD3 *Tulp3*<sup>-/-</sup> cells, IMCD3  *$\beta$ -Arr1/2*<sup>-/-</sup> cells showed a significant increase in SMO signal in absence of SHH stimuli compared to unstimulated WT cells. However, after treatment with SAG cilia SMO signal increased in IMCD3  *$\beta$ -Arr1/2*<sup>-/-</sup> cells (Fig. 20A and C). This data is consistent with previous studies (Mukhopadhyay *et al.*, 2010; Nachury, 2018). In contrast, changes in PALD1 accumulation were observed in both knock out cell lines (Fig. 20A and B). In IMCD3  *$\beta$ -Arr1/2*<sup>-/-</sup> cells, PALD1 accumulation is generally more comparable to WT cells but still shows no significant differences after induction (Fig. 20D); however, in IMCD3 *Tulp3*<sup>-/-</sup> cells, the accumulation of PALD1 is significantly impaired.

The present data indicates that PALD1 is related to GPCR trafficking, especially GPR161, which is also dependent to TULP3 and  $\beta$ -arrestins. Both GPR161 and SMO accumulation affect ciliary cAMP levels, and the latter occurs in parallel with PALD1 (Mukhopadhyay *et al.*, 2013; Praktiknjo *et al.*, 2018). Therefore, it can be assumed that the accumulation of PALD1 might also be dependent on changes in cAMP levels. In this case, there could also be a link to one of the cAMP-dependent key regulators of SHH signaling, PKA. No potential substrate of PALD1 has yet been identified, nor has any functional phosphatase activity of PALD1 been demonstrated. Consequently, the possibility that PALD1 functions as an anti- or pseudo-phosphatase should be considered (Roffers-Agarwal *et al.*, 2012; Nitzsche *et al.*, 2020). Since no catalytic activity can be detected in the class of anti-phosphatases despite structural similarities to phosphates, it has long been assumed that they consequently have no particular function. Today, we know that anti-phosphatases can regulate other enzymes, albeit especially other phosphates, by direct interaction, e.g. by blocking catalytic sites (Reiterer *et al.*, 2014). It is conceivable that PALD1 could bind kinases in analogy to a possible anti-phosphatase activity. Accordingly, a connection between PALD1 and PKA can also be suspected on the basis of a possible cAMP dependence of PALD1. The idea that PALD1 might bind PKA would be one way to explain the function of PALD1 in SHH signaling.



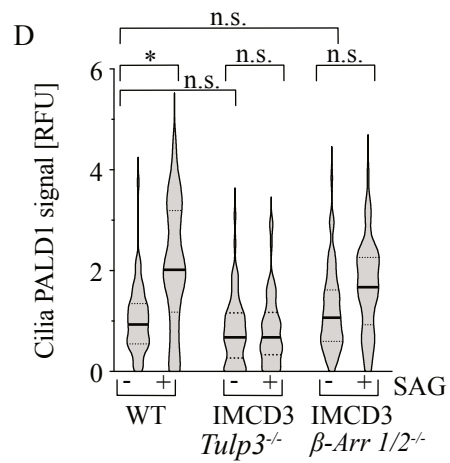
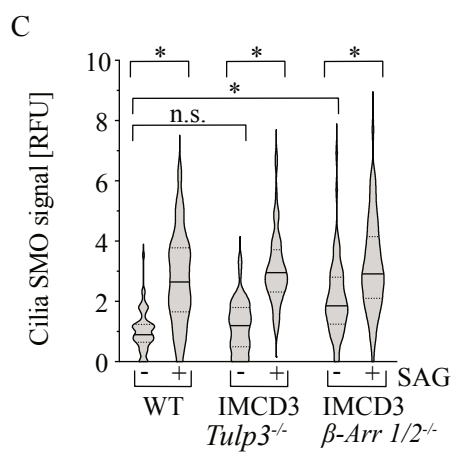
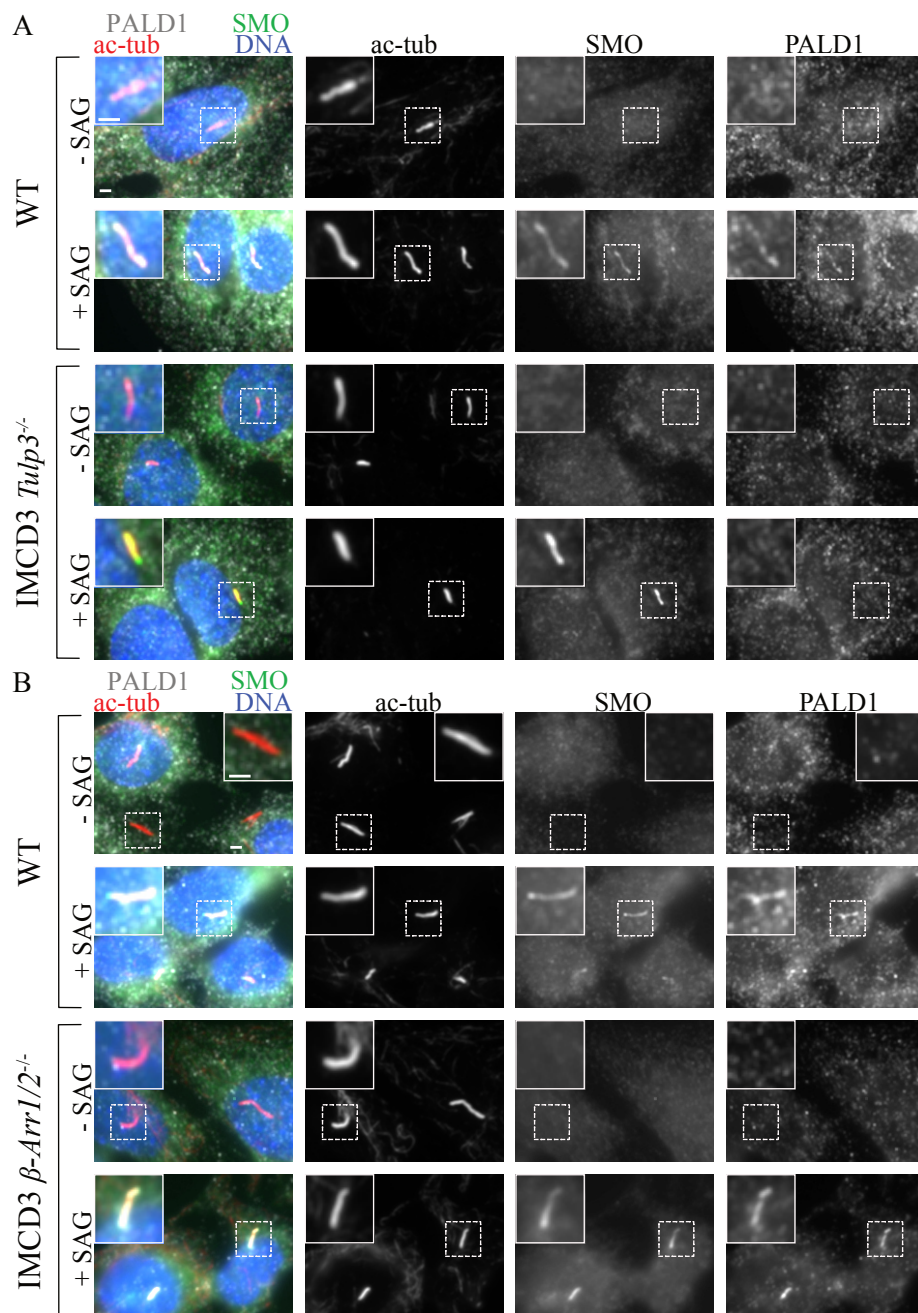


**Fig. 20: PALD1 accumulation in the primary cilium is TULP3 dependent.**

(A, B) Representative IF micrographs of WT, IMCD3 *Tulp3*<sup>-/-</sup> and IMCD3 *β-Arr1/2*<sup>-/-</sup> cells, treated 24h prior to experimentation with SAG and stained with specific antibodies against PALD1, SMO and ac-tub. The scale bar represents a distance of 2μm (C) Quantitative analysis of (A) and (B). 30 – 27 cilia signals of PALD1 were quantified per condition from two independent, biological replicates (n<sub>Total</sub> = 57 cilia). Signals were analyzed relative to ac-tub in RFUs. Statistic significance was assessed by two-way ANOVA with Sidak's multiple comparison, p < 0.0001 ((D) Quantitative analysis of (A) and (B) as described in (C) Signals were analyzed relative to ac-tub in RFU, p < 0.0001.

### 6.7. PALD1 accumulation is dependent on cAMP

The activity of PKA can be abolished in presence of a small protein kinase A inhibitory peptide (PKI) that mimics the natural substrate of PKA (Knighton *et al.*, 1991; Dalton & Dewey, 2006). For the following experiment, IMCD3 cells expressing a cilia-localized version of NPHP3[1-203]-GFP-PKI (Cilia-PKI; Mick *et al.*, 2015) were used. It has been shown that cilia localized PKI leads to ciliary PKA-C localization (unpublished data, David Mick.) Based on these observations, it can be assumed that if PALD1 binds to PKA or one of its subunits (e.g. PKA-C), PALD1 accumulation will be altered in the described cilia-PKI cell line. This could be because I.) PALD1 directly interacts with a PKA subunit and localizes to the primary cilium with the respective subunit or II.) PKA is inhibited in Cilia-PKI which in turn activates SHH signaling as GLI3 modification and subsequent processing would be abolished. Consequently, PALD1 should accumulate in the primary cilia of the Cilia-PKI cell line in the presence and absence of SHH inducing reagents. To test this hypothesis, Cilia-PKI and a control cell line expressing a PKI-4A, a 4-residue mutant that is also cilia-localized but inactivated and consequently fails to block PKA activity (Control-PKI; Mick *et al.*, 2015), were treated 24h prior to fixation with Shh-N. After that, cells were analyzed in IF microscopy with antibodies against PALD1 and ac-tub. The ciliary signals of PALD1 were evaluated relative to the cilia marker ac-tub. GFP signals confirmed localization of PKI.

Inhibition of PKA or the presence of a catalytic subunit in the cilium appears to latently decrease the presence of PALD1. This can be concluded from the fact that ciliary PALD1 levels in stimulated cilia-PKA cells are not significantly different compared with restimulated control-PKI cells (Fig. 21). However, this observation does not hinder a significant PALD1 accumulation after addition of Shh-N in Cilia-PKI and Control-PKI (Fig. 21B). Accordingly, PALD1 does not appear to be related to PKA in the way presumed. Whether PALD1 is possibly regulated analogously to PKA via changes in cAMP levels will be discussed below.

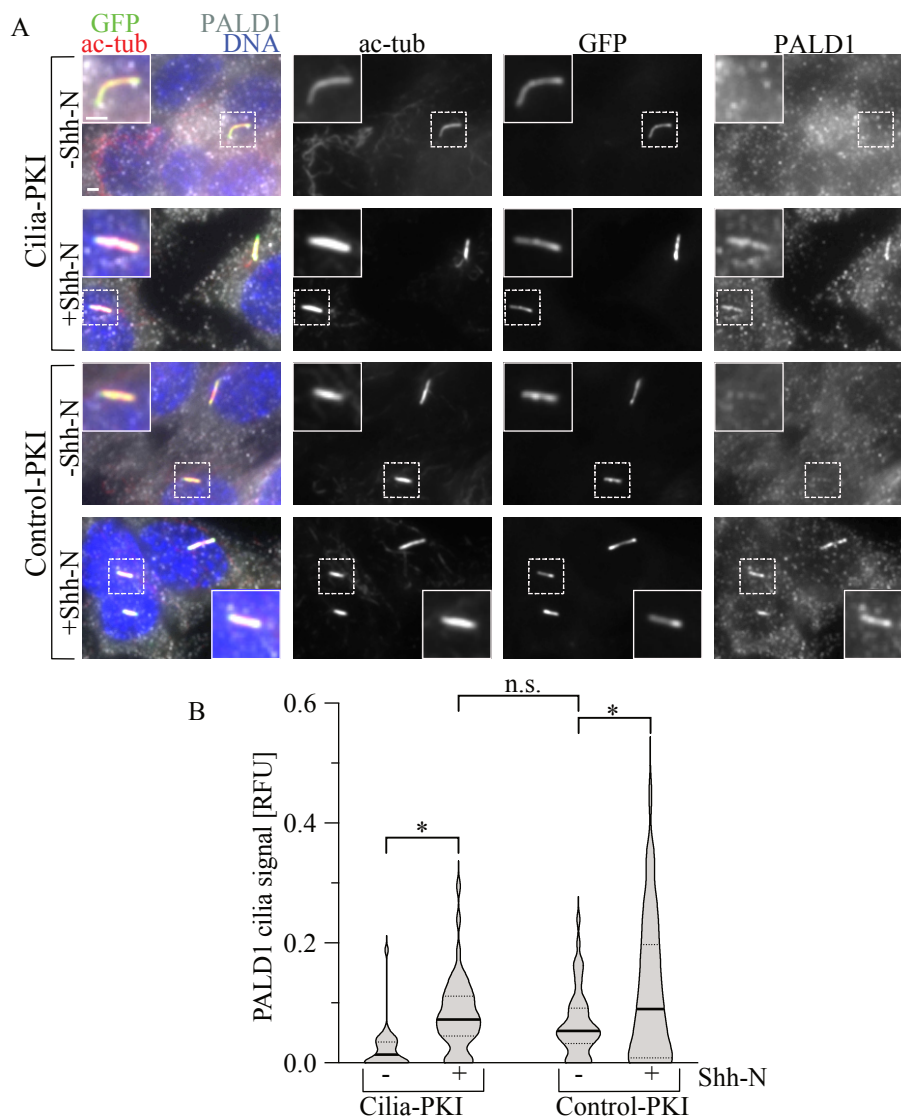


**Fig. 21: PALD1 accumulation in stimulated Cilia-PKI cells does not differ from unstimulated Control-PKI cells.**

(A) Representative IF micrographs of Cilia-PKI and Control-PKI cells. Cells were fixed and stained in the presence and absence of Shh-N with antibodies against PALD1 and ac-tub. Incubation with Shh-N was executed for 24h prior to fixation. The scale bar shows 2 $\mu$ m (B) Quantification of 30 cilia signals of PALD1 relative to ac-tub in RFUs per condition from 3 independent biological replicates ( $n_{\text{total}} = 90$  cilia). Statistic significance was assessed by two-way-ANOVA with Tukey's multiple comparison test;  $p < 0.01$ .

To address the question whether PALD1 accumulation is cAMP dependent, artificial somatostatin signaling in the cilia of IMCD3 cells was investigated. Somatostatin (sst) is an inhibitory peptide secreted by endocrine cells as well as the central nervous system (Ampofo *et al.*, 2020). Sst binds to the sst receptor (SSTR3), which regulates a variety of processes such as inhibiting the secretion of glucagon and insulin as well as inhibiting the secretion of various hormones. These processes take place through the activation of a  $G\alpha_i$ -protein and subsequent inhibition of adenylyl cyclases (Mykytyn & Askwith, 2017; Ampofo *et al.*, 2020). Hippocampal neurons express cilia-membrane localized SSTR3 (Berbari

*et al.*, 2007). As WT IMCD3 cells do not harbor SSTR3, SSTR3 was ectopically expressed and localized specifically to the cilium of IMCD3 cells to induce changes in ciliary cAMP levels upon activation (Nager *et al.*, 2017). Accordingly, the IMCD3 cell line used expresses NeonGreen (NG) labeled SSTR3 (SSTR3<sup>NG</sup>) in the primary cilium (IMCD3 SSTR3<sup>NG</sup>; Fig. 22; Nager *et al.*, 2017). After addition of sst, it binds to SSTR3 and activates the receptor. The receptor activates the G $\alpha_i$  protein, resulting in the corresponding decrease in cAMP level and is internalized afterwards for inactivation (Green *et al.*, 2015; Mykytyn & Askwith, 2017). Thus, based on the previous hypothesis that PALD1 accumulation may be cAMP dependent, activation of SSTR3 should result in a change in ciliary cAMP levels. To test the general ability of IMCD3 SSTR3<sup>NG</sup> cells to accumulate PALD1 in the primary cilium, an additional sample was treated with SAG.

After addition of sst, the receptor was activated and removed from the cilium for inactivation as expected (REF). This is evident from the loss of green signal within the cilium (Fig. 22A). Interestingly, cells treated with either SAG or sst both show ciliary accumulation of PALD1. Only after treatment with SAG is this accompanied by no change in SSTR3<sup>NG</sup> (Fig. 22A). Ciliary signals after addition of sst were quantified and evaluated for SSTR3<sup>NG</sup> and PALD1, respectively, relative to the ciliary marker ac-tub. After activation, with sst, a significant reduction in the ciliary SSTR3<sup>NG</sup> signal is observed. Meanwhile, the ciliary PALD1 signal increases significantly (Fig. 22B).

Based on these findings, it can be speculated that PALD1 may fulfill a more general role in cellular signaling. This role is probably not limited to SHH signaling, as PALD1 accumulates in the cilium by a change in cAMP levels. While such a change occurs in the context of SHH signaling, it also occurs in relation to other signaling pathways (Besschetnova *et al.*, 2010; Jiang *et al.*, 2019; Sherpa *et al.*, 2019). It is therefore possible that PALD1 exerts different signal-dependent roles in cellular signaling depending on the cell type.

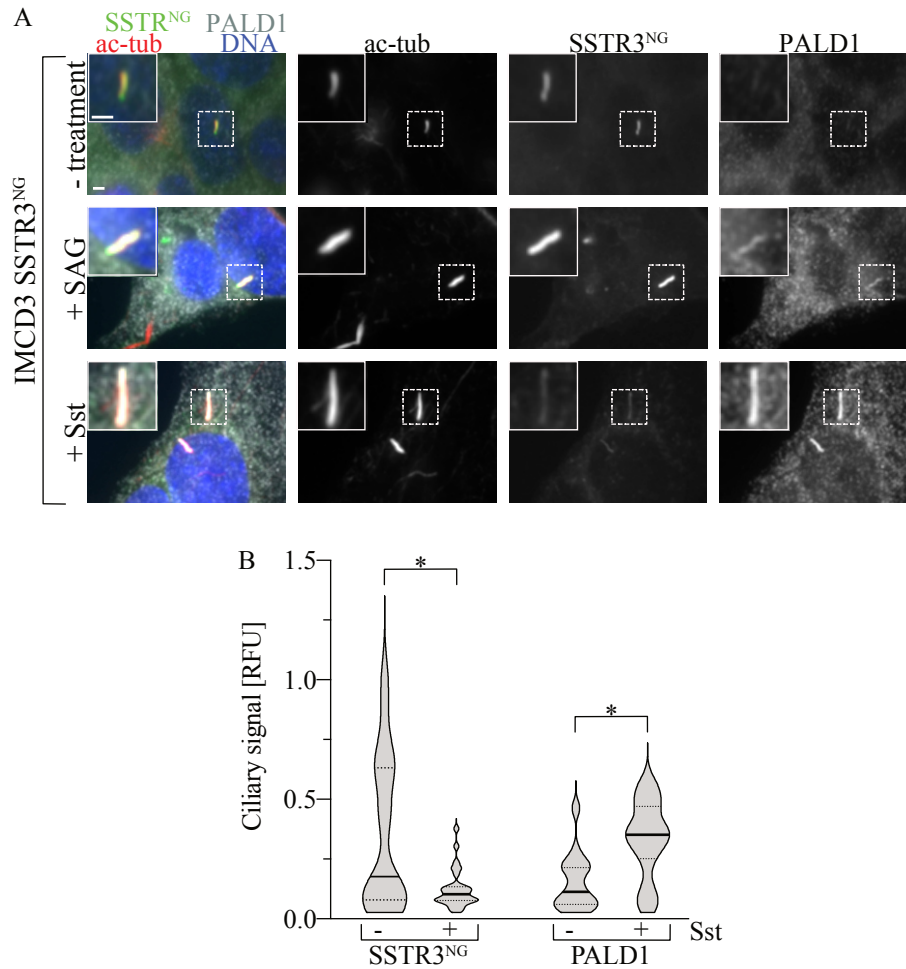


**Fig. 22: PALD1 accumulation is induced by changes in cAMP levels.**

(A) Representative IF micrographs of IMCD3 SSTR3<sup>NG</sup> cells treated with SAG, sst or vehicle and stained with antibodies against PALD1 and ac-tub. The scale bar represents 2 $\mu$ m (B) Quantification of 1 experiment out of 2 biological replicates with the same qualitative results. 30 cilia were quantified per condition (n = 30). Statistic significance was assessed by 2way ANOVA with Sidak's multiple comparisons test; p < 0.05.

## 6.8. PALD1 in SHH related and non-related ciliary signaling of C2C12 and 3T3 cells.

In IMCD3 cells, PALD1 accumulates in response to changes in cAMP levels and attenuates SHH signaling. As PALD1 is also expressed in 3T3 cells, in which it does not accumulate in primary cilia during SHH signaling, it could be a general factor of ciliary signaling. Consequently, the question arises which role PALD1 could play in 3T3 cells. Another question that has risen is whether PALD1 possesses a function in SHH signaling in C2C12 cells or mediates SHH signaling dependent processes, as it accumulates in primary cilia of C2C12 cells. Further, other ciliary signaling pathways could be affected by PALD1. To address these questions, a *Pald1* knock out was generated in C2C12 cells (C2C12 *Pald1*<sup>-/-</sup>) and 3T3 cells (3T3 *Pald1*<sup>-/-</sup>). For this purpose, the CRISPR-cas9 system was used, as described previously, for the generation of the IMCD3 *Pald1*<sup>-/-</sup> cell line. After generation of potential knock out cells, cells were screened *via* quantitative fluorescence WB analysis to confirm for the complete loss of PALD1.

The WB screen confirmed efficient knock out of *Pald1* in C2C12 and in 3T3 cells (Fig. 23). The generation of the knock out was so efficient that no PALD1 was detected in a pool of cells consisting of 100 different cell clones that were sorted into one well during FACS sorting (C2C12 *Pald1*<sup>-/-</sup> Pool, 3T3 *Pald1*<sup>-/-</sup> Pool). As cell pool reduce single clone effects, they were chosen for the following experiments and will be referred to as C2C12 *Pald1*<sup>-/-</sup> and 3T3 *Pald1*<sup>-/-</sup> from hereafter.

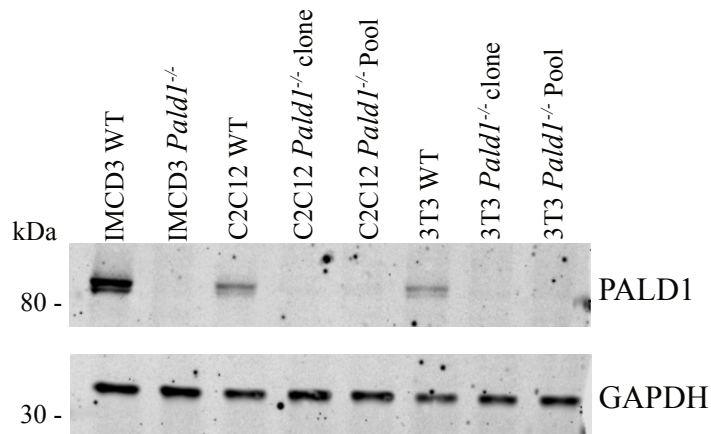


**Fig. 23: Generation of a *Pald1* knock out in C2C12 and 3T3 cells.**

After generation of the potential *Pald1*<sup>-/-</sup> cell lines *via* the CRISPR-cas9 system, the cell lines were screened for PALD1 expression in a quantitative fluorescence WB analysis. The WB analysis of the C2C12 parental cells (C2C12 WT), the 3T3 parental cells (3T3 WT) and their respective knock outs was done in comparison to IMCD3 WT and IMCD3 *Pald1*<sup>-/-</sup> cells. For C2C12 and 3T3 cells, single *Pald1*<sup>-/-</sup> clones were tested as well as the cell populations of potential knock out cells (modified after May *et al.*, 2021).

Because no PALD1 accumulation in primary cilia during SHH signaling was observed for 3T3 cells, the question remained whether PALD1 could regulate other ciliary signaling processes in 3T3 cells. 3T3 cells are fibroblasts that play an essential role in wound healing and have the ability to migrate (Schreier *et al.*, 1993). Previous studies have shown that PALD1 regulates cell migration in neural crest cells (Roffers-Agarwal *et al.*, 2012); therefore, it was investigated within this work whether the loss of PALD1 would affect the migration of 3T3 cells in a scratch assay. Scratches were introduced into a monolayer of 3T3 cells using the tip of a pipette. The width of the scratches was measured on the first day after scratching (T0) and every day thereafter. In 3T3 cells and in 3T3 *PalD1*<sup>-/-</sup> cells, the scratches began to heal immediately after application (Fig. 24A). The width of the scratches was measured and no significant differences were found between 3T3 and 3T3 *PalD1*<sup>-/-</sup> cells (Fig. 24B).

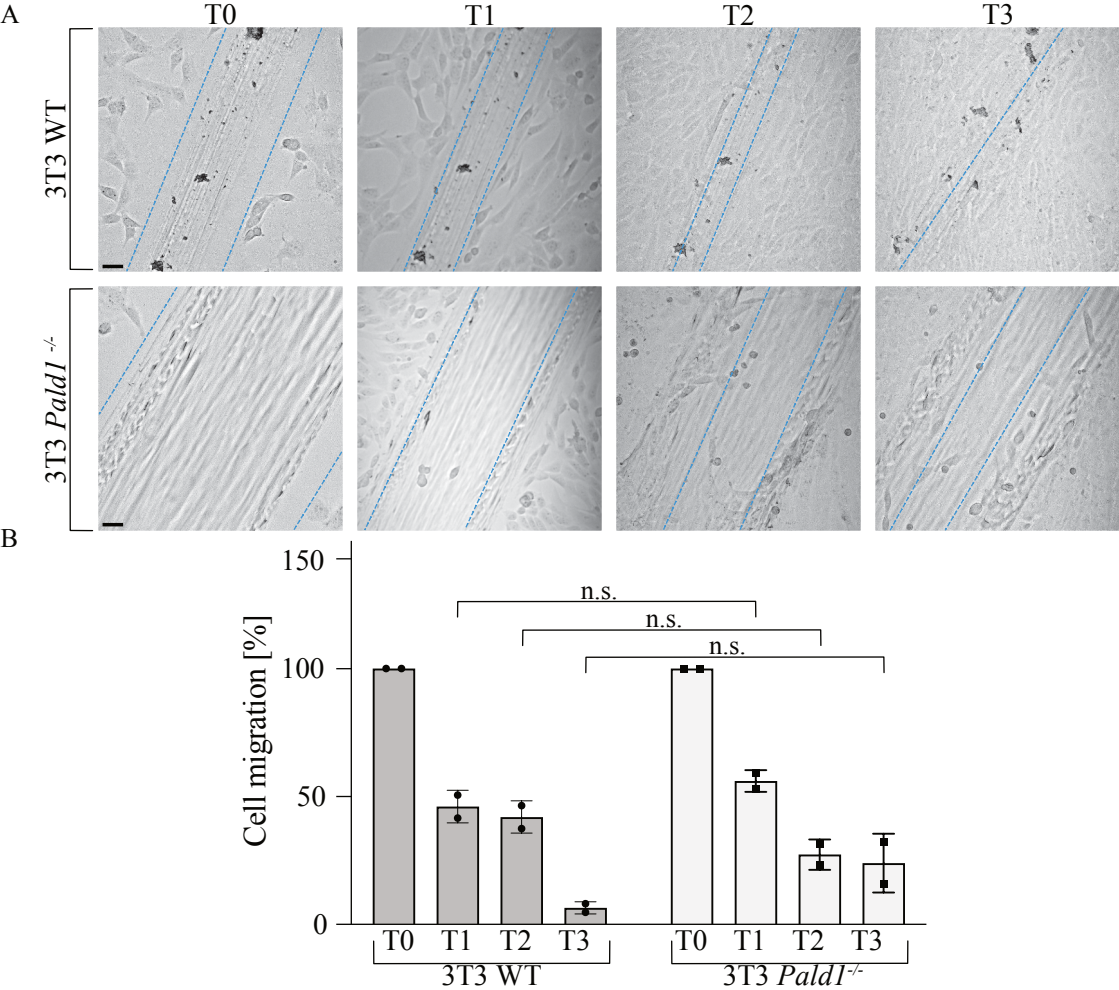


**Fig. 24: Scratch assay of 3T3 and 3T3 *PalD1*<sup>-/-</sup> cells showed no significant differences.**

(A) 3T3 and 3T3 *PalD1*<sup>-/-</sup> cells were seeded and grown in a monolayer. Scratches were introduced in the cell layer with a 5ml pipette tip. Images were taken from the cells immediately after introducing the scratch (Time point 0; T0) and every 24h until no scratch was visible in 3T3 WT cells (T1-T3). Yellow dotted lines indicate the cell border. The scale bar (black) shows 30µm. (B) The distance between two cell borders from (A) was measured from two technical replicates (n = 2). The width measured at T0 for the respective cell line was considered as 100% and

each time point was assessed in percentage of the width at T0. Statistic significance was assessed by 2way ANOVA with Sidak's multiple comparisons test.

The results for 3T3 cells are preliminary and will be critically discussed under 7. Discussion. However, the current lack of phenotype in 3T3 cells after loss of PALD1 in connection with the lack of ciliary PALD1 accumulation indicated that PALD1 could play a insignificant role in this cell line. Consequently, the investigation of C2C12 cells and C2C12 *Pald1*<sup>-/-</sup> was further pursued instead of 3T3 cells.

As mentioned previously, C2C12 cells have the ability to differentiate into myotubes which express specific muscle proteins. This process is dependent on SHH signaling and can be examined in a cell culture model and assessed by certain markers such as the protein myosin heavy chain (MYHI). After induction of differentiation into myotubes from C2C12 and C2C12 *Pald1*<sup>-/-</sup> cells, cell lysates were generated and examined by quantitative fluorescence WB. Here, MYHI was used as a differentiation marker and assessed relative to the GAPDH signals of each sample. Each day, samples of each cell line were taken and analyzed via quantitative fluorescence WB. The aim of the experiment was to compare the differentiation abilities of the two cell lines, and thus to investigate the influence of PALD1 on this process.

Reduced MYHI signal indicating a reduced differentiation capacity was observed in C2C12 cells after loss of PALD1. While during the first three days after induction of differentiation (time points (T) 1 – 3) no increase in MYHI signal was observed, C2C12 WT cells showed a clear increase in MYHI signals from day 4 (T4), indicating progressing differentiation into myotubes (Fig. 25A). In contrast, MYHI was barely detectable in C2C12 *Pald1*<sup>-/-</sup> cells even after more than a week (T5 = 7 days) of induced differentiation. The increase in MYHI was observed relative to the respective GAPDH signals and is significantly different in C2C12 WT cells as compared to C2C12 *Pald1*<sup>-/-</sup> cells (Fig. 25B). The latter show no changes in their MYHI signal, indicating insufficient differentiation into myotubes. These initial results, together with the observed accumulation of PALD1 in primary cilia of C2C12 WT cells, suggest that PALD1 controls SHH signaling-dependent processes like differentiation into myotubes. It is possible that PALD1 plays a similar role in C2C12 cells as it does in IMCD3 cells.



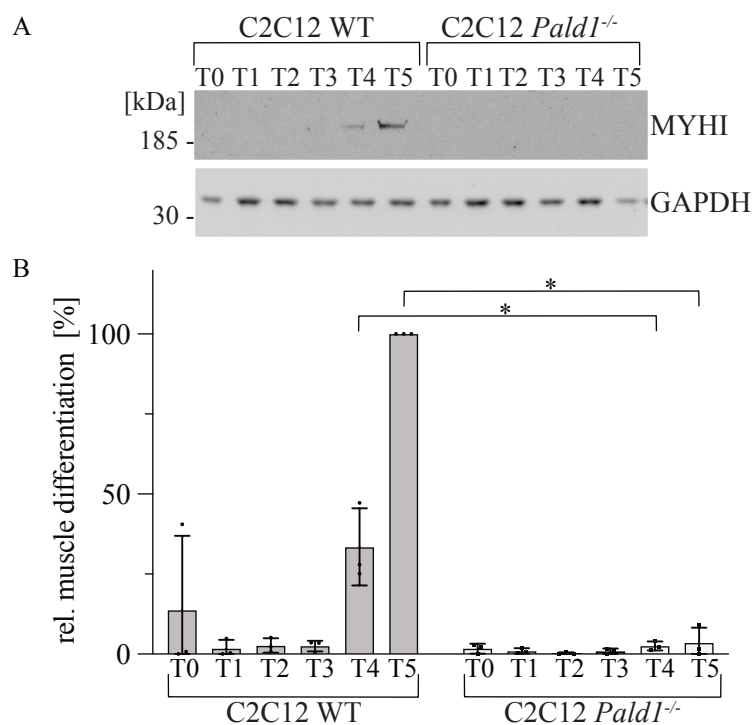


**Fig. 25: Muscle differentiation assay of C2C12 WT cells in comparison to C2C12 *Pald1*<sup>-/-</sup> cells.**

(A) Cell lysates prepared during different time points (T0-T5) of myoblast differentiation was analyzed in a quantitative fluorescence WB. T0 represents the time point before induction of muscle differentiation. GAPDH and MYHI were detected with specific antibodies. (B) Quantification of MYHI signals relative to respective GAPDH signals in C2C12 WT cells and C2C12 *Pald1*<sup>-/-</sup> cells. Analyzed were three biological replicates (n = 3). Values are shown in % of the maximum MYHI signal of each experiment in C2C12 WT cells. Statistic significance was assessed by two-way-ANOVA with Sidak's multiple comparisons test;  $p < 0.0001$ .

To further investigate the potential dependency of PALD1 on PKA already mentioned in previous experiments in IMCD3 cells, IF microscopy was performed. First, C2C12 WT and C2C12 *Pald1*<sup>-/-</sup> cells were stained with antibodies against PKA-C and SMO and ac-tub, as a corresponding cilia marker. The aim of this analysis was to detect potential differences in the localization of PKA-C or in the accumulation of SMO. In addition, the cilia length of C2C12 *Pald1*<sup>-/-</sup> was also assessed and compared with that of C2C12 WT cells.

In previous studies, PKA-C was shown to localize to the cilia base (Barzi *et al.*, 2010). No clear change in the localization of PKA-C between WT and C2C12 *Pald1*<sup>-/-</sup> cells was detected (Fig. 26A). In both cell lines, the protein continues to localize to the ciliary base. Ciliary SMO signals were quantified and assessed relative to the cilia marker ac-tub (Fig. 26B). No significant differences in ciliary SMO signals were found for C2C12 *Pald1*<sup>-/-</sup> compared with C2C12 WT cells. However, the signals appear to be less heterogeneous in C2C12 *Pald1*<sup>-/-</sup> than in the C2C12 WT cells. Cilia length was quantified and again no significant differences were found between C2C12 WT and C2C12 *Pald1*<sup>-/-</sup> cells (Fig. 26C).

That no significant, or if so, only minor differences were detected between WT and C2C12 *Pald1*<sup>-/-</sup> cells in this first experiment was initially surprising. This is because C2C12 cells, along with IMCD3 cells, are the only cell line to show detectable ciliary accumulation of PALD1. Because of these results, a more holistic approach was chosen by investigating SHH-mediated processes instead of single molecular defects to find out whether PALD1 controls SHH mediated processes in C2C12 cells. Since these defects suggest a SHH defect, the qPCR analysis was performed below.

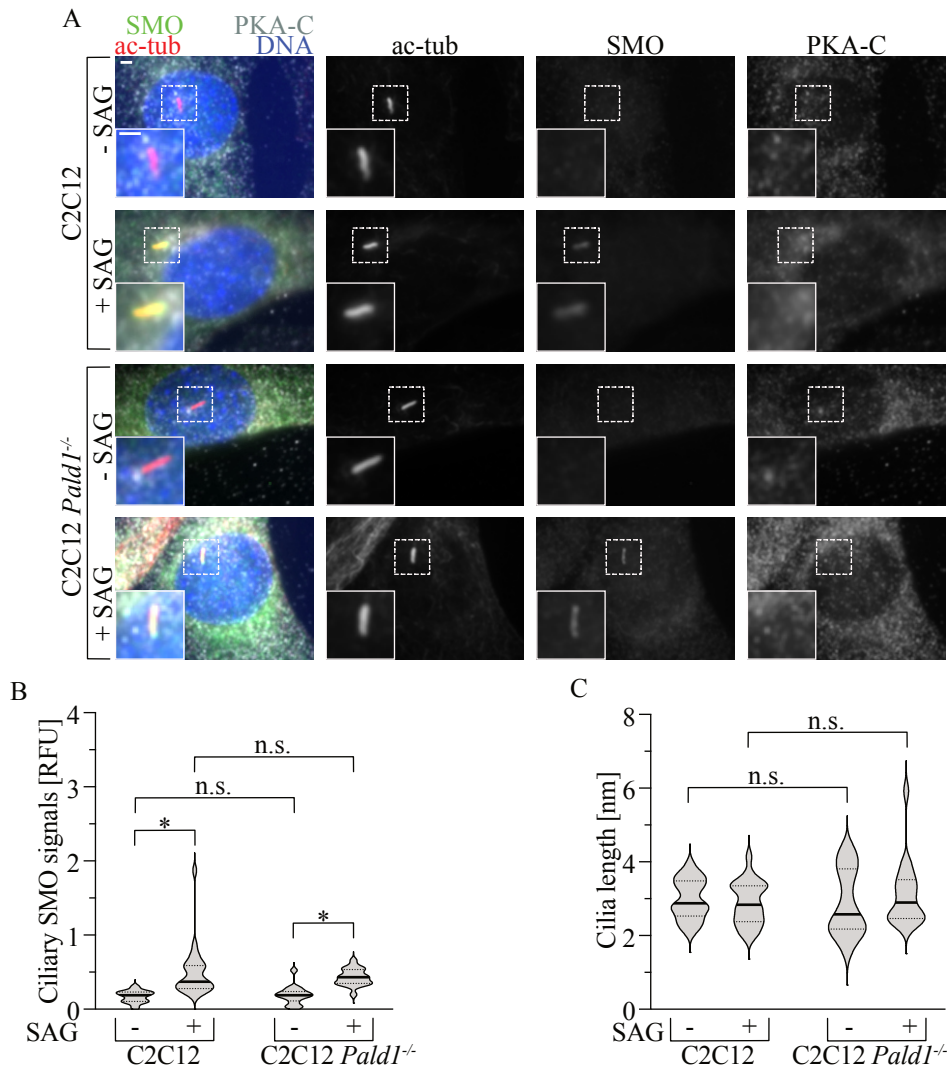


**Fig. 26: C2C12 *Pald1*<sup>-/-</sup> cells showed no SHH or cilia defects in comparison to C2C12 WT cells.**

(A) Representative IF micrographs of C2C12 WT and C2C12 *Pald1*<sup>-/-</sup> cells stained with specific antibodies against PKA-C, SMO and ac-tub. 24h before experiment, cells were treated with SAG. The scale bar represents 2 $\mu$ m. (B) Quantification of cilia signals of SMO relative to ac-tub in RFU. 30 cilia per condition were quantified from one experiment (n = 30). Statistic significance was assessed by two-way-ANOVA with Tukey's multiple comparisons test. (C) Cilia length was analyzed from 20 cilia (n = 20) based on IF microscopy from (A). Statistic significance was assessed by two-way-ANOVA with Sidak's multiple comparisons test; p < 0.05.

## 6.9. Prospect - pre-liminary qRT-PCR analysis confirms pre-activation of *Pald1*<sup>-/-</sup> in IMCD3s and surprisingly also in 3T3 but not in C2C12 cells

For the final analysis within this work of the PALD1 dependent transcriptional SHH response, IMCD3 *Pald1*<sup>-/-</sup>, C2C12 *Pald1*<sup>-/-</sup> and 3T3 *Pald1*<sup>-/-</sup> cell lines were analyzed by qRT-PCR in comparison to their respective WT cell lines. The qRT-PCR experiment aimed to identify potential transcriptional changes in SHH signaling in C2C12 *Pald1*<sup>-/-</sup>, 3T3 *Pald1*<sup>-/-</sup>, and also IMCD3 *Pald1*<sup>-/-</sup> cells and was performed in collaboration with the junior research group of Dr. Nicole Ludwig (Department of Human Genetics, UdS Homburg). RNA was isolated from the cell lines as described above and then, the corresponding qPCR assay was performed in cooperation with Esther Maldener and Dr. Nicole Ludwig. *Gli1* expression levels were determined using appropriate primers. In contrast to GLI3, GLI1 is not proteolytically processed. Instead, total expression levels change depending on the SHH signaling status of the cell. This results in decreased GLI1 levels in the absence of signal, making GLI1 a suitable marker to determine the transcriptional response of SHH signaling.

SHH pre-activation of IMCD3 *Pald1*<sup>-/-</sup> cells compared with IMCD3 WT cells was confirmed in this preliminary experiment. These results are consistent with previous data in this work. In fact, the observed effects on *Gli1* expression were very prominent. IMCD3 *Pald1*<sup>-/-</sup> cells showed, in the absence of Shh-N, a state of pre-activation, which is comparable to IMCD3 WT cells after treatment with Shh-N. However, as already observed for GLI3 in quantitative fluorescence WB, the status of activation was increased after treatment with Shh-N. The results for 3T3 cells surprisingly resembled the observations made in IMCD3 cells. 3T3 *Pald1*<sup>-/-</sup> cells showed increased *Gli1* expression compared to 3T3 WT cells. However, this effect was only visible in absence of Shh-N. After treatment with Shh-N, the observed pre-activation phenotype disappeared. This result differed from observations in IMCD3 cells where the activation was further increased after treatment with Shh-N. Moreover, the induction of 3T3 *Pald1*<sup>-/-</sup> cells was even weaker compared to 3T3 WT cells after treatment with Shh-N. It is notable that the effects were also significantly weaker than those observed in IMCD3 cells. Overall, the observed effects suggest a different role for PALD1 in 3T3 cells than in IMCD3 cells (Fig. 27). Surprisingly, C2C12 cells did not show strong effects in the qRT-PCR after PALD1 loss. While the non-induced samples of C2C12 WT and C2C12 *Pald1*<sup>-/-</sup> cells showed comparable induction, C2C12 *Pald1*<sup>-/-</sup> displayed a mild increase of *Gli1* after treatment with Shh-N compared to C2C12 WT. It should be noted when looking that the results for C2C12 cells show strong variations (Fig. 27).

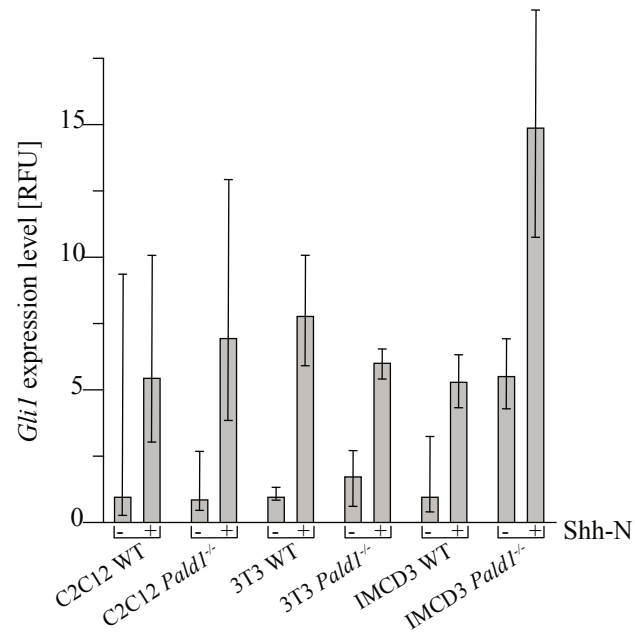


**Fig. 27: qRT-PCR analysis of *Pald1*<sup>-/-</sup> and respective WT cells reveals differences in signaling status.**

*Gli1* expression levels were measured via qPCR in cooperation with the group of Dr. Nicole Ludwig. All cell lines were serum starved for 48h in presence of absence of Shh-N. Shown are means of *Gli1* transcript levels relative to *Gapdh* of (n = 2) with relative  $R_{Q_{min}}$  and  $R_{Q_{max}}$  values.

## 7. Discussion

### 7.1. Improved Cilia-APEX2 study improves our understanding of the ciliary proteome.

During the last decades, primary cilia became more and more the focus of attention. Numerous now known ciliopathies highlighted the relevance of learning more about primary cilia (Reiter & Leroux, 2017). The aim is to better understand the molecular details and function of primary cilia in order to explore new therapeutic options for the rare, but very severe, cilia-dependent diseases. Unraveling the ciliary proteome improves our understanding of ciliary signaling and the role of primary cilia in various physiological processes. However, some challenges had to be overcome to study the ciliary proteome, e.g., the small reaction compartment of primary cilia. With a length that usually varies between 3 – 5  $\mu\text{m}$ , the ciliary reaction space is very small and the amount of proteins is accordingly low. Therefore, the use of very sensitive assays as well as the appropriate enrichment of the ciliary components is essential. The additional fact that cilia are not enclosed by a continuous membrane poses more difficulties in the purification of cilia. The combination of APEX labeling and MS analysis provided the first simple and feasible approach to study the ciliary proteome (Mick *et al.*, 2015). As innovative as this was, this method had certain limitations. For instance, low abundance of transmembrane proteins and TZ components were lacking from the analysis in the first Cilia-APEX study (Mick *et al.*, 2015). This fact considerably limited our understanding of important cilia-dependent processes and also prevented a detailed study of the SHH pathway. For this reason, it remained logical to further improve the APEX approach and thus eliminate previous weaknesses. APEX labeling was first refined by using a ciliary membrane localized, improved version of APEX, cmAPEX2. The cmAPEX2 version efficiently biotinylated ciliary membrane-associated proteins and identified actin-binding proteins as important cilia components (Kohli *et al.*, 2017). However, while significantly more membrane components were identified with the cmAPEX2 version compared to Cilia-APEX, some soluble proteins were lacking from the study, despite of the use of the improved APEX2 version (Mick *et al.*, 2015; Kohli *et al.*, 2017). Moreover, some low abundance transmembrane proteins such as GPR161 were still missing from the list of identified cilia proteins. By generating Cilia-APEX2, the new APEX cell line that labels cells with higher efficiency at lower transgene expression compared to Cilia-APEX, the identification of ciliary components was significantly improved in the subsequent study. Thus, both SHH and TZ components were identified in a new, improved Cilia-APEX2 study (May *et al.*, 2021). Nevertheless, a common weakness of the proteomic analyses described above remains that they were all performed in IMCD3 cells, and thus, potential differences in the proteomes of different cell lines remain unexplored by these approaches.

The cilia TZ forms an important barrier of the primary cilium, thereby enabling its function as a cellular signaling compartment. TZ components were absent in the first Cilia-APEX study (Mick *et al.*, 2015). However, by using Cilia-APEX2, approximately half of the known components from the ciliary TZ were successfully identified (May *et al.*, 2021). Interestingly, previous studies have established that the old concept of the TZ as a static construct is outdated. In contrast, it has been shown that the TZ forms a complex structure composed of static and non-static components that shuttle in and out of the primary

cilia in low amounts (Craigie *et al.*, 2010; Takao *et al.*, 2017). Interestingly, particularly those components that are considered dynamic were successfully identified using Cilia-APEX2 (May *et al.*, 2021). This indicates, on the one hand, a high sensitivity of the Cilia-APEX2 approach. On the other hand, it opens the possibility to observe signal- and cell-state-dependent changes of TZ components in the future and thus gain further insights into the various important functions of the TZ.

Most importantly, Cilia-APEX2 provided a better understanding of the SHH signaling pathway. Due to its importance in embryonic development and the adult organism, the SHH signaling pathway is a widely studied research topic (Gigante & Caspary, 2021). Nevertheless, many mechanisms remain poorly understood and many questions unanswered. Seven of the eight known SHH core components were identified in the Cilia-APEX2 study (May *et al.*, 2021). These components were namely SMO, which accumulates in the cilia after SHH activation, PTCH1 and GPR161, which exit the primary cilium when the SHH signaling state is active, and GLI2, GLI3, SUFU, and KIF7, which accumulate at the ciliary tip after SHH activation (Liem *et al.*, 2009; Hsu *et al.*, 2011; He *et al.*, 2014; May *et al.*, 2021). The only known SHH signaling component not identified in the Cilia-APEX2 study was the transcriptional activator GLI1. Independent of this, it was observed for the first time that a regulatory subunit of PKR1 $\alpha$  leaves the primary cilium together with GPR161 after induction of SHH signaling. Among others, it was speculated that GPR161, PKR1 $\alpha$ , and PKA-C are removed from the cilium after activation as a holoenzyme, but this has not yet been experimentally confirmed (May *et al.*, 2021).

## **7.2. Identification of PALD1 as a new component of SHH signaling.**

In addition to the observations described, the potential phosphatase PALD1 was linked to SHH signaling for the first time through the Cilia-APEX2 study (May *et al.*, 2021). While previous studies have already identified PALD1 as an important signaling factor in various cellular signaling pathways, its association with SHH signaling was novel (Huang *et al.*, 2009; Wallgard *et al.*, 2012; Roffers-Agarwal *et al.*, 2012; Nitzsche *et al.*, 2020). In 2012, PALD1 expression was detected in pre-migratory and migratory neural crest cells (Roffers-Agarwal *et al.*, 2012). Furthermore, PALD1 was shown to have a regulatory influence on cell migration during embryonic development (Roffers-Agarwal *et al.*, 2012). However, because the observations described appeared to be independent of the conserved cysteines within the PTP catalytic domains of PALD1, it was suspected at the time that PALD1 exerts its regulatory function in the role of an antiphosphatase and not as a PT phosphatase, as initially suspected on the basis of sequence similarities (Roffers-Agarwal *et al.*, 2012). However, the notion of PALD1 as an antiphosphatase needed further confirmation as phosphatase assays completely lacked from this study.

Another group identified PALD1 as a novel inhibitor of insulin signaling (Huang *et al.*, 2009). The mechanism involving PALD1 is suggested to inhibit the upstream insulin-stimulated AKT phosphorylation. While the group suspects that PALD1 targets a component upstream of AKT, the study lacks identification of a target protein of PALD1. Subsequently, the question of whether PALD1 regulates AKT via phosphatase activity or as an antiphosphatase could not be addressed. However, this

study further clarifies that PALD1 is an important general factor in cellular signaling (Huang *et al.*, 2009). Although, many questions about the precise mechanisms and overall role of PALD1 remain unanswered, the study provides further relevant evidence on the function of PALD1.

Shown within this work in independent IF microscopy, PALD1 co-accumulated together with SMO in primary cilia of IMCD3 and C2C12 cells after induction of SHH signaling. This co-accumulation appeared to be independent of the degree of pathway activation (see Fig. 10 and Fig. 13) and underwent a similar kinetic (May *et al.*, 2021). The most obvious interpretation was, that the co-accumulation of PALD1 and SMO was due to the complexation of the two proteins. However, this idea could be rebutted by the treatment of IMCD3 cells with the SHH blocking reagent CYC (see Fig. 11). CYC treatment resulted in an accumulation of SMO in primary cilia with inactive SHH signaling. PALD1 lacked from cilia under these conditions which indicated an accumulation only after SHH pathway activation. Moreover, SMO was permanently detected in primary cilia of IMCD3 *Ift27<sup>-/-</sup>* cells while PALD1 accumulation in IMCD3 *Ift27<sup>-/-</sup>* cells was impaired, which was additional proof that PALD1 and SMO do not form a permanent complex (see Fig. 15). Therefore it can be concluded that I.) PALD1 does not stably interact with SMO and it was also confirmed that II.) SMO accumulation in primary cilia is not sufficient to induce PALD1 accumulation. Consequently, PALD1 accumulation needs to be induced by further mechanisms upstream or downstream of SMO. As PALD1 accumulates after physiological pathway activation via binding of the ligand Sonic to PTCH1 (induction with Shh-N) and after pathway activation via direct binding of an agonist of SMO (induction with SAG), it can be suspected that PALD1 functions downstream of SMO in SHH signaling.

Based on previous studies, it was not surprising that PALD1 was detected in different murine and human cell lines. In all cell lines tested, steady state expression levels appeared to be independent of SHH induction. This observation suggested that the role of PALD1 in SHH signaling depends primarily on its localization and that expression levels appear less important for the function of PALD1. However, it is possible that PALD1 exerts more significant roles in cell lines with generally higher steady-state expression levels such as IMCD3 cells.

This theory could be one possible explanation why PALD1 has not been identified in previous SHH screens in 3T3 cells, as 3T3 cells displayed weaker steady state *Pald1* expression levels than IMCD3 cells, which were used for the Cilia-APEX2 study (May *et al.*, 2021). 3T3 cells showed neither a ciliary accumulation of PALD1 after stimulation with SHH-inducing reagents nor a significant defect in a cell migration assay (see Fig. 13 and Fig. 24). This suggests that polarization and migration, which are essential for wound healing, are not disrupted in 3T3 cells lacking PALD1. To further validate this first data generated from the cell migration assays, additional assays of this type could be performed in which the normalization of scratch width is optimized. In addition, scratches of different widths could be generated to test how this affects the ability of 3T3 WT and 3T3 *Pald1<sup>-/-</sup>* cells to migrate. When transcriptional activation of SHH signaling was investigated *via* qPCR, no significant differences between 3T3 cells and 3T3 *Pald1<sup>-/-</sup>* cells were detected. Summarized, these initial data could not identify

the role of PALD1 in 3T3 cells. The analysis of 3T3 cells could be extended by further methods to investigate the transcriptional response of 3T3 cells to different SHH signals. In addition to further qPCR experiments, a luciferase assay would be a valuable tool, as well as the investigation of the transcription factor GLI in WB analysis (Watanabe *et al.*, 2003; Hwang *et al.*, 2021). Nevertheless, based on the underlying data already available, it can be speculated that the role of PALD1 in 3T3 cells is less significant than the role of PALD1 in IMCD3 cells.

In C2C12 cells, *Pald1* steady state expression and accumulation of PALD1 in cilia were detected after treatment with SHH-inducing reagents. This observation suggested that C2C12 *Pald1*<sup>-/-</sup> cells should show distinct defects compared to C2C12 WT cells in IF microscopy. However, analysis by qPCR assay in C2C12 cells showed only a slightly stronger response to the SHH stimuli in C2C12 *Pald1*<sup>-/-</sup> cells. No strong effects for C2C12 *Pald1*<sup>-/-</sup> cells could be observed without activation of SHH signaling that would indicate the previously observed phenotype of pre-activation in IMCD3 cells. It must be clarified that the qPCR analysis is more of an experimental outlook that requires further investigation. Nevertheless, it was observed that loss of PALD1 prevented differentiation of C2C12 cells into myotubes, indicating that PALD1 may play an important role in cilia signaling in C2C12 cells, specifically SHH signaling. Additionally, experiments that investigate the transcriptional response of SHH signaling in C2C12 *Pald1*<sup>-/-</sup> could bring further information on molecular mechanisms and confirm preliminary data (Mok *et al.*, 2018). Future experiments could further investigate the ciliary GPR161 levels in C2C12 *Pald1*<sup>-/-</sup> compared to C2C12 WT cells.

In addition to the cell lines described above, *Pald1* steady state expression was also detected in the murine MIN6 $\beta$  cells. Although the steady state expression levels of *Pald1* are relatively high, no accumulation in the primary cilia of MIN6 $\beta$  cells could be detected here. While this initially contradicts the assumption that high *Pald1* expression levels are associated with strong PALD1 function in the corresponding cell line, the observation here in MIN6 $\beta$  cells here can be explained by the lack of a SHH response. It could be suggested that PALD1 accumulates in cilia of MIN6 $\beta$  cells in response to stimuli other than SHH signaling but remains to be investigated. As it was shown that PALD1 accumulates in the cilia of IMCD3 cells in response to changes in cAMP levels (see Fig. 22), PALD1 accumulation in other cell lines could also be associated with changes in ciliary cAMP levels that are independent of SHH signaling. Since PALD1 has been previously identified as a negative regulator of insulin signaling as described previously (Huang *et al.*, 2009), the possibility that PALD1 accumulates in MIN6 $\beta$  cells in response to changes in the extracellular glucose levels remains to be investigated. This hypothesis could be tested by IF microscopy as the ciliation rate in MIN6 $\beta$  cells is high. However, the responsiveness of the cell line to glucose must be established as this would be crucial for this experiment. PALD1 was further detected in HEK cells, but lacked from human RPE cells. Thus, analysis of additional human cell lines may be of interest for the future investigation of PALD1.

After showing that *Pald1* expression is neither restricted to IMCD3 cells nor to murine cell lines, the question regarding the evolutionary conservation of *Pald1* arose. The simultaneous gain or loss of



different genes during evolution can provide information about their function (Pellegrini *et al.*, 1991). Therefore, the CLIME gene analysis was performed with the aim to gain further insights into a potential function of PALD1. While other SHH signaling components were of particular interest, *Pald1* clustered with the gene of the IFT-B component *Ift25*, among others, in the comparative CLIME gene analysis. This indicates a coevolution of *Ift25* and *Pald1*, implying a similarity in their function or an interdependence. IFT25 is an IFT-B subcomplex component that is conserved among some but not all ciliated species and is not essential for cilia assembly. However, IFT25 regulates ciliary export of SHH components and plays a role in early kidney development (Keady *et al.*, 2012; Eguether *et al.*, 2014). As IFT25 physically interacts with IFT27 through complexation, loss of IFT27 leads to degradation of IFT25 and *vice versa* (Wang *et al.*, 2009). The IFT27/IFT25 complex is essential for the export of SMO from primary cilia in an inactive SHH signaling state. IFT27, thus also an IFT-B sub-complex component, promotes ARL6-mediated exit of SHH components through the BBsome (Keady *et al.*, 2012, Eguether *et al.*, 2014, Eguether *et al.*, 2018). Because of the IFT25 loss in IMCD3 *Ift27<sup>-/-</sup>* cells, the relation between PALD1 and IFT25 was investigated using IMCD3 *Ift27<sup>-/-</sup>* cells. SHH signaling has been shown to be generally attenuated by loss of IFT27/IFT25, as indicated by reduced GLI2 levels (Eguether *et al.*, 2014). Within this work it was shown that ciliary SMO accumulation in IMCD3 *Ift27<sup>-/-</sup>* cells can be further increased after stimulation with SHH reagents. In contrast to the earlier assumption that SMO accumulates in cilia only in the active signaling state, SMO has since been shown to shuttle in and out of the primary cilium without significant accumulation (Kim *et al.*, 2009; Goetz & Anderson, 2010). In response to a signal, ciliary SMO is retained and exit is prevented (Gigante & Caspary, 2020). The observed phenotype of SMO accumulation in IMCD3 *Ift27<sup>-/-</sup>* cells and the subsequent weakening of the SHH signaling pathway may be the result of insufficient SMO removal. Impaired ciliary exit of SMO could attenuate the SHH response through a constitutive negative feedback. In this condition, SHH signaling would never be completely turned off, which could permanently weaken the ability of cells to respond to stimuli (Gigante & Caspary, 2020). However, the mechanisms explained could also be the result of the complex function of IFT27 downstream of SMO in SHH signaling (Eguether *et al.*, 2018). The mislocalization of several SHH components associated with the loss of IFT27 could also be the result of a weakened response to the signal (Eguether *et al.*, 2014; Eguether *et al.*, 2018).

As discussed above, ciliary PALD1 accumulation is not purely dependent on ciliary SMO accumulation. It seems logical to expect that disturbed PALD1 accumulation in IMCD3 *Ift27<sup>-/-</sup>* cells is the result of general SHH defects and depends, for example, on a mislocalized pathway component downstream of SMO. Apart from that, the impaired PALD1 accumulation in IMCD3 *Ift27<sup>-/-</sup>* cells could also be a direct effect of the loss of IFT27. While both options are possible, based on the gene CLIME analysis, it seems more likely that PALD1 is dependent on IFT27/25.

Based on the gene CLIME analysis and IF microscopy of IMCD3 *Ift27<sup>-/-</sup>* cells, one could consider the possibility that PALD1 permanently complexes with IFT27 and IFT25. In that case PALD1, would represent an unknown IFT-B component. In principle, this theory could be tested by co-isolation experiments. However, even if PALD1 would interact with IFT27/25, which should be suspected, it is

likely that PALD1 does not permanently complex with IFT27/25 as it is not lost in IMCD3 *Ift27<sup>-/-</sup>* cells. In that respect, PALD1 would display some similarities to TULP3 with respect to IFT-A. TULP3 is a negative regulator of SHH signaling that localizes to primary cilia through interaction with the IFT-A complex. TULP3 is a protein that contains a tubby domain, a 260 amino acid long sequence that can bind both DNA and phosphorylated PIPs (Santagata *et al.*, 2001; Mukhopadhyay *et al.*, 2010). TULP3 is essential for the recruitment of GPR161, which is also impaired in IMCD3 *Pald1<sup>-/-</sup>* cells, and promotes PKA dependent SHH repression (Mukhopadhyay *et al.*, 2010). In this regard and based on the described similarities, it would be interesting to test whether PALD1 can be co-isolated with other IFT-B components suggesting that PALD1 could generally bind IFT-B components and execute a function similar to those of TULP3. In particular, it would be interesting to test whether the interaction partners change depending on SHH signaling status. Nevertheless, as PALD1 clustered specifically with IFT25 and is not conserved among all species that express IFT-B components, a specific interaction solely with the IFT25/27 complex appears to be more likely. Besides that, an interaction between PALD1 and TULP3 is also plausible. TULP3, like PALD1, has a negative regulatory role in SHH signaling and, like potentially PALD1, also interacts with IFTs. Within this work, it was observed that the loss of TULP3 indeed has an effect on the accumulation of PALD1. The fact that a link between PALD1 and IFT-B and PIPs could be established strongly resembling the mechanisms *via* TULP3 regulating SHH signaling.

Another interesting property of TULP3 is that the protein, consisting of a helix  $\beta$ -barrel structure, binds PI(4,5)P2 and PI(3,4)P2 (Santagata *et al.*, 2001). Recently, a group proposed PALD1 as a potential PI(4,5)P2 phosphatase (Nitzsche *et al.*, 2020). If the assumption that PALD1 possesses PIP phosphatase activity is true, it could regulate the SHH signaling status of the primary cilium via changes in the ciliary membrane composition. These changes could then be sensed by other SHH components such as TULP3 or GPR161 which would convert them into the appropriate signals. The ciliary membrane became the focus of scientific interest within the past years due to the discovery of similar mechanisms. Several exciting studies have demonstrated that the ciliary membrane plays an important regulatory role in regulating SHH signaling (Kowatsch *et al.*, 2019; Rudolf *et al.*, 2019; Kinnebrew *et al.*, 2019). For example, it has been demonstrated that the long enigmatic regulation of SMO by PTCH1 most likely occurs via changes in the accessibility of cholesterol in the ciliary membrane (Kinnebrew *et al.*, 2019). These are minute changes that are then sensed by SMO and lead to its retention in the cilium (Kinnebrew *et al.*, 2019). Similar mechanisms could conceivably be responsible for the regulation of GPR161 levels by PALD1. Nevertheless, the previous evidence for PALD1 as a PIP phosphatase remains critical as measurements of PALD1 phosphatase activity isolated from whole-cell lysates harbors the risk of contamination due to other cytosolic phosphatases that could falsify results. Therefore, the research group of our laboratory will investigate the PIP phosphatase activity of PALD1 with purified components *in vitro*. Finding and investigating potential interaction partners of PALD1 could shed further light on its function. Consequently, first experiments have been initiated which will certainly ensure exciting insights and new information on the role of PALD1.

Interestingly, *Pald1* was also clustered with other phosphatases as shown in the gene CLIME analysis, although these do not share structural similarities with the PT phosphatase group to which PALD1 belongs. In addition, PALD1 was clustered with other cilia-localized proteins that do not carry a phosphatase domain and some of which have unknown functions. This observation may suggest that PALD1 could function independently of any possible phosphatase function in SHH signaling or other cellular signaling pathways. In this case, PALD1 could regulate signaling through a mechanism that is independent of its potential phosphatase function. Pseudophosphatases and pseudokinases are catalytic inactive enzymes that have structural similarities to catalytic active phosphatases/kinases, but have structural defects in their active regions and, thus, lack catalytic activity (Reiterer *et al.*, 2014). These changes usually occur through viral insertion of genetic material into the gene site encoding the active domains (Reiterer *et al.*, 2014). While these pseudoenzymes were long thought to have no relevance in cellular signaling, it is increasingly coming to light that they perform important roles in cellular signaling by, for example, binding and inhibiting other enzymes, such as blocking a potential substrate via binding (Kharitidi *et al.*, 2014). This may also be the key to the observations made in preceding studies when the potential functions of PALD1 could not be attributed to phosphatase activity as described (Huang *et al.*, 2009; Wallgard *et al.*, 2012; Roffers-Agarwal *et al.*, 2012). Nevertheless, this idea is partially contradicted by the finding that PALD1 acts in a negative regulatory manner in insulin signaling by inhibiting AKT phosphorylation (Huang *et al.*, 2009). Since the exact mechanism is unknown, it would be possible that PALD1 directly interacts with AKT and removes the corresponding phosphates (Sarbasov *et al.*, 2005, Feng *et al.*, 2004). To date, no potential substrate for PALD1 has been identified. However, since phosphatase assays have proven to be challenging and error-prone, the mere absence of detected activity should not be sufficient to classify a protein as a pseudophosphatase. In contrast, detection of weak signals indicating a functional phosphatase could be equally misleading. To identify a pseudophosphatase, Kharitidi *et al.* propose an approach that involves gene alignment, mutagenesis of the potential domains, and purification of the potential pseudophosphatase in a eukaryotic system (Kharitidi *et al.*, 2014). Although this approach is laborious, this thorough testing should occur before a protein is classified.

An example of the complex regulation of pseudophosphatases are the myotubularin-related proteins MTMR9, 11, and 12, all three of which lack a catalytic activity. However, they are able to form dimers with active members of the myotubularin family and subsequently affect phosphatase activity (Kharitidi *et al.*, 2014). Parallels can be drawn here with INPP5E and PALD1. INPP5E is a cilia-localized PIP phosphatase that positively regulates SHH signaling. PALD1 could bind to INPP5E to antagonize its function as an anti-phosphatase and thus prevent signaling overactivation through INPP5E (Dyson *et al.*, 2016). With this knowledge, just as with an active phosphatase, the question as to what the potential binding partner for PALD1 in SHH signaling is must be asked. Considering this, the PTMs in SHH signaling that could be affected by PALD1 downstream of SMO need to be observed first and foremost. Obviously, besides PIP modifications through INPP5E, a modification that would come into consideration would be the well-studied modifications of GLI transcription factors that are regulated *via*

PKA. However, because GPR161 levels are reduced in the primary cilia of IMCD3 *Pald1*<sup>-/-</sup> cells, this suggests that PALD1 is either involved in a feedback loop or may function upstream of GLI proteins.

Consequently, GPR161 also represents a potential target protein of PALD1, as it is itself phosphorylated at its C-terminus. The C-terminus of GPR161 has several important functions, including representing the A Kinase Anchoring Protein (AKAP) for PKA and containing several protein kinase consensus sites (Bachmann *et al.*, 2016). The idea that PALD1 could bind to GPR161 and thus counteract its phosphorylation is intriguing for both mechanisms proposed in this work. Phosphorylation of GPR161 could be prevented by PALD1, and loss of PALD1 could subsequently lead to increased phosphorylation of GPR161 and its exit from primary cilia. The data obtained so far from IMCD3 *Pald1*<sup>-/-</sup> cell lines supports this idea. However, as a transmembrane protein with low abundance, detection of GPR161 remains challenging. In addition, GPR161 has a specific and important role in SHH signaling. As PALD1 was not associated with SHH signaling before this work, the before mentioned aspects would provide an explanation as to why GPR161 was not identified as a substrate or binding partner of PALD1. Perhaps PALD1 removed phosphates from GPR161 and this ability was evolutionarily lost, resulting in only binding and anti-phosphatase activity.

Loss of PALD1 in IMCD3 cells showed that PALD1 is an attenuator of SHH signaling by increasing Gli3<sup>FL/R</sup> signaling in the presence and absence of pathway activating reagents. Besides that, loss of PALD1 reduced ciliary GPR161 levels. The effect on ciliary GPR161 signaling suggests a possible link to  $\beta$ -arrestins.  $\beta$ -arrestins sense phosphorylation of GPR161 and mediate exit of GPR161 after activation of SHH signaling. Decreased ciliary GPR161 levels in IMCD3 *Pald1*<sup>-/-</sup> cells could indicate that PALD1 inhibits binding of  $\beta$ -arrestins to GPR161 to prevent hyper activation of SHH signaling. However, this theory has not yet been experimentally confirmed. Especially due to the fact that the loss of  $\beta$ -arrestin had no effect on PALD1 suggests that PALD1 functions upstream of  $\beta$ -arrestin. Accordingly,  $\beta$ -arrestin levels should be examined in *Pald1*<sup>-/-</sup> cells in future experiments. Thus, it was shown that PALD1 most likely accumulates in response to changes in the cAMP status of the primary cilium. This results in the hypothesis that PALD1 accumulation is initiated by a change in cAMP status provided by SMO and/or GPR161 in the SHH pathway. The same effect could be possibly achieved by other GPCRs unrelated to SHH signaling such as SSTR3 related signaling.

Two protein phosphatases, Protein phosphatase 1 (PP1) and Protein phosphatase 2A (PP2A), have been reported to dephosphorylate SMO and attenuate SHH signaling in *Drosophila* (Su *et al.*, 2011; Liu *et al.*, 2020). As *Drosophila* are the only organisms that do not require cilia for SHH signaling, the role of PP1 and PP2A remains unclear with respect to primary cilia. Nevertheless, PP2A and PP1 are abundant phosphatases in eukaryotes which suggests a similar function in mammals (Zhao *et al.*, 2017). PALD1 could have a function analogous to PP1 and PP2A, but the data generated here does not suggest this, so far. In mammals, the PIP-phosphatase INPP5E has been clearly shown to localize to cilia and regulate signaling by modifying the respective membrane environment (Xu *et al.*, 2016; Dyson *et al.*, 2017). This

could indicate that PALD1 exerts a lipid phosphatase activity, as well, and support the theory of Phosphatidylinositol (PiP) phosphatase.

### 7.3. The relation between PALD1 and PKA.

The data generated in this work has shown that ciliary PALD1 accumulation is regulated by changes in cAMP levels. This observation suggests a link between PALD1 and PKA, which was investigated in this work using an IMCD3 cilia-PKI cell line which expresses a cilia-localized version of the inhibitory peptide of PKA (Mick *et al.*, 2015). After successful SHH signal activation, adenylyl cyclases are inhibited leading to activation of the signaling pathway through inhibition of PKA. Interestingly, inhibition of ciliary PKA through PKI in IMCD3 cilia-PKI resulted in a reduction of ciliary PALD1 levels compared with a control cell line, while the opposite would be expected (see Fig. 21). So far, PKA-C has only been detected at the ciliary base (Barzi *et al.*, 2010; Tuson *et al.*, 2011). In several experiments within this work, attempts ensure undeniable detection of PKA-C in the primary cilium failed. A recent study that provided a multitude of new insights into ciliary cAMP signaling claimed to have detected PKA-C by fluorescence tag in primary cilia (Truong *et al.*, 2021). However, PKA-R1 $\alpha$  and PKA-C both were tagged within one cell line, using Yellow Fluorescent Protein (YF) and NG. The absorption spectra of YF and NG lie very close to each other, consequently this aspect of the study should be viewed extremely critically. Another very interesting study shows cilia localized PKA-C after stable expression of fluorescence tagged PKA-C in live cell imaging (Arveseth *et al.*, 2021). However, it must be criticized that the images were acquired in the absence of a reliable cilia marker such as ARL13B or ac-tub. Thus, possible background signals or fluorescence from cilia-like structures can be hardly distinguished from the protein of interest. A clear localization of PKA-C to primary cilia was shown by antibody staining in IMCD3 cilia-PKI cells (unpublished data, David Mick). This observation might be a first step in confirming the previously described theory of a cilia localized holoenzyme, that among others, consists of PKA-R1 $\alpha$  and PKA-C and exits the cilium after activation of SHH signaling (May *et al.*, 2021). The fact that detection of PKA-C has not yet been achieved in a physiological set-up could be explained by the possibility that PKA-C levels normally remain below the detection limits of microscopy experiments. PKI binds to PKA-C with a high affinity which in turn binds PKA-R1 $\alpha$  and could result in an increase of PKA-C levels that would raise them above detection limits (Knighton *et al.*, 1991; Dalton & Dewey, 2006). However, PKA-C could not be identified in primary cilia of WT cells neither in the MS analysis nor in IF microscopy (May *et al.*, 2021). Thus, if PKA-C does not localize to primary cilia in WT cells, mislocalization of PKA-C in IMCD3 cilia-PKI could perturb ciliary accumulation of PALD1 in a yet unknown mechanism.

To investigate this idea, an attempt was made to permanently localize PKA-R1 $\alpha$  to the cilia of IMCD3 and 3T3 cells within this work (data not shown.) For this purpose, a GFP tagged version of PKA-R1 $\alpha$  was permanently directed to primary cilia *via* the cilia targeting sequence of NPHP3. The approach of mislocating PKA-R1 $\alpha$  permanently to the primary cilium would bring information on how PKA activity

influences GPCR localization and with which proteins subunits of PKA interact during different stages of SHH signaling. However, this only applies if one assumes that such a dramatic permanent change of the cell can be carried out successfully, as the cells frequently lost the PKA-R1 $\alpha$  construct which unfortunately made it impossible to investigate its effects on SHH signaling within the time frame of this work. It should be noted that the permanent localization of PKA-R1 $\alpha$  in primary cilia represents a major change in the cell as PKA functions in a multitude of cellular processes beyond SHH signaling (Aley & Levine, 1999; Tuson *et al.*, 2011; Bachmann *et al.*, 2016). Consequently, ectopical localization of PKA subunits could pose corresponding problems and result in cell death or loss of the construct. While a similar attempt was recently performed by the group of Jeremy Reiter, the impact of such changes on the localization and activity of GPCRs remains uncertain (Truong *et al.*, 2021). Using a cell line that expresses permanently cilia localized PKA-R1 $\alpha$  could also bring information on the exact localization of PKA-C during SHH signaling. It would also be possible to investigate whether the possible detection of ciliary PKA-C in IMCD3 cilia-PKI cells is actually due to an increase in PKA-R1 $\alpha$  levels, as suspected here.

#### **7.4. Proposed mechanism and Perspectives.**

The improved Cilia-APEX2 cell line allowed new, important insights into one of the most important embryonic signaling pathways, the SHH signaling pathway. Based on the results described within this work, the following mechanism can be proposed. After SMO entry, which leads to a decrease in cAMP levels, PALD1 is transported to the primary cilia. As cilia PALD1 accumulation was impaired in IMCD3 *Ift27*<sup>-/-</sup> cells, this process is most likely mediated *via* IFT-B components. In particular, PALD1 accumulation should be achieved by the IFT25/27 sub-complex, which would explain why *Pald1* is appropriately co-conserved with *Ift25* in particular. After entering the primary cilia, PALD1 appears to attenuate signaling in a negative feedback loop. This could possibly occur *via* changes in the PIP status of the cell membrane, which is then sensed by GPR161 or  $\beta$ -arrestin (Gigante & Casparly, 2020). Thus, PALD1 could functionally act as an antagonist of  $\beta$ -arrestin2 or INPP5E, which is likely to prevent over-activation of SHH signaling. Respective excessive SHH signaling pathway activity bears concerning dangers, as it could lead to tumor formation and developmental defects (Bijlsma & Roelink, 2010). Loss of PALD1 results in decreased ciliary GPR161 levels and stronger SHH signaling responses, accordingly. It is possible that the accumulation of PALD1 is enhanced by direct interaction with TULP3, at least to the extent that a measurable signal is generated. This could be below the detection limit in the IMCD3 *Tulp3*<sup>-/-</sup> cell line. The described mechanism would thus play a crucial role, especially for the fine-tuning of the SHH signaling pathway. Accordingly, loss of PALD1 may lead to mild defects, especially in highly SHH active cells such as C2C12 and 3T3 cells.

As fascinating as the described mechanism may be, this proposed model awaits further confirmation. Therefore, further investigation of the transcriptional read-out of the respective knock out cell lines is recommended. More detailed information about potential interaction partners of PALD1 should be

obtained. In this way, the molecular mechanisms by which PALD1 regulates potential interaction partners can become clearer. More functional assays with PALD1 should be performed to learn about the activity by which PALD1 regulates the described interaction partners. Even if PIP phosphatase activity is suspected as it most likely is currently, this should be further confirmed experimentally. In addition, the possibility that PALD1 regulates SHH signaling pathway components as an anti-phosphatase should also be broadly investigated. In conclusion, knowledge of such finely regulating proteins such as PALD1 may have a crucial impact on the therapy of diverse SHH-dependent genetic diseases. The targeting of fine regulatory effectors could open up the possibility of treating patients without inducing a corresponding secondary disease by too strong interventions. For this reason, the investigation of corresponding fine regulators not only opens up a deeper understanding of the SHH signaling pathway, but also includes multiple promising therapeutic approaches.

## 8. References

1. **Abou Alaiwi**, Wissam A., Shao T. Lo, and Surya M. Nauli (2009)  
“Primary Cilia: Highly Sophisticated Biological Sensors.” *Sensors (Basel, Switzerland)* 9 (9): 7003–20. <https://doi.org/10.3390/s90907003>.
2. **Aley**, Kochuvelikakam O., and Jon D. **Levine** (1999)  
“Role of Protein Kinase A in the Maintenance of Inflammatory Pain.” *Journal of Neuroscience* 19 (6): 2181–86.  
<https://doi.org/10.1523/JNEUROSCI.19-06-02181.1999>.
3. **Alsolami**, Mona, Kuhns Stefanie, Alsulami Manal, and Blacque, Oliver E. (2019)  
“ERICH3 in Primary Cilia Regulates Cilium Formation and the Localisations of Ciliary Transport and Sonic Hedgehog Signaling Proteins.” *Scientific Reports* 9 (November).  
<https://doi.org/10.1038/s41598-019-52830-1>.
4. **Ampofo**, Emmanuel, Nalbach Lisa, Menger Michael D., and Laschke, Matthias W. (2020)  
“Regulatory Mechanisms of Somatostatin Expression.” *International Journal of Molecular Sciences* 21 (11).  
<https://doi.org/10.3390/ijms21114170>.
5. **Andrews**, Douglas, and **Nelson**, David L (1979)  
“Biochemical Studies of the Excitable Membrane of Paramecium Tetraurelia. II. Phospholipids of Ciliary and Other Membranes.” *Biochimica et Biophysica Acta (BBA) - Biomembranes* 550 (2): 174–87.  
[https://doi.org/10.1016/0005-2736\(79\)90205-0](https://doi.org/10.1016/0005-2736(79)90205-0).
6. **Anvarian**, Zeinab, Mykytyn Kirk, Mukhopadhyay Saikat, Bang Pedersen Lotte, and Tvorup Christensen, Søren. (2019).  
“Cellular Signalling by Primary Cilia in Development, Organ Function and Disease.” *Nature Reviews Nephrology* 15 (4):199–219.  
<https://doi.org/10.1038/s41581-019-0116-9>.
7. **Arveseth**, Corvin D., Happ, John T., Hedeem, Danielle S., Zhu, Ju-Fen, Capener, Jacob L., Shaw, Dana Klatt, Deshpande, Ishan, Liang Jiahao, Xu, Jiewei, Stubben ,Sara L., Nelson, Isaac B., Walker Madison F., Kawakami Kouki, MyersR. Benjamin *et al.*, (2021)  
“Smoothed transduces Hedgehog signals via activity-dependent sequestration of PKA Catalytic subunits.” *Plos Biology*, 3001191  
<https://doi.org/10.1371/journal.pbio.3001191>
8. **Avidor-Reiss**, Tomer, Maer Andreia M., Koundakjian Edmund, Polyanovsky Andrey, Keil Thomas, Subramaniam Shankar and Zuker, Charles S. (2004).  
“Decoding Cilia Function: Defining Specialized Genes Required for Compartmentalized Cilia Biogenesis,” 13.
9. **Ayers**, Katie L., and **Thérond** Pascal P. (2010)  
“Evaluating Smoothed as a G-Protein-Coupled Receptor for Hedgehog Signalling.”



- Trends in Cell Biology* 20 (5): 287–98.  
<https://doi.org/10.1016/j.tcb.2010.02.002>.
10. **Bachmann**, Verena A., Mayrhofer Johanna E., Ronit Ilouz, Philipp Tschaikner, Philipp Raffeiner, Ruth Röck, Mathieu Courcelles, *et al.* (2016)  
“Gpr161 Anchoring of PKA Consolidates GPCR and CAMP Signaling.”  
*Proceedings of the National Academy of Sciences of the United States of America* 113 (28): 7786–91.  
<https://doi.org/10.1073/pnas.1608061113>.
  11. **Baker**, Sheila A., Freeman Katie, Luby-Phelps Katherine, Pazour Gregory J., and Besharse Joseph C. (2003)  
“IFT20 Links Kinesin II with a Mammalian Intraflagellar Transport Complex That Is Conserved in Motile Flagella and Sensory Cilia \*.”  
*Journal of Biological Chemistry* 278 (36): 34211–18.  
<https://doi.org/10.1074/jbc.M300156200>.
  12. **Baldwin**, J. C., Karthikeyan A. S., and Raghothama K. G. (2001)  
“LEPS2, a Phosphorus Starvation-Induced Novel Acid Phosphatase from Tomato.” *Plant Physiology* 125 (2): 728–37.  
<https://doi.org/10.1104/pp.125.2.728>.
  13. **Bar**, Eli E., Chaudhry Aneeka, Lin Alex, Fan Xing, Schreck Karisa, Matsui William, Piccirillo Sara, *et al.* (2007)  
“Cyclopamine-Mediated Hedgehog Pathway Inhibition Depletes Stem-Like Cancer Cells in Glioblastoma.” *STEM CELLS* 25 (10): 2524–33.  
<https://doi.org/10.1634/stemcells.2007-0166>.
  14. **Barzi**, Mercedes, Berenguer Jordi, Menendez Anghara, Alvarez-Rodriguez, Ruben and Pons, Sebastian (2010)  
“Sonic-Hedgehog-Mediated Proliferation Requires the Localization of PKA to the Cilium Base.” *Journal of Cell Science* 123 (1): 62–69.  
<https://doi.org/10.1242/jcs.060020>.
  15. **Beales**, Phil, and **Jackson**, Peter K. (2012)  
“Cilia - the Prodigal Organelle.” *Cilia* 1 (1): 1.  
<https://doi.org/10.1186/2046-2530-1-1>.
  16. **Bear**, M. F.; Connors, B. W.; Paradiso, M. A.;  
Neurowissenschaften – ein grundlegendes Lehrbuch für Biologie, Medizin und Psychologie“  
Springer Spektrum, 2. Auflage 978-3-662-57262-7
  17. **Bergmann**, Carsten, Fliegau, Manfred, Ortiz Brüchle Nadina, Frank Valeska, Olbrich Heike , Kirschner Jan, Schermer Bernhard, *et al.* (2008)  
“Loss of Nephrocystin-3 Function Can Cause Embryonic Lethality, Meckel-Gruber-like Syndrome, Situs Inversus, and Renal-Hepatic-Pancreatic Dysplasia.” *American Journal of Human Genetics* 82 (4): 959–70.  
<https://doi.org/10.1016/j.ajhg.2008.02.017>.

18. **Bergmann**, Carsten, Guay-Woodford Lisa M., Harris Peter C., Horie Shigeo, Peters Dorian J. M., and Torres Vicente E. (2018)  
 “Polycystic Kidney Disease.” *Nature Reviews Disease Primers* 4 (1): 1–24.  
<https://doi.org/10.1038/s41572-018-0047-y>.
19. **Bernabé-Rubio**, Miguel, and **Alonso** Miguel A. (2017)  
 “Routes and Machinery of Primary Cilium Biogenesis.” *Cellular and Molecular Life Sciences* 74 (22): 4077–95.  
<https://doi.org/10.1007/s00018-017-2570-5>.
20. **Besschetnova**, Tatiana Y., Kolpakova-Hart Elona, Guan Yinghua, Zhou Jing, Olsen Bjorn R., And Shah Jagesh V. (2010)  
 “Identification of Signaling Pathways Regulating Primary Cilium Length and Flow-Mediated Adaptation.” *Current Biology : CB* 20 (2): 182–87.
21. **Bijlsma**, Maarten F., and **Roelink** Henk (2010)  
 “Non-Cell-Autonomous Signaling by Shh in Tumors: Challenges and Opportunities for Therapeutic Targets.” *Expert Opinion on Therapeutic Targets* 14 (7): 693–702.  
<https://doi.org/10.1517/14728222.2010.497488>.
22. **Blacque**, O. E., and **Leroux** M. R. (2006)  
 “Bardet-Biedl Syndrome: An Emerging Pathomechanism of Intracellular Transport.” *Cellular and Molecular Life Sciences: CMLS* 63 (18): 2145–61.  
<https://doi.org/10.1007/s00018-006-6180-x>.
23. **Blau**, H. M., Pavlath G. K., Hardeman E. C., Chiu C. P., Silberstein L., Webster S. G., Miller S. C., and Webster C. (1985)  
 “Plasticity of the Differentiated State.” *Science (New York, N.Y.)* 230 (4727): 758–66.  
<https://doi.org/10.1126/science.2414846>.
24. **Bloodgood**, Robert A. (2010)  
 “Sensory Reception Is an Attribute of Both Primary Cilia and Motile Cilia.” *Journal of Cell Science* 123 (4): 505–9.  
<https://doi.org/10.1242/jcs.066308>.
25. **Bodnar**, A. G., Ouellette M., Frolkis M., Holt S. E., Chiu C. P., Morin G. B., Harley C. B., Shay J. W., Lichtsteiner S., and Wright W. E. (1998)  
 “Extension of Life-Span by Introduction of Telomerase into Normal Human Cells.” *Science (New York, N.Y.)* 279 (5349): 349–52.  
<https://doi.org/10.1126/science.279.5349.349>.
26. **Bradford**, Marion M. (1976)  
 “A Rapid and Sensitive Method for the Quantitation of Microgram Quantities of Protein Utilizing the Principle of Protein-Dye Binding.” *Analytical Biochemistry* 72 (1): 248–54.  
[https://doi.org/10.1016/0003-2697\(76\)90527-3](https://doi.org/10.1016/0003-2697(76)90527-3).
27. **Brehm**, P., and Eckert R. (1978)  
 “An Electrophysiological Study of the Regulation of Ciliary Beating Frequency in

- Paramecium.” *The Journal of Physiology* 283 (October): 557–68.  
<https://doi.org/10.1113/jphysiol.1978.sp012519>.
28. **Breslow**, David K., Hoogendoorn Sascha, Kopp Adam R., Morgens David W., Vu Brandon K., Kennedy Margaret C., Han Kyuho, *et al.* (2018)  
 “A CRISPR-Based Screen for Hedgehog Signaling Provides Insights into Ciliary Function and Ciliopathies.” *Nature Genetics* 50 (3): 460–71.  
<https://doi.org/10.1038/s41588-018-0054-7>.
  29. **Bufalieri**, Francesca, Lospinoso Severini Ludovica, Caimano Miriam, Infante Paola, and Di Marcotullio Lucia (2020)  
 “DUBs Activating the Hedgehog Signaling Pathway: A Promising Therapeutic Target in Cancer.” *Cancers* 12 (6): 1518.  
<https://doi.org/10.3390/cancers12061518>.
  30. **Bustamante-Marin**, Ximena M., and Ostrowski Lawrence E. (2017)  
 “Cilia and Mucociliary Clearance.” *Cold Spring Harbor Perspectives in Biology* 9 (4).  
<https://doi.org/10.1101/cshperspect.a028241>.
  31. **Carvalho-Santos**, Zita, Machado Pedro, Branco Pedro, Tavares-Cadete Filipe, Rodrigues-Martins Ana, Pereira-Leal José B., and Bettencourt-Dias Mónica (2010)  
 “Stepwise Evolution of the Centriole-Assembly Pathway.” *Journal of Cell Science* 123 (9): 1414–26.  
<https://doi.org/10.1242/jcs.064931>.
  32. **Chen**, James K., Taipale Jussi, Cooper Michael K. and Beachy Philip A. (2002)  
 “Inhibition of Hedgehog Signaling by Direct Binding of Cyclopamine to Smoothed.” *Genes & Development* 16 (21): 2743–48.  
<https://doi.org/10.1101/gad.1025302>.
  33. **Chiang**, Chin, Ying Litingtung, Eric Lee, Keith E. Young, Jeffrey L. Corden, Heiner Westphal, and Philip A. Beachy. (1996)  
 “Cyclopia and Defective Axial Patterning in Mice Lacking Sonic Hedgehog Gene Function.” *Nature* 383 (6599): 407–13.  
<https://doi.org/10.1038/383407a0>.
  34. **Cohen**, Michael, Kicheva Anna, Ribeiro Ana, Blassberg Robert, Page Karen M., Barnes Chris P. and Briscoe James (2015)  
 “Ptch1 and Gli Regulate Shh Signalling Dynamics via Multiple Mechanisms.” *Nature Communications* 6 (1): 6709.  
<https://doi.org/10.1038/ncomms7709>.
  35. **Cole**, B. R. (1990)  
 “Autosomal Recessive Polycystic Kidney Disease.” In *The Cystic Kidney*, edited by Kenneth D. Gardner and Jay Bernstein, 327–50. Developments in Nephrology. Dordrecht: Springer Netherlands.  
[https://doi.org/10.1007/978-94-009-0457-6\\_13](https://doi.org/10.1007/978-94-009-0457-6_13).
  36. **Compton**, Steve J., and Jones Clive G. (1985)

- “Mechanism of Dye Response and Interference in the Bradford Protein Assay.”  
*Analytical Biochemistry* 151 (2): 369–74.  
[https://doi.org/10.1016/0003-2697\(85\)90190-3](https://doi.org/10.1016/0003-2697(85)90190-3).
37. **Cornec-Le Gall**, Emilie, Audrézet Marie-Pierre, Chen Jian-Min, Hourmant Maryvonne, Morin Marie-Pascale, Perrichot Régine, Charasse Christophe, *et al.* (2013)  
 “Type of PKD1 Mutation Influences Renal Outcome in ADPKD.” *Journal of the American Society of Nephrology : JASN* 24 (6): 1006–13.  
<https://doi.org/10.1681/ASN.2012070650>.
38. **Craige**, Branch, Brown Jason M., and Witman George B. (2013)  
 “Isolation of Chlamydomonas Flagella.” *Current Protocols in Cell Biology / Editorial Board, Juan S. Bonifacino ... [et Al.]* 0 3 (June): Unit-3.41.9.  
<https://doi.org/10.1002/0471143030.cb0341s59>.
39. **Byrne**, Eamon F. X., Sircar Ria, Miller Paul S., Hedger George, Luchetti Giovanni, Nachtergaele Sigrid, Tully Mark D., *et al.* (2016)  
 “Structural Basis of Smoothened Regulation by Its Extracellular Domains.” *Nature* 535 (7613): 517–22.  
<https://doi.org/10.1038/nature18934>.
40. **Christensen**, Søren T., Pedersen Lotte B., Schneider Linda, and Satir Peter (2007)  
 “Sensory Cilia and Integration of Signal Transduction in Human Health and Disease.” *Traffic* 8 (2): 97–109.  
<https://doi.org/10.1111/j.1600-0854.2006.00516.x>.
41. **Essner**, Jeffrey J., Vogan, Kyle J., Tabin, Clifford J., Yost Joseph, Brueckner, Martina. (2002)  
 “Conserved Function for Embryonic Nodal Cilia” *Nature* 418, 37-38  
<https://www.nature.com/articles/418037a>.
42. **Craige**, Branch, Tsao Che-Chia, Diener Dennis R., Hou Yuqing, Lechtreck Karl-Ferdinand, Rosenbaum Joel L., And Witman George B. (2010)  
 “CEP290 Tethers Flagellar Transition Zone Microtubules to the Membrane and Regulates Flagellar Protein Content.” *Journal of Cell Biology* 190 (5): 927–40.  
<https://doi.org/10.1083/jcb.201006105>.
43. **Dalgaard** OZ. 1957  
 “Bilateral polycystic disease of the kidneys: A follow-up of two hundred and eighty-four patients and their families.” *Acta Med Scand (Suppl)* 328:1—255
44. **Dalton**, George D., and Dewey William L. (2006)  
 “Protein Kinase Inhibitor Peptide (PKI): A Family of Endogenous Neuropeptides That Modulate Neuronal cAMP-Dependent Protein Kinase Function.” *Neuropeptides* 40 (1): 23–34.  
<https://doi.org/10.1016/j.npep.2005.10.002>.
45. **Desai**, Paurav B., Stuck Michael W., Lv Bo, and Pazour Gregory J. (2020)  
 “Ubiquitin Links Smoothened to Intraflagellar Transport to Regulate Hedgehog Signaling.” *Journal of Cell Biology* 219 (7).

- <https://doi.org/10.1083/jcb.201912104>.
46. **Dobell**, Clifford F.R.S. (1932).  
“Anthony van Leeuwenhoek and his “little animals.” Harcourt, Brace and Company.
  47. **Dyson**, Jennifer M., Conduit Sarah E., Feeney Sandra J., Hakim Sandra, DiTommaso Tia, Fulcher Alex J., Sriratana Absorn, *et al.* (2016)  
“INPP5E Regulates Phosphoinositide-Dependent Cilia Transition Zone Function.” *Journal of Cell Biology* 216 (1): 247–63.  
<https://doi.org/10.1083/jcb.201511055>.
  48. **Eguether**, Thibaut, Cordelieres Fabrice P., and Pazour Gregory J. (2018)  
“Intraflagellar Transport Is Deeply Integrated in Hedgehog Signaling.” *Molecular Biology of the Cell* 29 (10): 1178–89.  
<https://doi.org/10.1091/mbc.E17-10-0600>.
  49. **Eguether**, Thibaut, San Agustin Jovenal T., Keady Brian T., Jonassen Julie A., Liang Yinwen, Francis Richard, Tobita Kimimasa, *et al.* (2014)  
“IFT27 Links the BBSome to IFT for Maintenance of the Ciliary Signaling Compartment.” *Developmental Cell* 31 (3): 279–90.  
<https://doi.org/10.1016/j.devcel.2014.09.011>.
  50. **Elia**, Dafna, Madhala Dorit, Ardon Eti, Reshef Ram, and Halevy Orna. (2007)  
“Sonic Hedgehog Promotes Proliferation and Differentiation of Adult Muscle Cells: Involvement of MAPK/ERK and PI3K/Akt Pathways.” *Biochimica Et Biophysica Acta* 1773 (9): 1438–46.  
<https://doi.org/10.1016/j.bbamcr.2007.06.006>.
  51. **Erger**, Florian, Ortiz Brüchle Nadina, Gembruch Ulrich and Zerres Klaus (2017)  
“Prenatal Ultrasound, Genotype, and Outcome in a Large Cohort of Prenatally Affected Patients with Autosomal-Recessive Polycystic Kidney Disease and Other Hereditary Cystic Kidney Diseases.” *Archives of Gynecology and Obstetrics* 295 (4): 897–906.  
<https://doi.org/10.1007/s00404-017-4336-6>.
  52. **Everson**, Joshua L., Fink Dustin M., Chung Hannah M., Sun Miranda R., and Lipinski Robert J. (2018)  
“Identification of Sonic Hedgehog-Regulated Genes and Biological Processes in the Cranial Neural Crest Mesenchyme by Comparative Transcriptomics.” *BMC Genomics* 19 (1): 497.  
<https://doi.org/10.1186/s12864-018-4885-5>.
  53. **Fanconi**, G., E. Hanhart, A. von ALBERTINI, E. Uhlinger, Dolivo G., and Prader A. (1951)  
“[Familial, juvenile nephronophthisis (idiopathic parenchymal contracted kidney)].” *Helvetica Paediatrica Acta* 6 (1): 1–49.
  54. **Feldmann**, Georg, Fendrich Volker, McGovern Karen, Bedja Djahida, Bisht Savita, Alvarez Hector, Jan-Bart M. Koorstra, *et al.* (2008)  
“An Orally Bioavailable Small-Molecule Inhibitor of Hedgehog Signaling Inhibits Tumor Initiation and Metastasis in Pancreatic Cancer.” *Molecular Cancer Therapeutics* 7 (9): 2725–35.  
<https://doi.org/10.1158/1535-7163.MCT-08-0573>.

55. **Feng**, Jianhua, Tamaskovic Rastislav, Yang Zhongzhou, Brazil Derek P., Merlo Adrian, Hess Daniel, and Hemmings Brian A. (2004)  
“Stabilization of Mdm2 via Decreased Ubiquitination Is Mediated by Protein Kinase B/Akt-Dependent Phosphorylation \*.” *Journal of Biological Chemistry* 279 (34): 35510–17.  
<https://doi.org/10.1074/jbc.M404936200>.
56. **Forsythe**, Elizabeth, and Beales Philip L. (2013)  
“Bardet–Biedl Syndrome.” *European Journal of Human Genetics* 21 (1): 8–13.  
<https://doi.org/10.1038/ejhg.2012.115>.
57. **Firat-Karalar**, Elif Nur, Rauniyar Navin, Yates John R., and Stearns Tim (2014)  
“Proximity Interactions among Centrosome Components Identify Regulators of Centriole Duplication.” *Current Biology: CB* 24 (6): 664–70.  
<https://doi.org/10.1016/j.cub.2014.01.067>.
58. **Fliegauf**, Manfred, Benzing Thomas, and Omran Heymut (2007)  
“When Cilia Go Bad: Cilia Defects and Ciliopathies.” *Nature Reviews Molecular Cell Biology* 8 (11): 880–93.  
<https://doi.org/10.1038/nrm2278>.
59. **Gabow**, Patricia A. (1990)  
“Autosomal Dominant Polycystic Kidney Disease—More Than a Renal Disease.” *American Journal of Kidney Diseases* 16 (5): 403–13.  
[https://doi.org/10.1016/S0272-6386\(12\)80051-5](https://doi.org/10.1016/S0272-6386(12)80051-5).
60. **Gabow**, Patricia A., Duley Irene, and Johnson Ann M. (1992)  
“Clinical Profiles of Gross Hematuria in Autosomal Dominant Polycystic Kidney Disease.” *American Journal of Kidney Diseases* 20 (2): 140–43.  
[https://doi.org/10.1016/S0272-6386\(12\)80541-5](https://doi.org/10.1016/S0272-6386(12)80541-5).
61. **Gagnadoux**, M. F., Bacri J. L., Broyer M., and Habib R. (1989)  
“Infantile Chronic Tubulo-Interstitial Nephritis with Cortical Microcysts: Variant of Nephronophthisis or New Disease Entity?” *Pediatric Nephrology* 3 (1): 50–55.  
<https://doi.org/10.1007/BF00859626>.
62. **Garcia**, Galo, Raleigh David R., and Reiter Jeremy F. (2018)  
“How the Ciliary Membrane Is Organized Inside-Out to Communicate Outside-In.” *Current Biology* 28 (8): R421–34.  
<https://doi.org/10.1016/j.cub.2018.03.010>.
63. **Garcia-Gonzalo**, Francesc R., and Reiter Jeremy F. (2017)  
“Open Sesame: How Transition Fibers and the Transition Zone Control Ciliary Composition.” *Cold Spring Harbor Perspectives in Biology* 9 (2): a028134.  
<https://doi.org/10.1101/cshperspect.a028134>.
64. **Garcia-Gonzalo**, Francesc R., Cheng Phua Siew, Roberson Elle C., Galo Garcia, Monika Abedin, Schurmans Stéphane, Inoue Takanari, and Reiter Jeremy F. (2015)  
“Phosphoinositides Regulate Ciliary Protein Trafficking to Modulate Hedgehog Signaling.” *Developmental Cell* 34 (4): 400–409.

- <https://doi.org/10.1016/j.devcel.2015.08.001>.
65. **Ghossoub**, Rania, Molla-Herman Anahi, Bastin Philippe and Benmerah Alexandre (2011)  
“The Ciliary Pocket: A Once-Forgotten Membrane Domain at the Base of Cilia.” *Biology of the Cell* 103 (3): 131–44.  
<https://doi.org/10.1042/BC20100128>.
  66. **Gigante**, Eduardo D., and **Caspary** Tamara (2020)  
“Signaling in the Primary Cilium through the Lens of the Hedgehog Pathway.” *WIREs Developmental Biology* n/a (n/a): e377.  
<https://doi.org/10.1002/wdev.377>.
  67. **Gluzn**, Eva, Höög Johanna L., Smith Amy E., Dawe Helen R., Shaw Michael K., and Gull Keith (2010)  
“Beyond 9+0: Noncanonical Axoneme Structures Characterize Sensory Cilia from Protists to Humans.” *FASEB Journal: Official Publication of the Federation of American Societies for Experimental Biology* 24 (9): 3117–21.  
<https://doi.org/10.1096/fj.09-151381>.
  68. **Go**, Alan S., Yang Jingrong, Ackerson Lynn M., Lepper Krista, Robbins Sean, Massie Barry M., and Shlipak Michael G. (2006)  
“Hemoglobin Level, Chronic Kidney Disease, and the Risks of Death and Hospitalization in Adults with Chronic Heart Failure: The Anemia in Chronic Heart Failure: Outcomes and Resource Utilization (ANCHOR) Study.” *Circulation* 113 (23): 2713–23.  
<https://doi.org/10.1161/CIRCULATIONAHA.105.577577>.
  69. **Goetz**, S. C., and **Anderson**, K. V. (2010).  
The Primary Cilium: A Signaling Center during Vertebrate Development. *Nat. Rev. Genet.* 11, 331–344. Doi: 10.1038/Nrg2774. - *Nature Reviews Genetics* 11, 331-433.
  70. **Goodrich**, Lisa V., Milenković Ljiljana, Higgins Kay M., and Scott Matthew P. (1997)  
“Altered Neural Cell Fates and Medulloblastoma in Mouse Patched Mutants.” *Science* 277 (5329): 1109–13.  
<https://doi.org/10.1126/science.277.5329.1109>.
  71. **Gonçalves**, João, and **Pelletier** Laurence (2017)  
“The Ciliary Transition Zone: Finding the Pieces and Assembling the Gate.” *Molecules and Cells* 40 (4): 243–53.  
<https://doi.org/10.14348/molcells.2017.0054>.
  72. **Gui**, Miao, Ma Meisheng, Sze-Tu Erica, Wang Xiangli, Koh Fujiet, Zhong Ellen D., Berger Bonnie, *et al.* (2021)  
“Structures of Radial Spokes and Associated Complexes Important for Ciliary Motility.” *Nature Structural & Molecular Biology* 28 (1): 29–37.  
<https://doi.org/10.1038/s41594-020-00530-0>.
  73. **He**, Mu, Subramanian Radhika, Bangs Fiona, Omelchenko Tatiana, Liem Karel F., Kapoor Tarun M., and Anderson Kathryn V. (2014)  
“The Kinesin-4 Protein Kif7 Regulates Mammalian Hedgehog Signalling by Organizing the

- Cilium Tip Compartment.” *Nature Cell Biology* 16 (7): 663–72.  
<https://doi.org/10.1038/ncb2988>.
74. **Hernandez-Hernandez**, Victor, Pravincumar Priyanka, Diaz-Font Anna, May-Simera Helen, Jenkins Dagan, Knight Martin, and Beales Philip L. (2013)  
“Bardet–Biedl Syndrome Proteins Control the Cilia Length through Regulation of Actin Polymerization.” *Human Molecular Genetics* 22 (19): 3858–68.  
<https://doi.org/10.1093/hmg/ddt241>.
75. **Heuser**, Thomas, Raytchev Milen, Krell Jeremy, Porter Mary E., and Nicastró Daniela. (2009)  
“The Dynein Regulatory Complex Is the Nexin Link and a Major Regulatory Node in Cilia and Flagella.” *Journal of Cell Biology* 187 (6): 921–33.  
<https://doi.org/10.1083/jcb.200908067>.
76. **Hildebrandt**, Friedhelm, Benzing Thomas, and Katsanis Nichola (2011)  
“Ciliopathies.” *The New England Journal of Medicine* 364 (16): 1533–43.  
<https://doi.org/10.1056/NEJMra1010172>.
77. **Hsu**, Shu-Hsuan C., Zhang Xiaoyun, Yu Chunying, Li Zhu Juan, Wunder Jay S., Chi-Chung Hui, and Alman Benjamin A. (2011)  
“Kif7 Promotes Hedgehog Signaling in Growth Plate Chondrocytes by Restricting the Inhibitory Function of Sufu.” *Development* 138 (17): 3791–3801.  
<https://doi.org/10.1242/dev.069492>.
78. **Huang**, Ning, Zhang Donghui, Li Fangyuan, Chai Peiyuan, Wang Song, Teng Junlin, and Chen Jianguo. (2018)  
“M-Phase Phosphoprotein 9 Regulates Ciliogenesis by Modulating CP110-CEP97 Complex Localization at the Mother Centriole.” *Nature Communications* 9 (1): 4511.  
<https://doi.org/10.1038/s41467-018-06990-9>.
79. **Huang**, Shih-Min A., Hancock Michael K., Pitman Jeffrey L., Orth Anthony P., and Gekakis Nicholas (2009)  
“Negative Regulators of Insulin Signaling Revealed in a Genome-Wide Functional Screen.” *PLoS ONE* 4 (9).  
<https://doi.org/10.1371/journal.pone.0006871>.
80. **Huangfu**, Danwei, Liu Aimin, Rakeman Andrew S., Murcia Noel S., Niswander Lee, and Anderson Kathryn V. (2003)  
“Hedgehog Signalling in the Mouse Requires Intraflagellar Transport Proteins.” *Nature* 426 (6962): 83–87.  
<https://doi.org/10.1038/nature02061>.
81. **Huangfu**, Danwei, and Anderson Kathryn V. (2005)  
“Cilia and Hedgehog Responsiveness in the Mouse.” *Proceedings of the National Academy of Sciences* 102 (32): 11325–30.  
<https://doi.org/10.1073/pnas.0505328102>.
82. **Hwang**, Sun-hee, White Kevin A., Somatilaka Bandarigoda N., Shelton John M., Richardson James A., and Mukhopadhyay Saikat (2018)



- “The G Protein-Coupled Receptor Gpr161 Regulates Forelimb Formation, Limb Patterning and Skeletal Morphogenesis in a Primary Cilium-Dependent Manner.” *Development (Cambridge, England)* 145 (1).  
<https://doi.org/10.1242/dev.154054>.
83. **Inaba, Kazuo. 2011.**  
 “Sperm Flagella: Comparative and Phylogenetic Perspectives of Protein Components.” *Molecular Human Reproduction* 17 (8): 524–38.  
<https://doi.org/10.1093/molehr/gar034>.
84. **Ishikawa, Hiroaki, Thompson James, Yates John R., And Marshall Wallace F. (2012)**  
 “Proteomic Analysis of Mammalian Primary Cilia.” *Current Biology* 22 (5): 414–19.  
<https://doi.org/10.1016/j.cub.2012.01.031>.
85. **Jain, Raksha, Javidan-Nejad Cylen, Alexander-Brett Jennifer, Horani Amjad, Cabellon Michelle C., Walter Michael J. and Brody Steven L. (2012)**  
 “Sensory Functions of Motile Cilia and Implication for Bronchiectasis.” *Frontiers in Bioscience (Scholar Edition)* 4 (January): 1088–98.
86. **Jensen, Victor L, Li Chunmei, Bowie Rachel V., Clarke Lara, Mohan Swetha, Blacque Oliver E. and Leroux Michel R. (2015)**  
 “Formation of the Transition Zone by Mks5/Rpgrip1L Establishes a Ciliary Zone of Exclusion (CIZE) That Compartmentalises Ciliary Signalling Proteins and Controls PIP2 Ciliary Abundance.” *The EMBO Journal* 34 (20): 2537–56.  
<https://doi.org/10.15252/embj.201488044>.
87. **Kanie, Tomoharu, Abbott Keene Louis, Mooney Nancie Ann, Plowey Edward Douglas, Demeter Janos, and Jackson Peter Kent. (2017)**  
 “The CEP19-RABL2 GTPase Complex Binds IFT-B to Initiate Intraflagellar Transport at the Ciliary Base.” *Developmental Cell* 42 (1): 22-36.e12.  
<https://doi.org/10.1016/j.devcel.2017.05.016>.
88. **Keady, Brian T., Samtani Rajeev, Tobita Kimimasa, Tsuchya Maiko, San Agustin Jovenal T., Follit John A., Jonassen Julie A., Subramanian Ramiah, Lo Cecilia W., and Pazour Gregory J. (2012)**  
 “IFT25 Links the Signal-Dependent Movement of Hedgehog Components to Intraflagellar Transport.” *Developmental Cell* 22 (5): 940–51.  
<https://doi.org/10.1016/j.devcel.2012.04.009>.
89. **Kharitidi, Dmitri, Manteghi Sanaz, and Pause Arnim. (2014)**  
 “Pseudophosphatases: Methods of Analysis and Physiological Functions.” *Methods, Protein Tyrosine Phosphatase Methods*, 65 (2): 207–18.  
<https://doi.org/10.1016/j.ymeth.2013.09.009>.
90. **Kim, Jynho, Kato Masaki, and Beachy Philip A. (2009)**  
 “Gli2 Trafficking Links Hedgehog-Dependent Activation of Smoothed in the Primary Cilium to Transcriptional Activation in the Nucleus.” *Proceedings of the National Academy of Sciences*

- 106 (51): 21666–71.  
<https://doi.org/10.1073/pnas.0912180106>.
91. **Kinnebrew**, Maia, Iverson Ellen J., Patel Bhaven B., Pusapati Ganesh V., Kong Jennifer H., Johnson Kristen A., Luchetti Giovanni, *et al.* (2019)  
“Cholesterol Accessibility at the Ciliary Membrane Controls Hedgehog Signaling.” *ELife* 8 (October).  
<https://doi.org/10.7554/eLife.50051>.
92. **Knighton**, D. R., Zheng J. H., Eyck L. F. Ten, Xuong N. H., Taylor S. S., and Sowadski J. M. (1991)  
“Structure of a Peptide Inhibitor Bound to the Catalytic Subunit of Cyclic Adenosine Monophosphate-Dependent Protein Kinase.” *Science (New York, N.Y.)* 253 (5018): 414–20.  
<https://doi.org/10.1126/science.1862343>.
93. **Kobayashi**, Tetsuo, and **Dynlacht** Brian D. (2011)  
“Regulating the Transition from Centriole to Basal Body.” *The Journal of Cell Biology* 193 (3): 435–44.  
<https://doi.org/10.1083/jcb.201101005>.
94. **Kohli**, Priyanka, Höhne Martin, Jüngst Christian, Bertsch Sabine, Ebert Lena K., Schauss Astrid C., Benzing Thomas, Rinschen Markus M. and Schermer Bernhard. (2017)  
“The Ciliary Membrane-associated Proteome Reveals Actin-binding Proteins as Key Components of Cilia.” *EMBO Reports* 18 (9): 1521–35.  
<https://doi.org/10.15252/embr.201643846>.
95. **Kowatsch**, Christiane, Woolley Rachel E., Kinnebrew Maia, Rohatgi Rajat, and Siebold Christian (2019)  
“Structures of Vertebrate Patched and Smoothed Reveal Intimate Links between Cholesterol and Hedgehog Signalling.” *Current Opinion in Structural Biology* 57 (June): 204–14.  
<https://doi.org/10.1016/j.sbi.2019.05.015>.
96. **Kozminski**, K. G., Beech P. L., and Rosenbaum J. L. (1995)  
“The Chlamydomonas Kinesin-like Protein FLA10 Is Involved in Motility Associated with the Flagellar Membrane.” *Journal of Cell Biology* 131 (6): 1517–27.  
<https://doi.org/10.1083/jcb.131.6.1517>.
97. **Kyttälä**, Mira, Tallila Jonna, Salonen Riitta, Kopra Outi, Kohlschmidt Nicolai, Paavola-Sakki Paulina, Peltonen Leena, and Kestilä Marjo (2006)  
“MKS1 , Encoding a Component of the Flagellar Apparatus Basal Body Proteome, Is Mutated in Meckel Syndrome.” *Nature Genetics* 38 (2): 155–57.  
<https://doi.org/10.1038/ng1714>.
98. **Lam**, Stephanie S., Martell Jeffrey D., Kamer Kimberli J., Deerinck Thomas J., Ellisman Mark H., Mootha Vamsi K., and Ting Alice Y. (2015)  
“Directed Evolution of APEX2 for Electron Microscopy and Proximity Labeling.” *Nature Methods* 12 (1): 51–54.  
<https://doi.org/10.1038/nmeth.3179>.

99. **Lambert**, Jean-Philippe, Tucholska Monika, Go Christopher, Knight James D. R., and Gingras Anne-Claude. (2015)  
 “Proximity Biotinylation and Affinity Purification Are Complementary Approaches for the Interactome Mapping of Chromatin-Associated Protein Complexes.” *Journal of Proteomics*, Protein dynamics in health and disease, 118 (April): 81–94.  
<https://doi.org/10.1016/j.jprot.2014.09.011>.
100. **Lechtreck**, Karl-Ferdinand, Johnson Eric C., Sakai Tsuyoshi, Cochran Deborah, Ballif Bryan A., Rush John, Pazour Gregory J., Ikebe Mitsuo, and Witman George B. (2009)  
 “The Chlamydomonas Reinhardtii BBSome Is an IFT Cargo Required for Export of Specific Signaling Proteins from Flagella.” *Journal of Cell Biology* 187 (7): 1117–32.  
<https://doi.org/10.1083/jcb.200909183>.
101. **Leitch**, Carmen C., Lodh Sukanya, Prieto-Echagüe Victoria, Badano Jose L, and Zaghoul Norann A. (2014)  
 “Basal Body Proteins Regulate Notch Signaling through Endosomal Trafficking.” *Journal of Cell Science* 127 (11): 2407–19.  
<https://doi.org/10.1242/jcs.130344>.
102. **Li**, Yiwei, Maitah Ma'in Y, Ahmad Aamir, Kong Dejuan, Bao Bin, and Sarkar Fazlul H. (2012)  
 “Targeting the Hedgehog Signaling Pathway for Cancer Therapy.” *Expert Opinion on Therapeutic Targets* 16 (1): 49–66.  
<https://doi.org/10.1517/14728222.2011.617367>.
103. **Liao**, Xiaoyun, Siu Michelle K. Y., Au Christy W. H., Wong Esther S. Y., Chan Hoi Yan, Ip Philip P. C., Ngan Hextan Y. S., and Cheung Annie N. Y. (2009)  
 “Aberrant Activation of Hedgehog Signaling Pathway in Ovarian Cancers: Effect on Prognosis, Cell Invasion and Differentiation.” *Carcinogenesis* 30 (1): 131–40.  
<https://doi.org/10.1093/carcin/bgn230>.
104. **Liew**, Gerald M., Ye Fan, Nager Andrew R., Murphy J. Patrick, Lee Jaclyn S., Aguiar Mike, Breslow David K., Gygi Steven P. and Nachury Maxence V. (2014)  
 “The Intraflagellar Transport Protein IFT27 Promotes BBSome Exit from Cilia through the GTPase ARL6/BBS3.” *Developmental Cell* 31 (3): 265–78.  
<https://doi.org/10.1016/j.devcel.2014.09.004>.
105. **Liu**, Hongjun, Fergusson Maria M., Castilho Rogerio M., Liu Jie, Cao Liu, Chen Jichun, Malide Daniela, *et al.* (2007)  
 “Augmented Wnt Signaling in a Mammalian Model of Accelerated Aging.” *Science* 317 (5839): 803–6.  
<https://doi.org/10.1126/science.1143578>.
106. **Liu**, Min, Liu Aiguo, Wang Jie, Zhang Yansong, Li Yajuan, Su Ying, and Zhu Alan Jian (2020)  
 “Competition between Two Phosphatases Fine-Tunes Hedgehog Signaling.” *Journal of Cell Biology* 220 (e202010078).  
<https://doi.org/10.1083/jcb.202010078>.
107. **Luchetti**, Giovanni, Sircar Ria, Kong Jennifer H., Nachtergaele Sigrid, Sagner Andreas,

- F.X. Byrne Eamon, Covey Douglas F., Siebold Christian and Rohatgi Rajat (2016)  
 “Cholesterol Activates the G-Protein Coupled Receptor Smoothed to Promote Hedgehog Signaling.” *ELife* 5 (October).  
<https://doi.org/10.7554/eLife.20304>.
108. **Ma**, Pengcheng, Song Ning-Ning, Li Yongxin, Zhang Qiong, Zhang Lei, Zhang Longlong, Kong Qinghua, *et al.* (2019)  
 “Fine-Tuning of Shh/Gli Signaling Gradient by Non-Proteolytic Ubiquitination during Neural Patterning.” *Cell Reports* 28 (2): 541-553.e4.  
<https://doi.org/10.1016/j.celrep.2019.06.017>.
109. **May**, Elena A., Kalocsay Marian, D’Auriac Inès Galtier, Schuster Patrick S., Gygi Steven P., Nachury Maxence V., and Mick David U. (2021)  
 “Time-Resolved Proteomics Profiling of the Ciliary Hedgehog Response.” *Journal of Cell Biology* 220 (5): e202007207.  
<https://doi.org/10.1083/jcb.202007207>.
110. **May**, Elena A., Sroka Tommy J. and Mick David U. (2021)  
 “Phosphorylation and Ubiquitylation Regulate Protein Trafficking, Signaling, and the Biogenesis of Primary Cilia.” *Frontiers in Cell and Developmental Biology* 9.  
<https://doi.org/10.3389/fcell.2021.664279>.
111. **McKenzie**, Casey W., Branch Craige, Kroeger Tiffany V., Finn Rozzy, Wyatt Todd A., Sisson Joseph H., Pavlik Jacqueline A. *et al.* (2015)  
 “CFAP54 Is Required for Proper Ciliary Motility and Assembly of the Central Pair Apparatus in Mice.” *Molecular Biology of the Cell* 26 (18): 3140–49.  
<https://doi.org/10.1091/mbc.E15-02-0121>.
112. **Mecke**, S., And Passarge E. (1971)  
 “Encephalocele, Polycystic Kidneys, and Polydactyly as an Autosomal Recessive Trait Simulating Certain Other Disorders: The Meckel Syndrome.” *Annales De Genetique* 14 (2): 97–103.
113. **Mick**, David U., Rodrigues Rachel B., Leib Ryan D., Adams Christopher M., Chien Allis S., Gygi Steven P., and Nachury Maxence V. (2015)  
 “Proteomics of Primary Cilia by Proximity Labeling.” *Developmental Cell* 35 (4): 497–512.  
<https://doi.org/10.1016/j.devcel.2015.10.015>.
114. **Mok**, Gi Fay, Lozano-Velasco Estefania, Maniou Eirini, Viaut Camille, Moxon Simon, Wheeler, Grant and Münsterberg Andrea (2018)  
 “MiR-133-Mediated Regulation of the Hedgehog Pathway Orchestrates Embryo Myogenesis.” *Development* 145 (12).  
<https://doi.org/10.1242/dev.159657>.
115. **Molla-Herman**, A., Ghossoub R., Blisnick T., Meunier A., Serres C., Silbermann F., Emmerson C., *et al.* 2010.  
 “The Ciliary Pocket: An Endocytic Membrane Domain at the Base of Primary and Motile Cilia.” *Journal of Cell Science* 123 (10): 1785–95.

- <https://doi.org/10.1242/jcs.059519>.
116. **Morante**, Nicholas, Abedin Sigg Monika, Strauskulage Luke, Raleigh David R. And Reiter Jeremy F. (2020)  
“DYRK2 Is a Ciliary Kinase Involved in Vertebrate Hedgehog Signal Transduction.” *BioRxiv*, August, 2020.08.31.275511.  
<https://doi.org/10.1101/2020.08.31.275511>.
117. **Mukhopadhyay**, Saikat, Wen Xiaohui, Chih Ben, Nelson Christopher D., Lane William S., Scales Suzie J., and Jackson Peter K. (2010)  
“TULP3 Bridges the IFT-A Complex and Membrane Phosphoinositides to Promote Trafficking of G Protein-Coupled Receptors into Primary Cilia.” *Genes & Development* 24 (19): 2180–93.  
<https://doi.org/10.1101/gad.1966210>.
118. **Moyer**, J. H., Lee-Tischler M. J., Kwon H. Y., Schrick J. J., Avner E. D., Sweeney W. E., Godfrey V. L., Cacheiro N. L., Wilkinson J. E., and Woychik R. P. (1994)  
“Candidate Gene Associated with a Mutation Causing Recessive Polycystic Kidney Disease in Mice.” *Science (New York, N.Y.)* 264 (5163): 1329–33.  
<https://doi.org/10.1126/science.8191288>.
119. **Mukhopadhyay**, Saikat, Wen Xiaohui, Ratti Navneet, Loktev Alexander, Rangell Linda, Scales Suzie J. and Jackson Peter K. (2013)  
“The Ciliary G-Protein-Coupled Receptor Gpr161 Negatively Regulates the Sonic Hedgehog Pathway via CAMP Signaling.” *Cell* 152 (1): 210–23.  
<https://doi.org/10.1016/j.cell.2012.12.026>.
120. **Mykytyn**, Kirk, and Askwith Candice. (2017)  
“G-Protein-Coupled Receptor Signaling in Cilia.” *Cold Spring Harbor Perspectives in Biology* 9 (9): a028183.  
<https://doi.org/10.1101/cshperspect.a028183>.
121. **Nachury**, Maxence V. (2018)  
“The Molecular Machines That Traffic Signaling Receptors into and out of Cilia.” *Current Opinion in Cell Biology, Cell Signalling*, 51 (April): 124–31.  
<https://doi.org/10.1016/j.ceb.2018.03.004>.
122. **Nachury**, Maxence V., Loktev Alexander V., Zhang Qihong, Westlake Christopher J., Peränen Johan, Merdes Andreas, Slusarski Diane C, *et al.* (2007)  
“A Core Complex of BBS Proteins Cooperates with the GTPase Rab8 to Promote Ciliary Membrane Biogenesis.” *Cell* 129 (6): 1201–13.  
<https://doi.org/10.1016/j.cell.2007.03.053>.
123. **Nager**, Andrew R., Goldstein Jaclyn S., Herranz-Pérez Vicente, Portran Didier, Ye Fan, Garcia-Verdugo Jose Manuel, and Nachury Maxence V. (2017)  
“An Actin Network Dispatches Ciliary GPCRs into Extracellular Vesicles to Modulate Signaling.” *Cell* 168 (1–2): 252-263.e14.  
<https://doi.org/10.1016/j.cell.2016.11.036>.
124. **Nakata**, Kana, Shiba Dai, Kobayashi Daisuke, and Yokoyama Takahiko. (2012)

- “Targeting of Nphp3 to the Primary Cilia Is Controlled by an N-Terminal Myristoylation Site and Coiled-Coil Domains.” *Cytoskeleton* 69 (4): 221–34.  
<https://doi.org/10.1002/cm.21014>.
125. **Nakayama**, Kazuhisa, and Katoh Yohei (2020)  
 “Architecture of the IFT Ciliary Trafficking Machinery and Interplay between Its Components.” *Critical Reviews in Biochemistry and Molecular Biology* 55 (2): 179–96.  
<https://doi.org/10.1080/10409238.2020.1768206>.
126. **Nauli**, Surya M., Alenghat Francis J., Luo Ying, Williams Eric, Vassilev Peter, Li Xiaogang, Elia Andrew E. H., *et al.* (2003)  
 “Polycystins 1 and 2 Mediate Mechanosensation in the Primary Cilium of Kidney Cells.” *Nature Genetics* 33 (2): 129–37.  
<https://doi.org/10.1038/ng1076>.
127. **Nieuwenhuis**, Joppe, Adamopoulos Athanassios, Bleijerveld Onno B., Mazouzi Abdelghani, Stickel Elmer, Celie Patrick, Altelaar Maarte, *et al.* (2017)  
 “Vasohibins Encode Tubulin Detyrosinating Activity.” *Science* 358 (6369): 1453–56.  
<https://doi.org/10.1126/science.aao5676>.
128. **Niewiadomski**, Paweł, Niedziółka Sylwia M., Markiewicz Łukasz, Uśpieński Tomasz, Baran Brygida, and Chojnowska Katarzyna (2019)  
 “Gli Proteins: Regulation in Development and Cancer.” *Cells* 8 (2): 147.  
<https://doi.org/10.3390/cells8020147>.
129. **Nishijima**, Yuya, Hagiya Yohei, Kubo Tomohiro, Takei Ryota, Katoh Yohei, and Nakayama, Kazuhisa. (2017)  
 “RABL2 Interacts with the Intraflagellar Transport-B Complex and CEP19 and Participates in Ciliary Assembly.” *Molecular Biology of the Cell* 28 (12): 1652–66.  
<https://doi.org/10.1091/mbc.e17-01-0017>.
130. **Nitzsche**, Anja, Pietila Riikka, Testini Chiara, Ninchoji Takeshi, Smith Ross O., Ekvarn Elisabet, Larsson Jimmy, *et al.* (2020)  
 “Paladin Is a PI(4,5)P2 Phosphoinositide Phosphatase That Regulates Endosomal Signaling and Angiogenesis.” *BioRxiv*.  
<https://doi.org/10.1101/2020.02.11.943183>.
131. **Nonaka**, S., Tanaka Y., Okada Y., Takeda S., Harada A., Kanai Y., Kido M., and Hirokawa N. (1998)  
 “Randomization of Left-Right Asymmetry Due to Loss of Nodal Cilia Generating Leftward Flow of Extraembryonic Fluid in Mice Lacking KIF3B Motor Protein.” *Cell* 95 (6): 829–37.  
[https://doi.org/10.1016/s0092-8674\(00\)81705-5](https://doi.org/10.1016/s0092-8674(00)81705-5).
132. **Nüsslein-Volhard**, C., and **Wieschaus** E. (1980)  
 “Mutations Affecting Segment Number and Polarity in *Drosophila*.” *Nature* 287 (5785): 795–801.  
<https://doi.org/10.1038/287795a0>.
133. **Ong**, Albert C. M., and **Harris** Peter C. (2005)

- “Molecular Pathogenesis of ADPKD: The Polycystin Complex Gets Complex.” *Kidney International* 67 (4): 1234–47.  
<https://doi.org/10.1111/j.1523-1755.2005.00201.x>.
134. **Párducz, Béla. (1967)**  
 “Ciliary Movement and Coordination in Ciliates” Translators’ Note: The Sudden Death of Dr. Párducz in February, 1964, Left the Text of the Present Manuscript Nearly Completed. A Small Part of Section IV Remained to Be Written; .(..)” In *International Review of Cytology*, edited by G. H. Bourne and J. F. Danielli, 21:91–128. Academic Press.  
[https://doi.org/10.1016/S0074-7696\(08\)60812-8](https://doi.org/10.1016/S0074-7696(08)60812-8).
135. **Parks, John E., Arion Janice W., and Foote R. H. (1987)**  
 “Lipids of Plasma Membrane and Outer Acrosomal Membrane from Bovine Spermatozoa.” *Biology of Reproduction* 37 (5): 1249–58.  
<https://doi.org/10.1095/biolreprod37.5.1249>.
136. **Pazour, Gregory J. (2004)**  
 “Comparative Genomics: Prediction of the Ciliary and Basal Body Proteome.” *Current Biology* 14 (14): R575–77.  
<https://doi.org/10.1016/j.cub.2004.07.017>.
137. **Pazour, Gregory J., Agrin Nathan, Leszyk John, and Witman George B. (2005)**  
 “Proteomic Analysis of a Eukaryotic Cilium.” *Journal of Cell Biology* 170 (1): 103–13.  
<https://doi.org/10.1083/jcb.200504008>.
138. **Pazour, Gregory J., Sheila A. Baker, James A. Deane, Douglas G. Cole, Bethany L. Dickert, Joel L. Rosenbaum, George B. Witman, and Joseph C. Besharse. 2002.**  
 “The Intraflagellar Transport Protein, IFT88, Is Essential for Vertebrate Photoreceptor Assembly and Maintenance.” *Journal of Cell Biology* 157 (1): 103–14.  
<https://doi.org/10.1083/jcb.200107108>.
139. **Pazour, Gregory J., Dickert Bethany L., Vucica Yvonne, Scott Seeley E., Rosenbaum Joel L., Witman George B., and Cole Douglas G. (2000)**  
 “Chlamydomonas IFT88 and Its Mouse Homologue, Polycystic Kidney Disease Gene Tg737, Are Required for Assembly of Cilia and Flagella.” *The Journal of Cell Biology* 151 (3): 709–18.
140. **Pazour, Gregory J., and Witman George B. (2003)**  
 “The Vertebrate Primary Cilium Is a Sensory Organelle.” *Current Opinion in Cell Biology* 15 (1): 105–10.  
[https://doi.org/10.1016/s0955-0674\(02\)00012-1](https://doi.org/10.1016/s0955-0674(02)00012-1).
141. **Pusapati, Ganesh V., Kong Jennifer H., Patel Bhaven B., Krishnan Arunkumar, Sagner Andreas, Kinnebrew Maia, Briscoe James, Aravind L., and Rohatgi Rajat. (2018)**  
 “CRISPR Screens Uncover Genes That Regulate Target Cell Sensitivity to the Morphogen Sonic Hedgehog.” *Developmental Cell* 44 (1): 113-129.e8.  
<https://doi.org/10.1016/j.devcel.2017.12.003>.
142. **Poitout, Vincent, Stout Laurence E., Armstrong Michael B., Walseth Timothy F., Sorenson Robert L., and Robertson R. Paul (1995)**

- “Morphological and Functional Characterization of BTC-6 Cells—an Insulin-Secreting Cell Line Derived From Transgenic Mice.” *Diabetes* 44 (3): 306–13.  
<https://doi.org/10.2337/diab.44.3.306>.
143. **Praktiknjo**, Samantha D., Saad Farah, Maier Dominic, Ip Pamela, and Hipfner David R. (2018)  
 “Activation of Smoothed in the Hedgehog Pathway Unexpectedly Increases Gas-Dependent CAMP Levels in Drosophila.” *Journal of Biological Chemistry* 293 (35): 13496–508.  
<https://doi.org/10.1074/jbc.RA118.001953>.
144. **Radhakrishnan**, Arun, Rohatgi Rajat, and Siebold Christian (2020)  
 “Cholesterol Access in Cellular Membranes Controls Hedgehog Signaling.” *Nature Chemical Biology* 16 (12): 1303–13.  
<https://doi.org/10.1038/s41589-020-00678-2>.
145. **Rauchman**, M. I., Nigam S. K., Delpire E., and Gullans S. R. (1993)  
 “An Osmotically Tolerant Inner Medullary Collecting Duct Cell Line from an SV40 Transgenic Mouse.” *American Journal of Physiology-Renal Physiology* 265 (3): F416–24.  
<https://doi.org/10.1152/ajprenal.1993.265.3.F416>.
146. **Reiter**, Jeremy F., and **Leroux** Michel R. (2017)  
 “Genes and Molecular Pathways Underpinning Ciliopathies.” *Nature Reviews Molecular Cell Biology* 18 (9): 533–47.  
<https://doi.org/10.1038/nrm.2017.60>.
147. **Reiterer**, Veronika, Eyers Patrick A., and Farhan Hesso (2014)  
 “Day of the Dead: Pseudokinases and Pseudophosphatases in Physiology and Disease.” *Trends in Cell Biology* 24 (9): 489–505.  
<https://doi.org/10.1016/j.tcb.2014.03.008>.
148. **Roberts**, Anthony J., Kon Takahide, Knight Peter J., Sutoh Kazu, and Burgess Stan A. (2013)  
 “Functions and Mechanics of Dynein Motor Proteins.” *Nature Reviews Molecular Cell Biology* 14 (11): 713–26.  
<https://doi.org/10.1038/nrm3667>.
149. **Roffers-Agarwal**, Julaine, Hutt Karla J., and Gammill Laura S. (2012)  
 “Paladin Is an Antiphosphatase That Regulates Neural Crest Cell Formation and Migration.” *Developmental Biology* 371 (2): 180–90.  
<https://doi.org/10.1016/j.ydbio.2012.08.007>.
150. **Ronquillo**, C.C., Bernstein P. S., and Baehr W. (2012)  
 “Senior-Løken Syndrome: A Syndromic Form of Retinal Dystrophy Associated with Nephronophthisis.” *Vision Research* 75 (December): 88–97.  
<https://doi.org/10.1016/j.visres.2012.07.003>.
151. **Roux**, Kyle J., Kim Dae In, Raida Manfred, and Burke Brian (2012)  
 “A Promiscuous Biotin Ligase Fusion Protein Identifies Proximal and Interacting Proteins in Mammalian Cells.” *The Journal of Cell Biology* 196 (6): 801–10.  
<https://doi.org/10.1083/jcb.201112098>.



151. **Roy**, Kasturi, and **Marin** Ethan P. (2019)  
“Lipid Modifications in Cilia Biology.” *Journal of Clinical Medicine* 8 (7).  
<https://doi.org/10.3390/jcm8070921>.
152. **Rudolf**, Amalie F., Kinnebrew Maia, Kowatsch Christiane, Ansell T. Bertie, Omari Kamel El, Benjamin Bishop, Els Pardon, *et al.* (2019)  
“The Morphogen Sonic Hedgehog Inhibits Its Receptor Patched by a Pincer Grasp Mechanism.”  
*Nature Chemical Biology* 15 (10): 975–82.  
<https://doi.org/10.1038/s41589-019-0370-y>.
153. **Salonen**, R., and P. Paavola. (1998)  
“Meckel Syndrome.” *Journal of Medical Genetics* 35 (6): 497–501.  
<https://doi.org/10.1136/jmg.35.6.497>.
154. **Salonen**, Riitta, John M. Opitz, and James F. Reynolds. (1984)  
“The Meckel Syndrome: Clinicopathological Findings in 67 Patients.” *American Journal of Medical Genetics* 18 (4): 671–89.  
<https://doi.org/10.1002/ajmg.1320180414>.
155. **Sang**, Liyun, Miller Julie J., Corbit Kevin C., Giles Rachel H, Brauer Matthew J., Otto, Edgar A. Lisa, Baye M., *et al.* (2011)  
“Mapping the Nephronophthisis-Joubert-Meckel-Gruber Protein Network Reveals Ciliopathy Disease Genes and Pathways.” *Cell* 145 (4): 513–28.  
<https://doi.org/10.1016/j.cell.2011.04.019>.
156. **Santagata**, Sandro, Boggon Titus J., Baird Cheryl L., Gomez Carlos A., Zhao Jin, Song Wei Shan, Myszka David G., and Shapiro Lawrence (2001)  
“G-Protein Signaling Through Tubby Proteins.” *Science* 292 (5524): 2041–50.  
<https://doi.org/10.1126/science.1061233>.
157. **Sherstha**, R., McKinley C., Russ P., Scherzinger A., Bronner T., Showalter R., And Everson G. T. (1997)  
“Postmenopausal Estrogen Therapy Selectively Stimulates Hepatic Enlargement in Women with Autosomal Dominant Polycystic Kidney Disease.” *Hepatology* 26 (5): 1282–86.  
<https://doi.org/10.1002/hep.510260528>.
158. **Shida**, Toshinobu, Cueva Juan G., Xu Zhenjie, Goodman Miriam B., And Nachury Maxence V. (2010)  
“The Major Alpha-Tubulin K40 Acetyltransferase AlphaTAT1 Promotes Rapid Ciliogenesis and Efficient Mechanosensation.” *Proceedings of the National Academy of Sciences of the United States of America* 107 (50): 21517–22.  
<https://doi.org/10.1073/pnas.1013728107>.
159. **Shinde**, Swapnil Rohidas, Nager Andrew R., And Nachury Maxence V. (2020)  
“Lysine63-Linked Ubiquitin Chains Earmark GPCRs for BBSome-Mediated Removal from Cilia.” Preprint. Cell Biology.  
<https://doi.org/10.1101/2020.03.04.977090>.

160. **Sorokin, Sergei (1962)**  
 “Centrioles and the formation of rudimentary cilia by fibroblast and smooth muscle cells.” *The Journal of Cell Biology* 15 (2): 363–77.
161. **Su, Xuefeng, Driscoll Kaitlin, Yao Gang, Raed Anas, Wu Maoqing, Beales Philip L., And Zhou Jing (2014)**  
 “Bardet-Biedl Syndrome Proteins 1 and 3 Regulate the Ciliary Trafficking of Polycystic Kidney Disease 1 Protein.” *Human Molecular Genetics* 23 (20): 5441–51.  
<https://doi.org/10.1093/hmg/ddu267>.
162. **Su, Ying, Ospina Jason K., Zhang Junzheng, Michelson Andrew P., Schoen Adam M., and Zhu Alan Jian (2011)**  
 “Sequential Phosphorylation of Smoothed Transduces Graded Hedgehog Signaling.” *Science Signaling* 4 (180): ra43.  
<https://doi.org/10.1126/scisignal.2001747>.
163. **Sutter, Michael, and Gregory G. Germino (2003)**  
 “Autosomal Dominant Polycystic Kidney Disease: Molecular Genetics and Pathophysiology.” *Journal of Laboratory and Clinical Medicine* 141 (2): 91–101.  
<https://doi.org/10.1067/mlc.2003.13>.
164. **Takabatake, Kiyofumi, Shimo Tsuyoshi, Murakami Jun, Anqi Chang, Kawai Hotaka, Yoshida Saori , Oo May Wathone, et al. (2019)**  
 “The Role of Sonic Hedgehog Signaling in the Tumor Microenvironment of Oral Squamous Cell Carcinoma.” *International Journal of Molecular Sciences* 20 (22): 5779.  
<https://doi.org/10.3390/ijms20225779>.
165. **Tobin, Jonathan L., and Beales Philip L. (2009)**  
 “The Nonmotile Ciliopathies.” *Genetics in Medicine* 11 (6): 386–402.  
<https://doi.org/10.1097/GIM.0b013e3181a02882>.
166. **Todaro, George J., and Green Howard. (1963)**  
 “Quantitative studies of the growth of mouse embryo cells in culture and their development into established lines.” *Journal of Cell Biology* 17 (2): 299–313.  
<https://doi.org/10.1083/jcb.17.2.299>.
167. **Truong, Melissa E., Bilekova Sara, Choksi Semil P., Li, Wan, Bugaj Lukasz J., Xu Ke and Reiter Jeremy F. (2021)**  
 “Vertebrate Cells Differentially Interpret Ciliary and Extraciliary CAMP.” *Cell* 184 (11): 2911–2926.e18.  
<https://doi.org/10.1016/j.cell.2021.04.002>.
168. **Tschaikner, Philipp, Enzler Florian, Torres-Quesada Omar, Aanstad Pia, and Stefan Eduard. (2020)**  
 “Hedgehog and Gpr161: Regulating CAMP Signaling in the Primary Cilium.” *Cells* 9 (1).  
<https://doi.org/10.3390/cells9010118>.
169. **Uhler, M. D., D. F. Carmichael, D. C. Lee, J. C. Chrivia, E. G. Krebs, and G. S. McKnight. (1986)**

- “Isolation of cDNA Clones Coding for the Catalytic Subunit of Mouse CAMP-Dependent Protein Kinase.” *Proceedings of the National Academy of Sciences* 83 (5): 1300–1304.  
<https://doi.org/10.1073/pnas.83.5.1300>.
170. **Uhler, M. D.,** Chrivia J. C., and McKnight G. S. (1986)  
 “Evidence for a Second Isoform of the Catalytic Subunit of CAMP-Dependent Protein Kinase.” *The Journal of Biological Chemistry* 261 (33): 15360–63.
171. **Veland, Iben R.,** Awan Aashir, Pedersen Lotte B., Yoder Bradley K., and Christensen Søren T. (2009)  
 “Primary Cilia and Signaling Pathways in Mammalian Development, Health and Disease.” *Nephron. Physiology* 111 (3): p39-53.  
<https://doi.org/10.1159/000208212>.
172. **Venkatesh, Deepak** (2017)  
 “Primary Cilia.” *Journal of Oral and Maxillofacial Pathology : JOMFP* 21 (1): 8–10.  
[https://doi.org/10.4103/jomfp.JOMFP\\_48\\_17](https://doi.org/10.4103/jomfp.JOMFP_48_17).
173. **Vertii, Anastassiia,** Hung Hui-Fang, Hehnlly Heidi, and Doxsey Stephen (2016)  
 “Human Basal Body Basics.” *Cilia* 5 (March).  
<https://doi.org/10.1186/s13630-016-0030-8>.
174. **Wali, Ravinder K.,** and William L. Henrich. 2005.  
 “Chronic Kidney Disease: A Risk Factor for Cardiovascular Disease.” *Cardiology Clinics* 23 (3): 343–62.  
<https://doi.org/10.1016/j.ccl.2005.03.007>.
175. **Wallgard, Elisabet,** Nitzsche Anja, Larsson Jimmy, Guo Xiaoyuan, Dieterich Lothar C., Dimberg Anna, Olofsson Tommie, *et al.* (2012)  
 “Paladin (X99384) Is Expressed in the Vasculature and Shifts from Endothelial to Vascular Smooth Muscle Cells during Mouse Development.” *Developmental Dynamics: An Official Publication of the American Association of Anatomists* 241 (4): 770–86.  
<https://doi.org/10.1002/dvdy.23753>.
176. **Wang, Lei,** and **Dynlacht Brian D.** (2018)  
 “The Regulation of Cilium Assembly and Disassembly in Development and Disease.” *Development (Cambridge, England)* 145 (18).  
<https://doi.org/10.1242/dev.151407>.
177. **Wang, Zhaohui,** Fan Zhen-Chuan, Williamson Shana M., and Qin Hongmin (2009)  
 “Intraflagellar Transport (IFT) Protein IFT25 Is a Phosphoprotein Component of IFT Complex B and Physically Interacts with IFT27 in Chlamydomonas.” *PLOS ONE* 4 (5): e5384.  
<https://doi.org/10.1371/journal.pone.0005384>.
178. **Wann, A. K. T.,** And **Knight M. M.** (2012)  
 “Primary Cilia Elongation in Response to Interleukin-1 Mediates the Inflammatory Response.” *Cellular and Molecular Life Sciences* 69 (17): 2967–77.  
<https://doi.org/10.1007/s00018-012-0980-y>.
179. **Wanner, A.,** Salathé M., And O’Riordan T. G. (1996)

- “Mucociliary Clearance in the Airways.” *American Journal of Respiratory and Critical Care Medicine* 154 (6 Pt 1): 1868–1902.  
<https://doi.org/10.1164/ajrccm.154.6.8970383>.
180. **Ward**, S., Thomson N., White J. G., and Brenner S. (1975)  
 “Electron Microscopical Reconstruction of the Anterior Sensory Anatomy of the Nematode *Caenorhabditis Elegans*.” *The Journal of Comparative Neurology* 160 (3): 313–37.  
<https://doi.org/10.1002/cne.901600305>.
181. **Watanabe**, Masaki, Inukai Kouichi, Katagiri Hideki, Awata Takuya, Oka Yoshitomo, and Katayama Shigehiro (2003)  
 “Regulation of PPAR $\gamma$  Transcriptional Activity in 3T3-L1 Adipocytes.” *Biochemical and Biophysical Research Communications* 300 (2): 429–36.  
[https://doi.org/10.1016/S0006-291X\(02\)02860-7](https://doi.org/10.1016/S0006-291X(02)02860-7).
182. **Wensel**, Theodore G., Zhang Zhixian, Anastassov Ivan A., Gilliam Jared C., He Feng, Schmid Michael F., and Robichaux Michael A. (2016)  
 “Structural and Molecular Bases of Rod Photoreceptor Morphogenesis and Disease.” *Progress in Retinal and Eye Research* 55 (November): 32–51.  
<https://doi.org/10.1016/j.preteyeres.2016.06.002>.
183. **Wright**, Kevin J., Baye Lisa M., Olivier-Mason Anique, Mukhopadhyay Saikat, Sang Liyun, Kwong Mandy, Wang Weiru, *et al.* (2011)  
 “An ARL3–UNC119–RP2 GTPase Cycle Targets Myristoylated NPHP3 to the Primary Cilium.” *Genes & Development* 25 (22): 2347–60.  
<https://doi.org/10.1101/gad.173443.111>.
184. **Wu**, Fujia, Zhang Yu , Sun Bo, McMahon Andrew P., And Wang Yu (2017)  
 “Hedgehog Signaling: From Basic Biology to Cancer Therapy.” *Cell Chemical Biology* 24 (3): 252–80.  
<https://doi.org/10.1016/j.chembiol.2017.02.010>.
185. **Xu**, Qingwen, Zhang Yuxia, Wei Qing, Huang Yan, Hu Jinghua and Ling Kun (2016)  
 “Phosphatidylinositol Phosphate Kinase PIPKI $\gamma$  and Phosphatase INPP5E Coordinate Initiation of Ciliogenesis.” *Nature Communications* 7 (February).  
<https://doi.org/10.1038/ncomms10777>.
186. **Yaffe**, David (1968)  
 “Retention of differentiation potentialities during prolonged cultivation of myogenic cells.” *Proc Natl Acad Sci USA*. Oct; 61(2): 477-483  
 Doi: 10.1073/pnas.61.2.477
187. **Yaffe**, David, and **Saxel** Ora (1977)  
 “Serial Passaging and Differentiation of Myogenic Cells Isolated from Dystrophic Mouse Muscle.” *Nature* 270 (5639): 725–27.  
<https://doi.org/10.1038/270725a0>.
188. **Ye**, Fan, Nager Andrew R., and Nachury Maxence V. (2018)  
 “BBSome Trains Remove Activated GPCRs from Cilia by Enabling Passage through the

- Transition Zone.” *Journal of Cell Biology* 217 (5): 1847–68.  
<https://doi.org/10.1083/jcb.201709041>.
189. **Yusifov**, Elkhan, Dumoulin Alexandre, and Stoeckli Esther T. (2021)  
 “Investigating Primary Cilia during Peripheral Nervous System Formation.” *International Journal of Molecular Sciences* 22 (6): 3176.  
<https://doi.org/10.3390/ijms22063176>.
190. **Zhao**, Long, Wang Liguu, Chi Chunli, Lan Wenwen, and Su Ying (2017)  
 “The Emerging Roles of Phosphatases in Hedgehog Pathway.” *Cell Communication and Signaling* 15 (1): 35.  
<https://doi.org/10.1186/s12964-017-0191-0>.
191. **Zhou**, Haiying, Kim Seokjoong, Ishii Shunsuke, and Boyer Thomas G. (2006)  
 “Mediator Modulates Gli3-Dependent Sonic Hedgehog Signaling.” *Molecular and Cellular Biology* 26 (23): 8667–82.  
<https://doi.org/10.1128/MCB.00443-06>.
192. **Zimmer**, Marc (2002)  
 “Green Fluorescent Protein (GFP): Applications, Structure, and Related Photophysical Behavior.” *Chemical Reviews* 102 (3): 759–82.  
<https://doi.org/10.1021/cr010142r>.
193. **Zimmermann**, K. W. (1898).  
 „Beiträge zur Kenntniss einiger Drüsen und Epithelien“. *Archiv für Mikroskopische Anatomie* 52, 552-706

## 9. Acknowledgements

With the completion of this work, a very defining, exciting and educational time comes to an end for me. Therefore, I would like to take this opportunity to thank some special people who stood beside me during this time.

First, I would like to thank Jun.–Prof. Dr. David Mick for allowing me to join the research group and for his support during this project. Thank you for always having an open ear, for many scientific discussions and for always encouraging me to find my own path. I have learned a lot during my time in the Mick working group and I am grateful for the opportunity to help shape and experience the development of this wonderful and growing team.

I would also like to thank all the members of the Mick working group, for the outstanding team spirit and mutual support on good and bad lab days. In particular, I would like to thank Tommy Sroka, Valerie Chaumet, Patrick Schuster and Lea Sannwald for their friendship and emotional and technical support during our shared time in the lab. Special thanks to Nicky Byers and Doris Jann, whose great technical support facilitated and enabled many experiments and processes during the end of my project. I would also like to thank the former members of the working group, Andreas Riske and Nicole Heim, for all the time we spent together in the lab. All of you made this time a special one and I will miss you very much.

Furthermore, I would also like to give special thanks to Martin van der Laan and his research group for their warm welcome, support and scientific discussions, as well as to all other members of the medical biochemistry department in Homburg.

Many thanks to Jun.–Prof. Dr. Nicole Ludwig and Esther Maldener from the Department of Human Genetics in Homburg for their assistance in performing the qPCR experiments as part of this project.

Many thanks also go to PD Dr. Elmar Krause from the Center for Integrative Physiology and Molecular Medicine in Homburg for technical assistance with FACS sorting.

I would like to say a very special thank you to my parents and grandparents who have supported and accompanied me on this path from the very beginning. Without you, none of this would have been possible. Thank you for your constant interest in my work and your belief in me.

I would also like to thank all my friends and especially my dear comrades-in-arms. Thank you for the many times where we could exchange ideas, encourage and support each other. I am very glad that you were by my side.

Last but not least, I would like to thank one special person who who rejoiced with me and suffered with me and was a consistent and strong support. Thank you Jens, for always being there for me, giving me patience, stability, strength and the courage to go on.

## 10. Publications

### 10.1. Research Article

**Elena A. May**; Marian Kalocsay; Inès Galtier D'Auriac; Patrick S. Schuster; Steven P. Gygi; Maxence V. Nachury; David U. Mick. **Time-resolved proteomics profiling of the ciliary Hedgehog response.** *J. Cell Biol.* 2021 Vol. 2020 No. 5; 2021;  
doi: 10.1083/jcb.202007207

### 10.2. Review Article

**Elena A. May**; Tommy J. Sroka; David U. Mick. **Phosphorylation and Ubiquitylation Regulate Protein Trafficking, Signaling, and the Biogenesis of Primary Cilia.** *Front. Cell. Dev. Biol.* 9:664279; 2021;  
doi: 10.3389/fcell.2021.664279

